Development of Modified polylysine based antibody conjugated nanoparticles with tumor-restricted, FcγR-independent stimulatory activity by targeting Fn14

Entwicklung modifizierter, mit Antikörpern konjugierter Nanopartikel auf Polylysinbasis mit tumorbeschränkter, FcγR-unabhängiger stimulierender Aktivität durch Ausrichtung auf Fn14

Doctoral thesis for a doctoral degree

at the Graduate School of Life Sciences,

Julius-Maximilians-University Wuerzburg

Section Biomedicine

Submitted by

Tengyu Zhang

Early Stage Researcher (ESR) From the European Union´s Horizon 2020 research and innovation programme under the Marie Sklodowska-Curie grant agreement No 813871

Würzburg 2023

Submitted on: ……

Members of the promotion committee:

Chairperson: Prof. Dr. Rüdiger Pryss

Primary Supervisor: Prof. Dr. Harald Wajant

Second Supervisor: Prof. Dr. Edwin Bremer

Third Supervisor: Prof. Dr. Dr. Andreas Beilhack

Date of Public Defense: ……

Date of Receipt of Certificates: ……..

Affidavit

I hereby confirm that my thesis entitled “Development of Modified polylysine based antibody conjugated nanoparticles with tumor-restricted, FcγR-independent stimulatory activity by targeting Fn14” is the result of my own work. I did not receive any help or support from commercial consultants. All sources and materials applied are listed and specified in the thesis.

Furthermore, I confirm that this thesis has not yet been submitted as part of another examination process neither in identical nor in similar form.

Würzburg ……

Date …… Signature ……

Eidesstattliche Erklärung

Hiermit erkläre ich an Eides statt, die Dissertation “ Entwicklung modifizierter, mit Antikörpern konjugierter Nanopartikel auf Polylysinbasis mit tumorbeschränkter, FcγR-unabhängiger stimulierender Aktivität durch Ausrichtung auf Fn14” eigenständig, d.h. insbesondere selbständig und ohne Hilfe eines kommerziellen Promotionsberaters, angefertigt und keine anderen als die von mir angegebenen Quellen und Hilfsmittel verwendet zu haben.

Ich erkläre außerdem, dass die Dissertation weder in gleicher noch in ähnlicher Form bereits in einem anderen Prüfungsverfahren vorgelegen hat.

Würzburg ……

Date …… Signature ……

Acknowledgement

At this juncture of my academic journey, I wish to express my profound gratitude towards my mentor, Prof. Dr. Harald Wajant, whose support, guidance, and inspiration were pivotal in the successful completion of my Ph.D. He provided me with the opportunity to carry out my research under his esteemed supervision. His valuable insights, constructive feedback, and constant encouragement have been instrumental in shaping my research pursuits. His open-door policy enabled a nurturing and collaborative environment, enriching my academic experience.

I am deeply appreciative of the support and encouragement from Prof. Dr. Edwin Bremer and Prof. Dr. Dr. Andreas Beilhack, my second and third supervisors. Their insightful comments and thoughtful criticism significantly contributed to my research and instilled in me a deeper understanding of my chosen field.

I am particularly grateful for the financial support from the European Union's Horizon 2020 Marie Curie Project, 'I-Direct,' which made this research possible. Moreover, support and professional guidance I received from my colleagues at the Department of Molecular Internal Medicine, Wuerzburg University have been a pillar of strength during my Ph.D. journey. I extend my sincere gratitude to InoCure from the Czech Republic for their support and collaboration.

To all those who have been a part of this journey, your support and contributions have been crucial to my research and personal growth. Thank you. I would like to extend special thanks to my esteemed colleague, Nienke Hesen, who accompanied me throughout the entirety of my Ph.D. study. Her companionship during challenging periods was invaluable. I also owe a deep debt of gratitude to my husband Johan and mother Longjuan for emotional support, helping me navigate the darker days during my Ph.D. journey.

Tengyu Zhang

Content:

1 Introduction

In recent years, immunomodulatory approaches that stimulate the host's immune system to fight against cancer have gained significant interest, as they exhibit milder side effects and stronger curing effects compared with traditional therapies such as chemotherapy, radiotherapy, and surgery. Not only does immunotherapy treat cancer by inducing a strong anti-tumor immune response, but it also controls metastasis and prevents its recurrence, hence representing a major advantage over traditional cancer treatments. Cancer immunotherapy, which activates/stimulates the host's immunity by the introduction of various cancer vaccines, monoclonal antibodies, immune checkpoint blockers, and cell-based therapies, has been proven to be very effective in many clinical studies (Lee Ventola, 2017). The tumor necrosis factor (TNF) receptor superfamily represents an attractive group of receptors for therapeutic targeting in cancer because of their immunostimulatory and cytotoxic activities. Several TNFRSF family members, including TNFR1, Fas/Apo1 and CD40 have been targeted in clinical studies.

1.1 TNFSF and TNF ligands

The communication between tumor necrosis factor (TNF) receptor superfamily (TNFRSF) receptors (TNFRs) and tumor necrosis factor (TNF) superfamily (TNFSF) ligands (TNFLs) is involved in a variety of biological processes, including cell apoptosis, cell differentiation, immune activation, regulation in inflammatory responses and induction of inflammatory mediators such as chemokines and cytokines. This renders TNFLs and TNFRs of interest for many clinical applications including targeted therapies against widespread human diseases such as atherosclerosis, osteoporosis, autoimmune disorders, allograft rejection, and cancer.

TNF receptor superfamily (TNFRSF)

The structures of TNFRs consist of three components: an extracellular domain, a transmembrane domain, and an intracellular domain. Almost all TNFRs are type 1 transmembrane proteins and the hallmark of TNFRs is the presence of

cysteine-rich domains (CRD) in their extracellular part of which the number varies from one in B-cell activating factor receptor (Baff) to six found in CD30 (Hehlgans & Pfeffer, 2005; Locksley et al., 2001). The CRDs fit in the “grooves” between protomers within the ligand trimer so as to bind the ligand. In general, TNFRs are divided into three subgroups based on their structural and functional features:

(1) TNFR associated factor (TRAF)-interacting or the so-called non-death receptors. This TRAF-interacting receptors contain one or more binding motifs for adapter proteins of the TRAF family in the cytoplasmic domain. This group includes fibroblast growth factor (FGF)-inducible 14 (Fn14), CD40 and several more. Linking of TRAF-interacting receptors to their intracellular signaling pathway activates the transcription factors of nuclear factor κB (NFκB) and mitogen-activated protein kinases (MAPK) cascades (Xie, 2013; Park, 2014).

(2) The death receptors. This group contains TNFRs such as TNFR1, CD95 (Fas) and TRAILR1 (DR4). The members of the death receptor group are characterized by an intracellular conserved protein–protein interaction domain, namely the death domain (DD) (Siegmund et al., 2017). The activation of death receptors triggers the apoptotic and/or necrotic cell death via DD-containing adapter proteins and caspase-8. However, not all death receptor mediated DD-mediated interactions result in cell death. Some DD-mediated interactions can stimulate non-cytotoxic signaling including TRAF-mediated engagement of NFκBs (Siegmund et al., 2017).

(3) The decoy receptors. This group of receptors lack an intracellular domain and consist of glycosylphosphatidylinositol (GPI)-anchored decoy receptors, soluble receptors, and a receptor with a non-functional DD.

1.1.1 TNF ligand superfamily

Most of TNF ligands (TNFLs) are type II proteins that can exist in both transmembrane form and soluble form. In the transmembrane form, TNFLs consist of an intracellular domain, a transmembrane domain (TM), a stalk region, and the C-terminal TNF homology domain (THD) which promotes the

assembly into homotrimeric molecules, or in rare cases the assembly of dimeric (murine GITRL) or heterotrimeric (LTαβ2) ligands (Wajant, 2015). By cleaving the stalk region via proteolytic processing or alternative splicing, the soluble TNFLs are obtained. As the soluble TNFLs still contain the THD, they can also assemble into trimers and are still able to present high affinity when interacting with TNFRs. The trimeric state of TNFLs is proven to be essential for the interaction with the corresponding TNFRs. However, not all the TNFRs react in a same way when interacting with the membrane bound and soluble TNFL forms. Based on the difference in their response to soluble ligand trimers, the TNFRs are divided into two groups, category I TNFRs such as TNFR1 and LTβR, and category II TNFRs such as Fn14 and CD40.

For the category I TNFRs, both soluble and membrane bound TNFL trimers are able to potently activate downstream signaling pathways; for the category II TNFRs, membrane bound TNFLs can activate receptor signaling, while the soluble TNFLs still retain the ability to interact with these TNFRs but do not activate downstream signaling (Wajant, 2015). For example, both TNFR1 and TNFR2 can efficiently bind soluble, or membrane bound TNF. However, TNFR1 can be fully activated by TNF of both forms, while TNFR2 is only fully activated by membrane bound TNF (Grell et al., 1995; Grell et al., 1998). Therefore, the TNFR-type intrinsic properties decide the responsiveness of TNFRs to TNFLs.

To fully support this statement, research have found that the potency of soluble TNFLs to category II TNFRs are fully recovered after they are modified into a membrane-associated form, or after they are physically linked between each other. For instance, soluble APRIL interacts with two of the category II TNFRs, transmembrane activator and cyclophilin ligand interactor (TACI) and B-cell maturation antigen (BCMA), but it partially or not at all activates the cell proliferation or B-cell activation effect respectively. However, after APRIL binds to proteoglycans through its N-terminally heparan sulfate proteoglycan binding motif, the receptor activation capability of APRIL is significantly augmented (Ingold et al., 2005; Joo et al., 2012). Likewise, single chain fragment variable (scFv) domains are used as anchor domains, since scFv domains are able to recognize cell surface-exposed tumor antigens or tumor stroma antigens (Wajant, 2015; Wajant, 2019). For example, antibodies against the TNFRSF

members CD40 and CD95 were genetically fused to a single-chain B-cell activating factor (scBaff) trimer as a C-terminal myeloma-specific anchoring domain (Nelke et al., 2020). The bispecific antibody fusion proteins obtained this way displayed strong agonistic effect when CD40- and CD95-responsive cells were co-cultured with BaffR, BCMA or TACI expressing anchoring cells, while only minor receptor stimulation was observed in cocultures with cells without expression of Baff-interacting receptors. It's noteworthy that the use of an anchor domain not only converts soluble TNFL or anti-TNFR antibody fusion proteins into potent TNFR agonists, but also give space to a second activity in a safe manner. Similarly, soluble TNFLs can be converted into potent category II TNFR agonists upon physical linkage of two or more ligand trimers (Kucka & Wajant, 2021).

The natural oligomerization of soluble TNFLs has been described previously. For instance, it has been shown that soluble CD95L present in the bronchoalveolar lavage fluid of patients suffering from acute lung injury can unexpectedly be highly apoptotic due to oxidation-triggered aggregation (Herrero et al., 2011). Moreover, the bronchoalveolar lavage fluid of acute lung injury patients was found to promote oligomerization of recombinant soluble CD95L in vitro, resulting in an enhanced ability to trigger CD95-mediated cell death (Herrero et al., 2011). Soluble Baff also occurs as a trimeric protein, as well as in the form of a 60-mer. However, the Baff 60-mer displays approximately 100-fold higher capacity than trimeric soluble Baff to trigger TACI signaling (Bossen et al., 2008). Likewise, oligomerization of soluble TNFL trimers can be achieved by genetically engineering recombinant TNFLs with an N-terminal tag, such as a Flag tag. This allows controlled oligomerization of soluble TNFL trimers by treatment with an anti-tag antibody. Furthermore, fusion with another multimerization domain often results in the formation of molecules with defined stoichiometry containing 6, 9, 12 or more TNFL protomers. For example, TNFL fusion proteins that harbor the dimerizing Fc domain of human IgG1 typically form hexameric molecules containing two parallel orientated trimeric "TNFL" subdomains (Bossen et al., 2008; Wyzgol et al., 2009; Medler et al., 2019).

In the past decades, various TNFLs have been engineered and generated as soluble Flag-tagged trimers or hexameric Fc-fusion proteins, and their agonistic activities to corresponding TNFRs have been investigated (table 1). In some studies, THD alone is sufficient to bind to TNFRs and activate TNFR, and in some cases, THD still binds to TNFRs but fails to activate them without oligomerization. This distinguished difference not only offer the essential experimental evidence needed to identify and define category I and category II TNFRs, but also clarifies that THD binding to TNFRs is not necessarily sufficient for activation of TNFRs (Kucka & Wajant, 2021). What is also worth mentioning is oligomerization of soluble TNFLs is proved to not increase their affinity for TNFRs (Fick et al., 2012; (Lang et al., 2012) . Based on the example of CD95L, where it has even been shown that the soluble ligand variant acts as an inhibitor of its transmembrane counterpart at least in the context of apoptosis induction, it is clear that the increased responsiveness of category II TNFRs to oligomerized soluble TNFL variants is not due to the increased receptor occupancy, but by the oligomerization (Suda et al., 1997; Kucka & Wajant, 2021).

Table 1. Activation of classical NFκB and cell death signaling by category I and category II TNFRs in response to soluble TNF ligands (sTNFLs). This table is modified according to (Kucka & Wajant, 2021).

TNFR	Category	TNFL	sTNF variant /activity (EC_{50} trimers: EC_{50} hexamer, etc.)	Reference	sTNF variant /activity (EC_{50} no anchoring: EC_{50} PM anchoring	Reference
TNFR1	I	TNF LTa	Flag-TNF / 1 Flag-TNC-LTa / 1		/	/
GITR	I	GITRL	Flag-TNC-GITRL / 5 HERA-GITRL / 10	(Wyzgol et al., 2009)(Richards et al., 2019)	Sc40-GITRL / 5	(Wyzgol et al., 2009)
BaffR	I	Baff	Flag-Baff / >100 Baff 64-mer / >100	(Bossen et al., 2008)	/	/
LTbR	I	$LTab_2$ LIGHT	Flag-sc$LTab_2$ /1 Flag-TNF-LIGHT / 1		/	/
41BB	II	41BBL	Flag-TNC-41BBL / >100	(Wyzgol et al., 2009)	Sc40-41BBL	(Wyzgol et al., 2009)
CD40	II	CD40L	Flag-CD40L / 20	(Holler et al., 2003)(Wyzgol et al., 2009)	Sc40-CD40L / >20	(Wyzgol et al., 2009)
			Flag-CD40L / >>100		ScFv: EpCAM-CD40L / 20	
CD27	II	CD27L	Flag-TNC-CD27L / >100	(Wyzgol et al., 2009)	/	/

Fn14	II	TWEAK	Flag-TWEAK / >1000	(Roos et al., 2010)	Sc40-TWEAK / >>100	(Roos et al., 2010)
TNFR2	II	TNF	Flag-TNF / 100 TNC-scTNF / >1000	(P. Schneider et al., 1998)(Prada et al., 2021)	/	/
TRAILR1	II	TRAIL	Flag-TNC-TRAILmutR1 /100	(Trebing, El-Mesery, et al., 2014)	scFv:CD70-TNC-TRAILmutR1 /100	(Trebing, El-Mesery, et al., 2014)
TRAILR2	II	TRAIL	Flag-TRAIL / >1000 Oligomeric TRAILs / >100	(P. Schneider et al., 1998) (Wajant, 2019)	AD-TRAILs / >100	(Wajant, 2019)

1.1.2 Fn14-Tweak pathway

Tumor necrosis factor like weak inducer of apoptosis (TWEAK) was identified in 1997 as a highly conserved and pro-apoptotic TNF-like protein in human HT-29 colon carcinoma cells (Chicheportiche et al., 1997; Locksley et al., 2001a). TWEAK exists in two forms: (1) as a 249 amino acids type II transmembrane protein and (2) as a 156 amino acids soluble, biologically active cytokine (sTWEAK) by furin-mediated proteolysis. As a member of the TNFSF, membrane-bound TWEAK consists of three parts (shown in the figure 1): (1) an extracellular TNF homology domain (THD) on the C-terminus, which mediates the formation of homotrimeric protein and binding of TWEAK with its receptor; (2) a transmembrane domain, which contains the cleavage site for serine proteases of the furin family allowing processing to soluble TWEAK; (3) a highly-reserved short intracellular N-terminal domain with a potential protein kinase C phosphorylation site, of which the function remains unclear (Wajant, 2013). Despite the fact that TWEAK expression being reported at the mRNA level in a variety of cells lines and cell types, cell surface expression of TWEAK is only identified in certain tumors and metastases tissue, including liver, colorectal, esophageal, bladder, pancreatic, ovarian, and prostate cancers as well as multiple sclerosis (Kawakita et al., 2004; Winkles et al., 2007; Wajant, 2013; Desplat-Jego et al., 2009; Tajrishi et al., 2014). TWEAK expression has also been reported in myeloid cells such as monocytes, dendritic cells as well as interferon-γ stimulated NK cells (Nakayama et al., 2000; Felli et al., 2005; Maecker et al., 2005). The

transcriptional regulation of TWEAK has been poorly investigated, though some studies indicated tissue damage and hypoxia might induce the expression of TWEAK, which in details proved the hypoxia-controlled interferon-γ and forkhead transcription factor FOXO3a has participated in up-regulation of TWEAK (Baxter et al., 2006; Wajant, 2013). Lipopolysaccharides (LPS) downregulate TWEAK mRNA in murine peritoneal macrophages, but the opposite was observed in human THP-1 monocytic cells (Chicheportiche et al., 2000; Winkles, 2008). It is assumed that TWEAK mRNA expression responses to the various cytokines depending on the cell type (Ratajczak et al., 2022). How the function of TWEAK protein is improved or maintained post-translationally also remains unclear. NFAT1-LCN2 was reported to stabilize TWEAK at the protein level (Gaudineau et al., 2012).

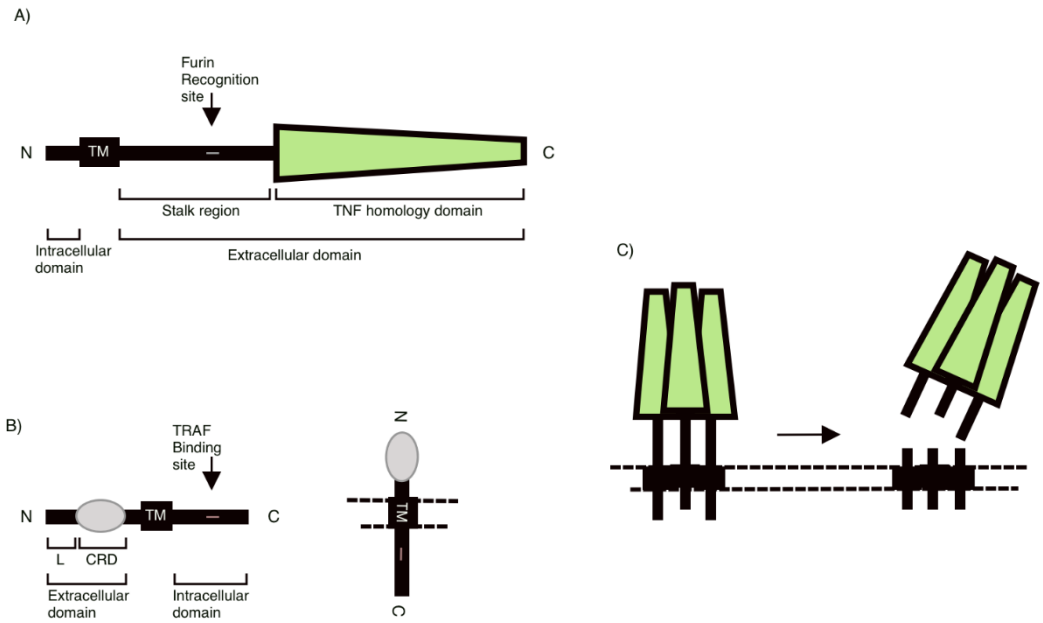

Figure 1: Domain architecture of TWEAK (A) and Fn14 (B). This figure is modified according to (Wajant, 2013).

Fibroblast growth factor-inducible 14 (Fn14) is a 129 amino acid type I transmembrane protein and is the smallest member of the TNFRSF with a molecular weight of 14 kDa (Figure 1) (Wiley et al., 2001). After identified as a transcriptional target of fibroblast growth factor-1 in NIH 3T3 fibroblasts, Fn14 has been categorized as a TNFRSF for transduction of TWEAK signals (Wiley et al., 2001). Besides Fn14, the type I transmembrane scavenger receptor CD163 has been proposed as a scavenger receptor for TWEAK (Bover et al., 2007). CD163 is expressed exclusively on the cells of the monocytic– macrophage linage and has been identified as the secondary, decoy receptor for TWEAK. However, the role of CD163 has not been well investigated and the downstream effect of TWEAK/CD163 interaction is also unclear

(Ratajczak et al., 2022). The extracellular ligand-binding region of Fn14 is made of 53 amino acid residues. Compared with extracellular regions of other TNF receptors containing two to six copies of CRDs in their ectodomain, Fn14 and B cell maturation, BaffR and the short isoform of transmembrane activator and calcium-modulator and cytophilin ligand interactor only contain a single CRD in their ectodomain (Locksley et al., 2001b). The cytoplasmic domain of Fn14 consists of 28 amino acid residues, and Fn14 is a typical TRAF-interacting TNFRSF receptor as there is a single TRAF binding motif in its cytoplasmic domain. Although Fn14 is widely expressed in a variety of non-lymphoid cells, including epithelial cells, endothelial cells, astrocytes, and neurons of the nervous system (L. Zheng et al., 2017), immunohistochemical investigation of human biopsy specimens and murine tissue samples showed a more differentiated expression pattern of Fn14 in vivo. In the healthy homeostatic tissue, only low expression of Fn14 is observed. On the contrary, high Fn14 expression was often observed on mesenchymal and epithelial progenitor cells and especially in context of tissue damage triggered by various insults such as mechanical or chemical injuries, oxidative stress, inflammation, hypoxia, and tumor growth (Winkles, 2008; Burkly et al., 2011). As a result, Fn14 expression has been reported in a variety of immune diseases, including rheumatic arthritis, glomerulonephritis, bowels disease, hepatitis and multiple sclerosis but also after stroke and heart attack as well as in atherosclerosis. What's more, the increased expression of Fn14 has been also detected in liver, colorectal, esophageal, bladder, pancreatic, ovarian and prostate cancers, as well as neuroblastoma, brain glioma, breast cancer, lung cancer, and melanoma (Chao et al., 2013; Gu et al., 2013; Huang et al., 2011; Li et al., 2014; Shimada et al., 2012; Tran et al., 2006; Watts et al., 2007; Yin et al., 2014; Yoriki et al., 2011; Zhou et al., 2014). Numerous growth factors associated with tissue repair processes such as VEGF and EGF, as well as cytokines, such as TNF, TGF-β, and IFN-γ have been reported to induce Fn14 expression (Donohue et al., 2003; Hosokawa et al., 2006; Kaur et al., 2009; Sanz et al., 2012; Whitsett et al., 2012).

1.1.3 Fn14/TWEAK-induced cell death

TWEAK was firstly named after its ability to induce cell death in INF-γ sensitized HT29 cells (Chicheportiche et al., 1997), and a few other cell lines such as OVCAR-4, Kym-1 and SKOV-3. However, it is still a rare exception of the TWEAK/Fn14 system to mediate cell death (Wajant, 2013). Other ligands of the TNFSF death receptors strongly stimulate cell death responses by activating corresponding death receptors, such as Fas, TNF-related apoptosis-inducing ligand (TRAIL) receptors-1 and 2, or TNFR1. Activation through these death receptors result in the activation of caspase-8 via their death domain and then triggering the

propagation of the apoptotic signal (Dickens et al., 2012). Under well-defined circumstances, death receptors also interact with the death domain-containing serine/threonine kinase RIP1 to activate an alternative necrotic form of programmed cell death (Dickens et al., 2012; Wajant, 2013).

Fn14 was reported to induce cell death by indirect mechanisms as it lacks a death domain. The mechanisms are induction of TNF and subsequent stimulation of the prototypic death receptor TNFR1 and depletion of TRAF2-cIAP1/2 (cellular inhibitor of apoptosis) complexes (Vince et al., 2008; Wicovsky et al., 2009; Dickens et al., 2012). When TNFR1 stimulation was blocked, studies showed that TWEAK fails to induce apoptosis. Moreover, TNF-induced cell death is strongly boosted after by Fn14 stimulation while TRAIL-induced cell death is not or only poorly boosted by the TWEAK/Fn14 system (Wicovsky et al., 2009). It was furthermore reported that Fn14 recruit TRAF2-cIAP1/2 complexes to enhance the TNFR1-induced apoptosis. TRAF2 is a classic member of the TRAF adapter protein family and has a RING domain with E3 ligase activity (Gonzalvez et al., 2012). cIAP1 and cIAP2 are also RING domain E3 ligases which have besides the RING domain a caspase recruitment domain and three baculovirus inhibitor of apoptosis (IAP) repeat domains involved in substrate recognition. As in most cells the expression of TRAF2-cIAP1/2 complexes are much lower than the expression of Fn14, recruitment of TRAF2-cIAP1/2 complexes to Fn14 via TWEAK activation results in exhaustion of the cytosolic pool of TRAF2-cIAP1/2 and thus limits their availability for TNFR1 (Vince et al., 2008; Wicovsky et al., 2009; Wajant, 2013). Other TRAF2 interacting receptors such as TNFR2, CD30 and CD40 can replace Fn14 in boosting TNFR1-induced cell death by depleting TRAF2 (Duckett & Thompson, 1997; Siemienski et al., 1997; Grell et al., 1999; Siegmund et al., 2018). Moreover, SMAC mimetics, a group of drugs targeting cancer also enhance TNFR1 signaling via triggering proteasomal degradation of cIAP1 and cIAP2 and also prevent the anti-apoptotic xIAP protein (Fulda & Vucic, 2012; Lalaoui et al., 2020). Although some publications showed TNF-independent cell death in normal human keratinocytes and cortical neurons via TWEAK/Fn14 induction, the underlying signaling mechanisms remain unclear (Haile et al., 2010; Sabour Alaoui et al., 2012).

1.1.4 Fn14-induced NFκB signaling

The TWEAK-Fn14 system through depletion of the cytoplasmic TRAF2, cIAP1, and cIAP2 complexes not only heightens TNFR1-induced caspase-8 activation, but also regulates NFkB signaling pathways (Wajant, 2013). Cytoplasmic TRAF2, cIAP1, and cIAP2 complexes play a crucial role in the stimulation of numerous transcription factors of the NFκB family via the TWEAK/Fn14 system. NFκBs are formed by five members of the Rel transcription factor family

(p50, p52, RelA, RelB, and c-Rel) in the form of homo- and heterodimers (Hoffmann et al., 2003; Hayden & Ghosh, 2012; Tsui et al., 2015). NFκBs can become activated in different ways and target different genes. The two prototypic signaling pathways that lead to the activation of distinct NFκB dimers are the classical and the alternative NFκB pathway (Figure 2) (Hayden & Ghosh, 2012; Mitchell et al., 2016). The TWEAK/FN14 system is able to stimulate both the classical and the alternative NFκB pathways. The key step in the alternative NFκB pathway is phosphorylation of the p100 precursor of p52 by the inhibitor of kappaB kinase (IKK)1. This leads to K48-ubiquitination and proteasomal processing of p100 to p52 and nuclear translocation of p52-containing NFκB dimers (Wajant, 2013). the activation of IKK1 needs phosphorylation by NIK, a cytosolic MAP3-kinase that is constitutively degraded in unstimulated cells by a TRAF2-cIAP1/2 complex-dependent mechanism. TRAF2 recruits NIK by interaction with the TRAF3, and as a result bind to NIK and subjected it so to K48-ubiquitination through the TRAF2-associated IAPs and subsequent proteasomal degradation (Mitchell et al., 2016). Therefore, when participating in the alternative NFκB pathway, cytosolic TRAF2-cIAP1/2 complexes play an inhibitory role that is blocked by their TWEAK-induced recruitment to membrane-bound Fn14. Stimulation of the classical NFκB pathway by TWEAK and several other ligands of the TNF family need stimulatory activities of TRAF2 and the cIAPs (Mitchell et al., 2016). In unstimulated cells, the activated NFκB dimers of the classical NFκB pathway are retained in the cytoplasm by forming a ternary complex with inhibitory proteins, the IκBs. The activation of the IKK complex which includes the scaffolding protein NEMO, IKK1 and IKK2 is the key step in the classical NFκB pathway, (Wajant, 2013). The IKK complex phosphorylates IκB proteins resulting in their proteasomal degradation and subsequent nuclear translocation of the released NFκB dimers. The TRAF2-cIAP1/2 complex plays a dual role in stimulation of the classical NFκB pathway. Whereas TRAF2 functions as an adapter protein being in charge of the recruitment of the IKK complex to receptors of the TNFRSF, the cIAPs K63-ubiquitinate the IKK subunit NEMO as well RIP in the framework of TNFR1 signaling, generating docking sites for various ubiquitin-binding proteins. The latter is crucial in IKK activation, such as TAB2-TAB3-TAK1 complex by IKK2 phosphorylation or the linear ubiquitin chain assembly complex (LUBAC), which creates extra docking sites for ubiquitin-binding proteins, but also recruits two deubiquitinating enzymes, A20 and Cyld (Bacher & Schmitz, 2005; Donohue et al., 2003; Nishikori, n.d.; Niu et al., 2012). The importance of TAK1, IKK2, cIAPs, and the TRAF2 for Fn14-mediated activation of the classical NFκB pathway was proved in siRNA experiments, dominant-negative ubiquitin-binding domains, IAP antagonists as well as knockout mice derived fibroblasts (Kumar et al., 2009; Saitoh et al., 2003; Sims et al., 2012; Varfolomeev et al., 2012).

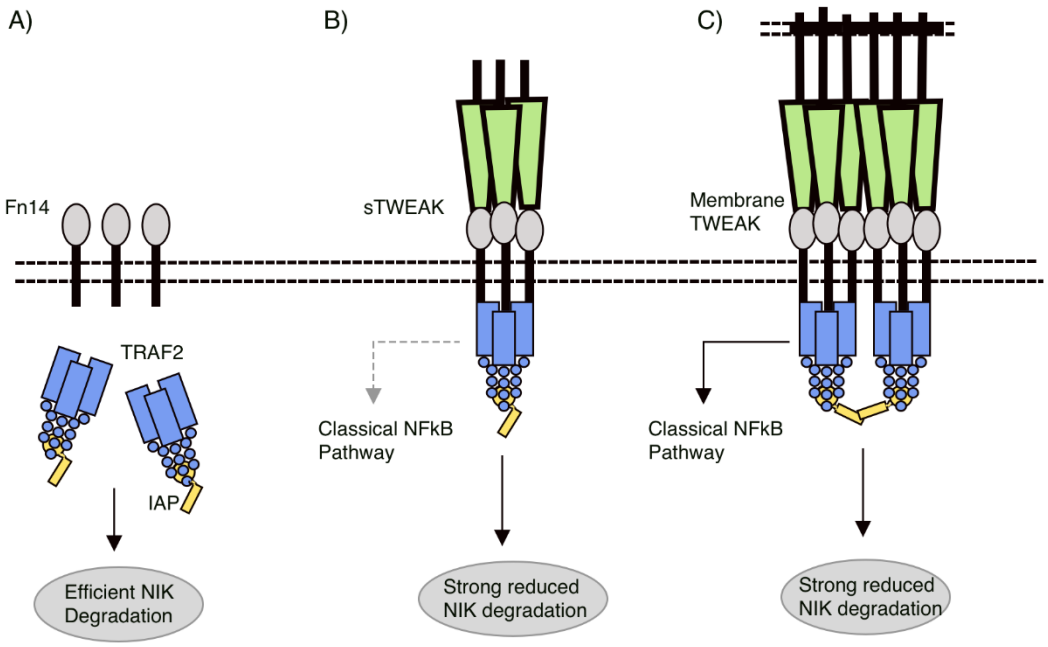

Figure 2: Activation of the classical and alternative NFκB pathway by soluble TWEAK and membrane TWEAK. A) In unstimulated cells, TRAF2-cIAP1/2 is distributed in the cytoplasm and efficiently activate degradation of NIK. B) Soluble TWEAK trimers trigger the alternative NFκB pathway. Binding of soluble TWEAK trimers to Fn14 leads to recruitment and depletion of cytosolic TRAF2-cIAP1/2 but not in the transactivation of the single inhibitor of apoptosis (IAP) molecules linked with a TRAF2 trimer. C) Membrane TWEAK triggers both classical and alternative NFκB pathway. Binding of membrane TWEAK to Fn14 not only leads to recruitment and depletion of cytosolic TRAF2-cIAP1/2 but also in the transactivation of TRAF2-associated IAP molecules.

What is worth to notice is that membrane-bound TWEAK can sufficiently activate both classical and alternative pathways efficiently, whereas soluble TWEAK only activates weak and delayed activation of the classical NFκB pathway but leads to intense stimulation of the alternative NFκB pathway (Wajant, 2013). Artificially immobilizing soluble TWEAK on a cell surface converts soluble TWEAK from a weak to a potent stimulator of classical NFκB signaling while not affecting the alternative NFκB pathway (Roos et al., 2010b; Wajant, 2013). Likewise, intense stimulation of the classical NFκB pathway can also be attained with dimerized or oligomerized trimers of soluble TWEAK. As a conclusion, the boosted efficacy to activate classical NFκB signaling by converting TWEAK from weak to potent stimulator indicates its correlation of the spatially restricted way of how membrane TWEAK is presented to Fn14 whereas the sequence information which is only available in membrane TWEAK is not required (Wajant, 2015). However, this has no significant effect on Fn14 occupation by

TWEAK or on the dose dependency of TWEAK-induced activation of the alternative NFκB pathway (Fick et al., 2012). Therefore, it seems that secondary interaction of two or more initially formed TWEAK-Fn14-TRAF2-cIAP1/2 complexes is required for classical NFκB signaling, whereas the single recruitment of the TRAF2-cIAP1/2 complex is sufficient for prompting of alternative NFκB signaling (Saitoh et al., 2003; Varfolomeev et al., 2012; Wajant, 2015).

1.1.5 Role of the TWEAK/Fn14 system in cancer

Numerous studies have indicated that the expression of TWEAK and Fn14 is highly upregulated in many solid tumors compared with healthy tissues as chronic inflammation and repetitive tissue damage happened in tumorigenesis contributes to the upregulation of TWEAK/Fn14 (Bossen et al., 2006; Brown et al., 2010; Chicheportiche et al., 1997; Dwyer et al., 2021). The upregulation of TWEAK at the mRNA level has been confirmed in numerous tumor cell lines and solid tumor entities by immunohistochemistry, and expression of membrane TWEAK on cell surface has also been stated for various cancers including liver, colorectal, esophageal, bladder, pancreatic, ovarian, and prostate cancers as well as neuroblastoma (Gu et al., 2013; Ho et al., 2004; Kawakita et al., 2004; Lin et al., 2012; Pettersen et al., 2013; Shimada et al., 2012; Yin et al., 2014; Yoriki et al., 2011).

The vast majority of cellular effects prompted by the TWEAK/Fn14 system are apparently of potential advantage for tumor development (Hu et al., 2017; Wajant, 2013). The proliferation of endothelial cells is an important step in the formation of blood vessels, which is required for tumor growth. The proliferation of normal endothelial cells, keratinocytes infected by human papillomavirus (HPV), and hepatocellular carcinoma cells has been reported to be promoted by TWEAK (C. S. Schneider et al., 2015; Kawakita et al., 2004). Moreover, the TWEAK/Fn14 pathway is proved to be important for the invasion and migration of tumors (Hu et al., 2017). For instance, TWEAK/Fn14 signaling stimulates the invasion and migration glioblastoma cells through TRAF2 (Cherry et al., 2015). TWEAK has also been found to play a crucial role in stimulating the morphogenic phenotype of Eph4 mammary epithelial cells, and this morphogenesis can be inhibited by blocking Fn14 expression (Michaelson et al., 2005). In this context, some agents that target TWEAK or Fn14 have been generated to inhibit the progression of tumors, and these agents have achieved initial success in clinical and pre-clinical trials.

However, TWEAK also induces apoptosis of some tumor cell lines, such as interferon-γ treated PC-3 prostate cancer cells, Kym-1 cells, HSC3 (oral squamous cell carcinoma) cells

and HT-29 (colon adenocarcinoma) (Nakayama et al., 2002, 2003; Sanz et al., 2012). These results indicate that TWEAK has cytotoxic activity on some human tumor cells, but this function needs co-culturing with sensitizing agents in most cases, suggesting that TWEAK-induced cell death is cytokine-dependent. In colorectal cancer, high TWEAK expression is associated with improved overall and disease-free survival, and this suggests an inhibitory effect of TWEAK on the invasiveness of colon cancer cell lines in vitro (Lin et al., 2012).

1.1.6 Role of TWEAK/Fn14 in cancer prognosis, prediction, and treatment

Since TWEAK/Fn14 signaling correlates closely with multiple biological activities of tumors, TWEAK and Fn14 are considered as potential therapeutic target for caner prognosis, prediction, and treatment. It has been reported to use high Fn14 expression as an independent prognostic factor in non-small cell lung cancer, gastric cancer, and hepatocellular carcinoma (Kwon et al., 2012; N. Li et al., 2013; Sun et al., 2016). Moreover, low TWEAK/CD136 expression ratio in tumors is associated with poor prognosis, and the low blood level of sTWEAK is related to locoregional failure in patients with squamous cell carcinoma in head and neck (Avilés-Jurado et al., 2015). Regarding cancer treatment, various Fn14- and TWEAK-targeting agents have been developed in recent years, and some are listed in Table 2 below.

Table 2: TWEAK- or Fn14-targeting therapeutic agents to treat cancers.

Name	Type	Target	Results	Reference
RG7212	Neutraliing mAb	TWEAK	Tumor inhibition	(Lassen et al., 2015)
Fn14-TRAIL (KAHR-101)	Fusion protein	TWEAK	Tumor inhibition	(Aronin et al., 2013)
18D1	Agonistic mAb	Fn14	Reduced metastasis	(Chopra et al., 2015); (Trebing, Lang, et al., 2014)

PDL192 (enavatuzumab)	Agonistic mAb	Fn14	Tumor inhibition	(De Plater et al., 2014); (Salzmann et al., 2013)
BIIB036	Agonistic mAb	Fn14	Tumor inhibition	(Michaelson et al., 2011, 2012)
Anti-Fn14 antibody conjugated nanoparticles	Antibody-conjugated nanoparticle	Fn14	Tumor inhibition	(Aido et al., 2021b); (C. S. Schneider et al., 2015)

For instance, RG7212 is a neutralizing monoclonal antibody (mAb) targeting TWEAK. RG7212 showed significant efficacy on suppressing the growth of solid tumors by blocking TWEAK/Fn14 signaling, NF-κB activation, and cytokine secretion in cultured tumor cells (Lassen et al., 2015). In some circumstances, the crosstalk between TNF and TWEAK leads to induction of apoptosis, and consequently it can be used for cancer treatment by promoting tumor cell death using agonistic Fn14-antibodies or recombinant TWEAK (Wajant, 2013). Based on that, some monoclonal antibodies targeting Fn14 are also developed, such as PDL192, 18D1 and BIIB036 (Cherry et al., 2015; Chopra et al., 2015; De Plater et al., 2014; Kawakita et al., 2004b; Michaelson et al., 2011, 2012; Salzmann et al., 2013; Trebing, Lang, et al., 2014). These three agents all suppress tumor growth in vivo through various mechanisms, including inhibition of TWEAK-Fn14 engagement, induction of antibody-dependent cellular cytotoxicity (ADCC), and blockage of Fn14. PDL192 and BIIB036 exhibited impressive anti-tumor efficacy in vivo by activation of NF-κB pathway, stimulates the production of IL-8, and induces death of human cancer cells (E. Cheng, Armstrong, Galisteo, & Winkles, 2013; De Plater et al., 2014; Michaelson et al., 2012; Salzmann et al., 2013). The 18D1 antibody exhibits potent inhibition efficacy on metastatic colony formation of RENCA (murine renal cell carcinoma) cells predominantly via ADCC (Trebing, Lang, et al., 2014).

However, some studies found potent side effects of PDL192, 18D1 and BIIB036 antibodies. PDL192 showed significant liver and pancreatic toxicity in a Phase I clinical trial (Cheng et al., 2013). Therefore, developing other formulations with higher safety and effectiveness is necessary for mAbs targeting Fn14/TWEAK.

1.2 Nanoparticles based immunotherapy

Despite the aforementioned advantages of the existing immunotherapy compared with the traditional therapies, its application is still limited by challenges such as induction of destructive auto-immunity, lack of effective delivery of cancer antigens to immune cells, off-target effect, self-attenuation of TME, and poor penetration of immunotherapeutic agents through tumoral abnormal ECM (extracellular matrix) (Buabeid et al., 2020a; Munn & Bronte, 2016; Phan et al., 2003). Current existing cancer treatment of immunotherapy relies on three significant factors: (i) the effective transfer of cancer antigens to immune cells, especially APCs (antigen-presenting cells), for example dendritic cells; (ii) the induction of antitumor immune response after cancer antigen delivery; (iii) the modulation of the TME to induce a response to the antitumor immunotherapeutic agents (Buabeid et al., 2020b). Nanotechnology provides the opportunity to improve cancer immunotherapy by overcoming the shortcomings of current immunotherapy, and thus makes it more effective. Nanoparticles (NPs) are one of the representative of nanotechnology, and they have several unique properties that make them ideal for use in various biomedical applications, including adjustable particle size and shape, flexibility for function modification, enhanced in-vivo and electronic properties (Buabeid et al., 2020b). A major goal of using NPs in cancer immunotherapy is to improve the therapeutic index by delivering immunotherapeutic agents directly to the site of interest, enhancing the site-accumulation and potency at the region, while simultaneously minimizing the dose-dependent systemic toxicity (Buabeid et al., 2020b). The combination of immunotherapy with nanoparticulate system, which made by stimuli-sensitive materials, can initiate immune cells or organs (such leukocytes or lymphoid organs) response with a low concentration of immune-stimulating drugs. This is different from the traditional strategy of delivering chemotherapeutic agents to cancer cells, which demands a high drug concentration to kill all the target cells to be effective (Din et al., 2017; Riley et al., 2019). Moreover, the combination of nanoparticulate systems with immunotherapy can be multifunctional, such as co-delivery of multiple therapeutic agents or therapeutic agent with imaging agents by integrating them into the core and on the surface of multifunctional nanoparticles (Sau et al., 2018). In one study, immunogenic melanoma antigen, tyrosinase-related protein 2 (TRP2), along with Toll-like receptor (TLR) ligand (7-acyl lipid A) were encapsulated into poly(lactic-co-glycolic acid) (PLGA) nanoparticles as a vaccine, and it was injected into mice bearing melanoma B16 tumors (Hamdy et al., 2008). This vaccine was able to have a therapeutic anti-tumor effect by activating TRP2-specific CD8 T cells to secrete interferon (IFN)-γ at lymph nodes and spleens of the mice. Moreover, the TRP2/7-acyl lipid nanoparticles treated group showed an increased level of pro-inflammatory cytokines compared to control group. A recent study found that nanoliposomes can deliver tumor-specific antigens and immunostimulatory therapeutic

supplements simultaneously, with a multifaceted immunomodulatory effect (Noh et al., 2017). The study found that this approach (using nanoliposomes 100 nm in size, which the study termed “tumosomes”) can lead to enhanced anticancer immunity, reduction in tumor growth, and improved survival of mouse tumor models. The tumosomes used in the study contained two immunostimulatory therapeutic supplements, i.e., MPLA (3-O-desacyl-4′-monophosphoryl lipid A) and DDA (dimethyl-dioctadecylammonium) as a danger signal and a cell-invasion domain, respectively.

This approach has the potential to overcome the issue of autoimmunity that can occur when using self-antigens, and the therapeutic efficacy of this modality can be further improved by using it with other therapeutic approaches including chemotherapy.

1.2.1 The composition and type of nanoparticles

Various nanoparticle systems have been studied for cancer immunotherapy in recent years (figure 3). Among a wide array of nanoparticles that are currently being studied for cancer immunotherapy, polymer-based nanoparticles are the most popular. This is due in part to the fact that the Food and Drug Administration (FDA) has approved a variety of polymers for the synthesis of these nanoparticles. Some examples of these polymers include polyethylene glycol (PEG), PLGA, and chitosan. Another reason why polymer-based nanoparticles are so popular is because they are biodegradable, biocompatible, and nontoxic. Other commonly used nanoparticulate systems include the inorganic (such as gold nanoparticles) and the lipid-based nanoparticles (such as liposomes). All these nanoparticles show promise for targeting cancer and delivering antigens and supplements to the target site with good accuracy and precision for the activation of the immune system.

Most of nanoparticulate systems with immunomodulatory effect fit in two categories: immunosuppressive or immunostimulatory, both of have been used for the treatment of various types of diseases (Jiao et al., 2014). Immunosuppressive nanoparticles are used for the treatment of autoimmune and inflammatory diseases, whereas immunostimulatory nanoparticles are used for the treatment of some other infectious diseases and cancer (Feng et al., 2019). The applications of immunostimulatory nanoparticles for the treatment cancers and their compositions are shown in table 3.

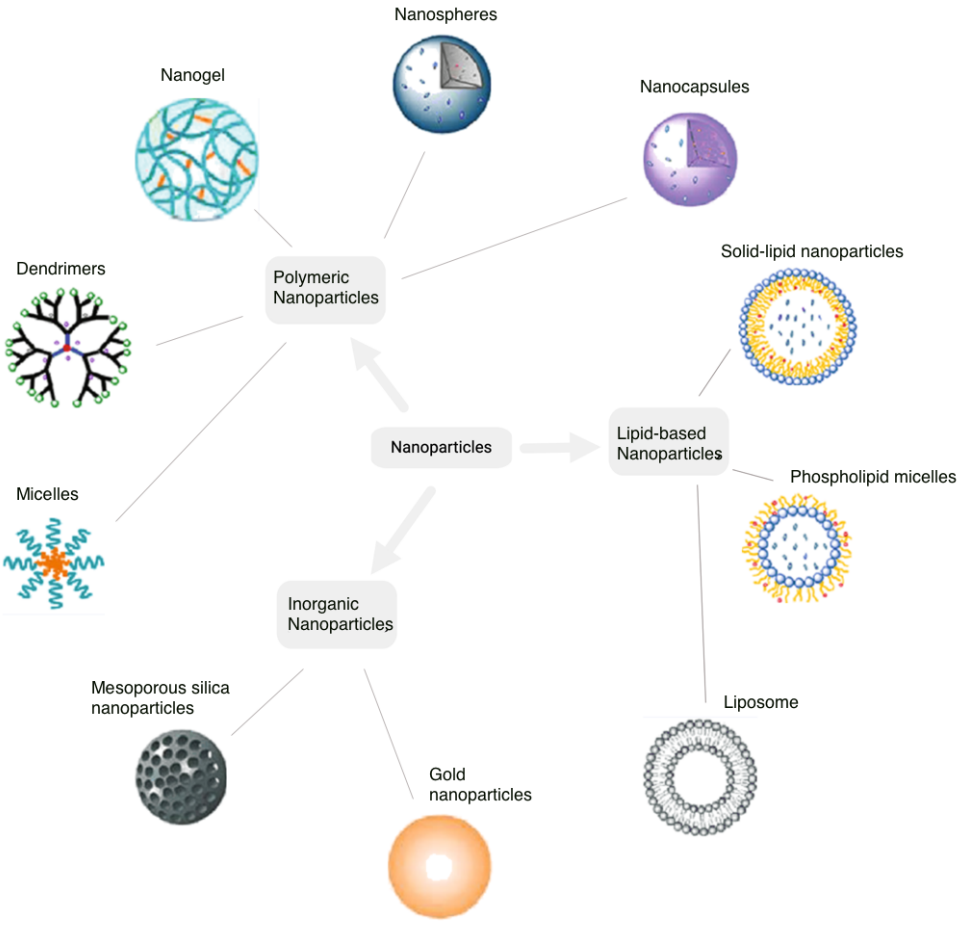

Figure 3: The representative examples of currently studied nanoparticles (polymeric, lipidic, and inorganic) for cancer immunotherapy.

Table 3: Nanoparticle-based immunomodulatory systems for cancer immuno-therapy

Immunomodulatory effect	Nanoparticle composition	Load	Target	Reference
Antigen presenting cells activation	PLGA nanoparticle	TLR7/8 agonist		(Kim et al., 2018a)
	PLGA nanoparticle	OVA, Pam3Csk4, and Poly(I:C)	CD40 on dendritic cells	(Rosalia et al., 2015)
	Chitosan nanoparticle	Cell lysate from B16 melanoma	Mannose receptor on dendritic cells	(Rosalia et al., 2015)

	Lipo-CpG micelle	CpG	Albumin hitchhiking	(Liu et al., 2014)
	mBiNE	CRT	HER-2 on tumor cells	(Yuan et al., 2017)
T cell activation	Magnetic nanocluster	MHC1-OVA, anti-CD28, leukocyte	Magnetic navigation	(Q. Zhang et al., 2017)
	polyPAA	OVA	-	(Qiu et al., 2018)
	CNT	MHC1-OVA, anti-CD28, and PLGA NPs encapsulating IL-2 and magnetite	-	(Fadel et al., 2014)
	PEG-PLA nanoparticles	CTLA-4 siRNA	-	(S. Y. Li et al., 2016)
	PEG-PLGA nanoparticles	Anti-PDL1 antibodies	-	(Mi et al., 2018)
	Super-paramagnetic iron oxide nanoparticles	Anti-PDL1 antibodies, anti-CD3/anti-CD28 antibodies, fucoidan, and dextran	Magnetic navigation	(Chiang et al., 2018)
Regulation of TME	Lipid coated PLGA nanoparticle	Imatinib	Nrp 1 receptor on Tregs	(Ou et al., 2018)
	CD-lysine nanoparticles	R848	-	(Rodell et al., 2018)
	HDL nanoparticles	-	Scavenger receptor B1 on MDSCs	(Plebanek et al., 2018)
	PEGylated LNC	ImGem	-	(Sasso et al., 2016)
	LPH nanoparticles	HMGA 1 siRNA	Sigma receptor on tumor cells	(Y. Wang et al., 2018)

	LCP nanoparticles	TGF-β siRNA, tumor antigen, and CpG	-	(Xu et al., 2014)
	PEG-PLGA nanoparticles	SD-208	PD-1 on T cells	(Schmid et al., 2017)
	Nanoparticle assembled from DEAP molecule, PD-L1 antagonist, NGL919, and a substrate peptide of MMP-2		-	(K. Cheng et al., 2018)
Combination with other therapy	NDP based on cationic liposome and HA	CpG and mitoxantrone-induced DTC	-	(Fan et al., 2017)
	Netrophil-based cationic liposome	Paclitaxel	-	(Xue et al., 2017)
	PLGA nanoparticles	Indocyanine green and imiquimod	-	(Chen et al., 2016)
	Hollow silica nanoparticles	Catalase and Ce6	Mitochondria	(Yang et al., 2018)
	PEG–PLGA nanoparticles	Indocyanine green, titanium dioxide, and NH_4HCO_3	Mannose receptor on TAM	(Shi et al., 2018)
	PLGA nanoparticles	Catalase and imiquimod	-	(Chen et al., 2019)

1.2.1.1 Gold nanoparticles (AuNPs)

Among all the immunostimulatory nanoparticulate systems, gold nanoparticles (AuNPs) are a good system contributed by their low cytotoxicity, tunable surface chemistry, and easily controllable shape and size (Q. Zhou et al., 2016). AuNPs are a significant type of immunostimulatory nanoparticles that have been shown to activate macrophages and their subsequent differentiation into dendritic-like cells, leading to T cell proliferation and subsequent cytokine release (Fallarini et al., 2013). AuNPs have also been found to be useful as an adjuvant for antibody production in mice, and their immunogenic property is further increased when used in combination with other immunostimulants (Dykman et al., 2018; Saha et al., 2016). Moreover, AuNPs alone can inhibit tumor growth by modulating the tumor

microenvironment (Saha et al., 2016). In a study, PEG-functionalized AuNPs were used as a platform for conjugating anti-Fn14 antibodies (Aido et al., 2021a). Conjugation of antibodies to AuNPs proved to immobilize the antibodies while maintained their binding capacity to the corresponding receptors. Furthermore, the conjugation and immobilization of antibodies assisted the antibody crosslinking, and consequently converted them into potent agonist. This study indicates that AuNPs can be used to immobilize anti-TNFR antibodies and help to enhance their agonistic activity via mimicking the effect of cell-anchored antibodies or membrane-bound TNF ligands. Additionally, this provides the opportunity to develop new generations of drug delivery systems according to their biocompatibility and their tunable synthesis process.

Yet, there are certain limitations associated with this approach. The delivery of large biomolecules via AuNP to cells not only requires targeting to a site but also cellular internalization and sometimes intracellular release of the cargo (Amina & Guo, 2020). When antibodies are conjugated to the surface of AuNPs, they are potent agonists and can exert strong immunostimulatory effects, which might cause significant side effects. Therefore, further in vivo investigation or modifications of AuNPs-conjugated antibodies are needed for transferring this system into clinical applications.

1.2.1.2 Polymeric Nanoparticles

Polymeric nanoparticles are a type of immunostimulatory NP that are widely used due to their excellent biodegradability, biocompatibility, water solubility, chemical stability, and high capacity to encapsulate immunostimulants (S. Li et al., 2018). The most common polymeric nanoparticles in cancer immunotherapy are poly ethylenimine (PEI), poly (D,L-lactide-co-glycolide) (PLG), poly (g-glutamic acid) (PGA), PEG, PLGA, and chitosan NPs (Zhao et al., 2014). Nanoparticles based on these polymers have been utilized as an effective immunostimulatory adjuvant in immunotherapies. For example, a study has shown that encapsulating a toll-like receptor 7/8 (TLR 7/8) agonist within PLGA nanoparticles can significantly increase the expression of costimulatory molecules (CD40, CD80, and CD86) via activation of bone marrow-derived dendritic cells (BMDCs), as compared to administering the agonist alone (Kim et al., 2018b). Furthermore, subcutaneous administration of the TLR7/8-encapsulated PLGA nanoparticles results in their migration to the draining lymph nodes, where they subsequently activate CD8+ T cells and DCs, leading to increased antitumoral response in renal carcinoma, melanoma, and bladder models. These findings suggest that PLGA nanoparticles could be used as potent immunostimulatory adjuvants for cancer immunotherapy.

Recently, Chen et.al (Qian et al., 2020) assembled a drug-peptide conjugate with a modified polylysine (MPL) shell. The MPL shell exhibited pH-dependent dissolution performance, namely the shell remained stable in neutral or basic buffer environment (pH greater or equal to 7.0), but the shell broke into pieces when exposing to acid buffer environment (pH less than 7.0). The principle lies in the charge switch of MPL that the MPL carries a negative charge in normal body tissue, while the charge of MPL switched to positive when exposing to acidic tumor microenvironment (TME), and as a result releasing the positive drug-peptide conjugate. After injecting the MPL-shelled drug-peptide conjugate into mice, no positive reaction detected in sections from the liver, heart, kidney or spleen, whereas the tumor site showed significant accumulation of MPL-shelled drug-peptide conjugate, which indicates the successful delivery of therapeutic agents and high biocompatibility of MPL-shelled drug-peptide conjugate (Qian et al., 2020). Meanwhile, in vivo antitumor and inhibition of metastasis efficacy were observed when mice were treated with MPL-shelled drug-peptide conjugate, compared with no effect observed when treated with control. This suggests that MPL shows great potential as a biocompatible polymeric delivery system for big biomolecules.

2 Materials and Methods

2.1. Chemicals, reagents and cell culture mediums

Table 4: Chemicals, reagents and cell culture media

Substance	Company
1-ethyl-3-(3-dimethylaminopropyl) carbodiimide hydrochloride (EDC)	Thermo Scientific, Erlangen, Germany
2-(N-morpholino) ethane sulfonic acid (MES)	VWR chemicals, Darmstadt, Germany
2,3-dimethyl maleic anhydride (DMMA)	Thermo Scientific, Erlangen, Germany
Acetic acid	J. T. Baker, Leibzig, Germany
Acrylamide (30 %)	Carl Roth, Karlsruhe, Germany
Agarose	Carl Roth, Karlsruhe, Germany
Ammonium persulfate (APS)	AppliChem, Darmstadt, Germany
Anti-Flag M2 agarose beads	Sigma, Deisenhofen, Germany
Bovine serum albumin (BSA)	Sigma, Deisenhofen, Germany
Dimethyl sulfoxide (DMSO)	Carl Roth, Karlsruhe, Germany
Disodium phosphate	AppliChem, Darmstadt (Germany)
Ethanol 96 %, denatured	J. T. Baker, Leibzig, Germany
Ethidium bromide	Carl Roth, Karlsruhe, Germany
Ethylenediaminetetraacetic acid (EDTA)	Carl Roth, Karlsruhe, Germany
Fetal bovine serum (FBS)	PAA, Pasching, Austria
Flag peptide	Sigma, Deisenhofen, Germany
Glycerol (86 %)	Carl Roth, Karlsruhe, Germany
Gold (III) chloride acid trihydrate	VWR International, Czech Republic
Hydrochloric Acid (1M)	VWR, Darmstadt, Germany
Isopropyl alcohol (2-propanol)	Sigma-Aldrich, Schnelldorf, Germany
Methanol	PAA, Pasching, Austria
N-hydroxysuccinimide(1-hydroxy-2,5 pyrrolidine Dione) sodium salt (NHS)	Sigma-Aldrich, Schnelldorf, Germany
Nonfat dried milk powder	J. T. Baker, Leibzig, Germany
Paraformaldehyde	Sigma, Deisenhofen, Germany
mPEG-Thiol (5 kDa)	Biochempeg, Watertown, MA, USA
Penicillin-Streptomycin (100 x)	Carl Roth, Karlsruhe, Germany
Peptone	PAA, Pasching, Austria
Phosphate buffered saline (PBS)	Sigma-Aldrich, Darmstadt, Germany

Poly-L-Lysine hydrochloride (3kDa)	Nanosoft Polymer, USA
Polymyxin B (PMB)	PAA, Pasching, Austria
Pre-stained protein marker (broad range)	InvivoGen, Toulouse, France
Protein G agarose	Roche, Mannheim, Germany
Blue Protein standards	New England Biolabs, Frankfurt, Germany
RPMI 1640 Medium	Roche, Mannheim, Germany
Silver staining marker (low molecular weight)	GE Healthcare Life Sciences, Garching, Austria
Sodium acetate	Carl Roth, Karlsruhe, Germany
Sodium carbonate	Carl Roth, Karlsruhe, Germany
Sodium chloride	Sigma-Aldrich, Schnelldorf, Germany
Sodium dodecyl sulfate (SDS)	GE Healthcare, Garching, Dassel, Germany
Sodium Hydroxide	Carl Roth, Karlsruhe, Germany
Sodium phosphate	Carl Roth, Karlsruhe, Germany
Sucrose	Carl Roth, Karlsruhe Garching, Germany
Tetramethylethylenediamine (TEMED)	Sigma, Deisenhofen, Germany
Thiol-PEG-Acetic Acid (5 kDa)	Biochempeg, Watertown, MA, USA
Triethylamine ≥99%, TECHNICAL	VWR International, Czech Republic
Tris	Sigma, Deisenhofen, Germany
Trisodium citrate	Thermo Scientific, Erlangen, Germany
Triton X-100	Carl Roth, Karlsruhe, Germany
Trypsin-EDTA solution (10X)	Sigma, Deisenhofen, Germany
Tween-20	PAA, Pasching, Austria
Yeast extract	Carl Roth, Karlsruhe, Germany
β-Mercaptoethanol	Carl Roth, Karlsruhe, Germany

2.2 Antibodies

Table 5: Antibodies

Antibody	Source	Company
Anti-Flag mAb M2	Mouse IgG1 monoclonal	Sigma, Deisenhofen, Germany
Anti- Fn14	Rabbit monoclonal	Cell Signaling Technology, Beverly, MA, USA
Anti-hBaffR-PE	Mouse IgG1 monoclonal	Biosciences, Heidelberg, Germany
Anti-hBCMA-PE	Mouse IgG2 monoclonal	Biolegend, San Diego, USA
Anti-hCD19-FITC	Mouse IgG2 monoclonal	Biolegend, San Diego, USA
Anti-hCD20-PE	Mouse IgG2 monoclonal	Biolegend, San Diego, USA
Anti-hCD25-APC	Mouse IgG1 monoclonal	Biolegend, San Diego, USA
Anti-hCD38-FITC	Mouse IgG1 monoclonal	Miltenyi Biotec, Bergisch Gladbach, Germany
Anti-hCD70-FITC	Mouse IgG3 monoclonal	Biosciences, Heidelberg, Germany
Anti-mCD20-PE	Rat IgG2 monoclonal	Biolegend, San Diego, USA
Anti-mCD70-PE	Rat IgG2 monoclonal	Biolegend, San Diego, USA
Anti-mIgG1κ-PE	Isotype control	R&D Systems, Minneapolis, USA
Anti-mIgG2a-PE	Isotype control	R&D Systems, Minneapolis, USA
Anti-mIgG2b-PE	Isotype control	R&D Systems, Minneapolis, USA
Anti-mIgG-PE	Goat polyclonal	Sigma-Aldrich, Darmstadt, Germany
Anti-mouse IRDye 800	Goat polyclonal	LI-COR Bioscience, Bad Homburg, Germany
Anti-mouse-HRP	Rabbit polyclonal	Dako-Cytomation, Denmark
Anti-PARP	Mouse IgG1, clone 7D3-6	BD Biosciences, Heidelberg, Germany
Anti-PDL1-PE	Mouse IgG1 monoclonal	Biolegend, San Diego, USA
Anti-rabbit-HRP	Goat polyclonal	Dako-Cytomation, Glostrup, Denmark
Anti-rabbit-HRP	Goat polyclonal	Cell Signaling Technology, Beverly, MA, USA

2.3 Kits

Table 6: Kits

Kit	Company
BioLux *Gaussia* Luciferase Assay Kit	New England Biolabs, Frankfurt
OptEIA IL8-ELISA	BD Biosciences, Heidelberg, Germany
Pierce ECL Western Blotting Substrate	Fermentas, St. Leon-Rot, Germany
Pierce® Silver Stain	Fermentas, St. Leon-Rot, Germany

2.4 Instruments and disposable materials/equipments

Table 7: Instruments and disposable materials/equipments

Instrument or material/equipment	Company
96-well ELISA plates (high binding)	Greiner, Frickenhausen, Germany
Advanced magnetic hotplates stirrers	VWR International, Czech Republic
Agfa Curix 60 processing maschine	Agfa, Düsseldorf, Germany
Casting chambers for SDS-PAGE	PeqLab, Erlangen, Germany
Cell culture bottles	Greiner, Frickenhausen, Germany
Cell culture petri dishes	Greiner, Frickenhausen, Germany
Cell culture plates	Greiner, Frickenhausen, Germany
Centrifuge Rotana 460R	Hettich, Tuttlingen, Germany
CO2 incubator Heraeus Cell Safe	Heraeus, Hanau, Germany
Cryotubes	Greiner, Frickenhausen, Germany
Dialysing tubes, Viking, MWCO 15kDa	Carl Roth, Karlsruhe, Germany
Dialysis membrane Spectra/Por® 4, 1kDa	VWR International, Czech Republic
Electrophoresis system	BioRad, München, Germany
ELISA-reader	Anthos Labtec, Krefeld, Germany
Eppendorf tubes, 1,5 ml und 2 ml	Eppendorf, Hamburg, Germany
Equibio EasyjecT Plus electroporator	PeqLab, Erlangen, Germany
Flow cytometer FACScaliber	BD Biosciences, Heidelberg, Germany
Flow cytometry tubes	Falcon, Heidelberg, Germany
Heat block	PeqLab, Erlangen, Germany
IRAffinity-1S - FTIR Spectrometers	SHIMADZU, Kyoto, Japan

LI-COR Odyssey® Infrared Imager	LI-COR Biosciences, Lincoln, USA
MACS LS columns	Miltenyi Biotec, Bergisch Gladbach, Germany
MACS multistand	Miltenyi Biotec, Bergisch Gladbach, Germany
MACS separator	Miltenyi Biotec, Bergisch Gladbach, Germany
Microcentrifuge 5417C	Eppendorf, Hamburg, Germany
Nanodrop	
Nitrocellulose membranes, 0,2 µM pore size	Whatman, Dassel, Germany
PCR-Thermocycle Primus	MWG Biotech, Ebersberg, Germany
Pipetus	Hirschmann Laborgeräte, Eberstadt, Germany
Polyallomer tubes	Seton, Los Gatos, CA, USA
Polypropylene tubes	Greiner, Frickenhausen, Germany
Power supply EPS 301	GE Healthcare, Garching, Germany
Sterile filters (0,2µm)	Sarstedt, Nümbrecht, Germany
Sterile plastic Pasteur pipettes	Hartenstein, Würzburg / Versbach, Germany
Tube Rotator	VWR International, Czech Republic
Ultracentrifuge OPTIMA-L70	Beckman Coulter, Krefeld, Germany
Well plates for cell culture	Greiner, Frickenhausen, Germany
Wet/tank blotting system	PeqLab, Erlangen, Germany
Zetasizer Nano ZS	Malvern Panalytical, Malvern, United Kingdom

2.5: Preparations and buffer

Table 8: Preparations and buffers

Preparation	Prescription
Assay diluent	1 x PBS
	10 % (v/v) FCS
Blot buffer 10x	0,025 M Tris
	0,192 M glycin
	20 % (v/v) methanol
	pH 8,3
CV staining solution	20 % (v/v) methanol
	0,5 % (w/v) CV powder
ELISA coating buffer	8,4 g/l NaHCO3
	3,56 g/l Na2CO3

	pH 9,5
Laemmli buffer (SDS-PAGE, 4 x)	8 % (w/v) SDS
	10 % β-Mercaptoethanol
	40 % gycerol
	0,2 M Tris pH 8
	0,04 % bromphenol blue
LB medium	10 g peptone
	5 g yeast extract
	10 g/l NaCl
PBS	0,02 M Na phosphate
	0,7 % (w/v) NaCl
	pH 7,2
PBST	1 x PBS
	0,05 % (v/v) tween-20
PBST in milk	1 x PBS
	0,05 % (v/v) tween-20
	5 % (w/v) nonfat dried milk powder
Running buffer 10x (SDS-PAGE)	0,05 M Tris
	0,38 M glycin
	0,004 M SDS
	pH 8,3
Separating gel buffer (SDS-PAGE)	1,5 M Tris
	0,015 M SDS
	pH 8,8
Stacking gel buffer (SDS-PAGE)	0,5 M Tris
	0,015 M SDS
	pH 6,8
TBS	0,02 M Tris
	8 % (w/v) NaCl
	pH 7,6
TBST	1 x TBS
	0,05 % (v/v) tween-20
TBST in milk	1 x TBS
	0,05 % (v/v) Tween-20
	5 % (w/v) nonfat dried milk powder

2.6 Cells:

The human cancer cell lines used for this work were already accessible in the Division of Molecular Internal Medicine, University Hospital of Würzburg.

Table 9: Cells

Cell line	Source	Origin of Cancer
HEK293	Institution's own stock	Human embryonic kidney
HT1080	Institution's own stock	Human Fibrosarcoma

3. Methods

3.1 Cell culture

The cell cultures were maintained in RPMI-1640 medium, supplemented with 10% heat-inactivated fetal bovine serum (FBS), and incubated at 37 °C under a 5% CO2 atmosphere. Following washing with 1X Phosphate-Buffered Saline (PBS), cells were detached using trypsin-EDTA solution, with an incubation period of 10 minutes. After this, cells were centrifuged at a speed of 1200 rpm for 4 minutes. Then cells were counted using a hemocytometer under a microscope prior to seeding in cell culture plates for downstream experiments. The remaining cells were further propagated by serial dilution, ranging from 1:3 to 1:10 in fresh medium containing 10% FBS. Periodically, cells were cryopreserved at -80 °C in cryotubes. The freezing medium consisted of 10% Dimethyl Sulfoxide (DMSO) in FBS, with a final volume of 1 ml per cryotube.

3.2 Protein production

The expression plasmid encoding the corresponding antibody was transfected into HEK293 cells using Polyethylenimine (PEI) as a transfection agent. The transfection process was executed as follows: A solution of 1 mg/ml PEI in water was gradually added to 2 ml of serum-free RPMI 1640 medium containing 12 µg of plasmid DNA, creating a plasmid-PEI complex. This mixture was incubated for 10 minutes at room temperature to facilitate the formation of the complex. Following incubation, the complex was introduced to nearly confluent HEK293 cells in a 15 cm tissue culture dish, which had been recently refreshed with 15 ml of serum-free medium. The following day, the medium was replaced with RPMI 1640 medium supplemented with 1% Penicillin/Streptomycin (P/S) and 2% Fetal Bovine Serum (FBS). After 7 days, the culture supernatant was harvested and centrifuged at 4600 rpm for 10 minutes to remove cell debris. The production of the desired protein was regularly monitored by quantifying protein concentrations using Western blot analysis. Protein samples were prepared by boiling for 5 minutes at 95 °C. The samples were then loaded onto a nitrocellulose membrane (see section 3.6). The membrane was incubated overnight with the anti-Flag monoclonal antibody M2. The following day, after washing off the primary antibody, the membrane was incubated for one hour with the secondary

antibody, anti-mouse IRDye 800. Finally, the nitrocellulose membranes were scanned using the LI-COR Odyssey® Infrared Imager. Protein concentrations were determined based on the intensity of the corresponding protein bands relative to a standard protein of known concentration.

3.3 Protein purification

Protein-containing supernatants, produced by HEK293 cells, were subsequently purified using affinity chromatography with anti-Flag M2 agarose beads. These beads were packed into a column and thoroughly rinsed with autoclaved Tris-Buffered Saline (TBS). The supernatant was then loaded onto the column, maintaining a flow rate of at least one drop per 30 seconds. After the supernatant was loaded, the column was stored at 4 °C until all the flow-through was collected. Subsequently, the beads were washed again with TBS. Bound protein molecules were then eluted from the beads in 0.5 ml fractions using TBS containing 100 µg/ml of Flag peptide, with a flow rate of at least one drop per minute. The eluted proteins were subsequently dialyzed against Phosphate-Buffered Saline (PBS) overnight at 4 °C. Following dialysis, the proteins were sterile filtered and stored at -20 °C for further analysis. The efficiency of protein recovery post-purification was assessed by measuring the protein concentrations in the original supernatant prior to purification, the flow-through, the eluted fractions, the post-purification TBS wash flow-through, and the remaining beads.

3.4 Silver staining.

The purified protein was resolved via Sodium Dodecyl Sulfate Polyacrylamide Gel Electrophoresis (SDS-PAGE), as detailed in section 3.6. Following electrophoretic separation, the gel was stained using the Pierce® Silver Stain Kit, in accordance with the manufacturer's guidelines.

3.5 FACS analysis

The surface expression of various receptors was assessed using flow cytometry. A cell count of 5x10^5 cells was transferred to a U-bottom 96-well plate. The plate was

then centrifuged at 1200 rpm for 4 minutes, and the cells were washed twice with ice-cold PBS. Following the washes, cells were incubated for 1 hour at 4 °C with an antibody, following the manufacturer's guidelines. An appropriate isotype control antibody was used to account for nonspecific binding. Subsequently, cells were washed three times with PBS, resuspended in 300 µl of PBS, and transferred into flow cytometry tubes. The samples were analyzed on a BD FACS Calibur flow cytometer. Data generated from the flow cytometry analysis were further analyzed using WinMDI 2.8 software.

3.6 Western Blot

3.6.1 SDS-PAGE

Protein separation was achieved using SDS-PAGE. The separating gel was first prepared with the following components: 0.374 M Tris buffer (pH 8.8), 0.0035 M SDS, distilled H_2O, and either 12% or 10% acrylamide. The gel was polymerized using 0.1% Ammonium persulfate (APS) and 0.1% Tetramethylethylenediamine (TEMED). To create a level surface, isopropanol was gently layered on top of the separating gel solution immediately after it was poured and before polymerization. Once the separating gel had polymerized, the isopropanol was carefully removed. The stacking gel, consisting of 6% acrylamide in 0.123 M Tris buffer (pH 6.8), 0.00375 M SDS, 0.1% APS, and 0.1% TEMED, was then layered on top of the polymerized separating gel. The gel comb, which creates the sample wells, was inserted into the stacking gel before it polymerized. After polymerization of the stacking gel, the comb was removed, and the protein samples were loaded into the wells using a micropipette. The electrophoretic separation was run at 120 V and 400 mA for 95 minutes for smaller gels, and for 105 minutes for larger gels.

3.6.2 Blotting on nitrocellulose membrane

Proteins separated by SDS-PAGE were transferred onto nitrocellulose membranes using a wet/tank blotting system. The nitrocellulose membranes and Whatman filter papers were cut to match the dimensions of the gels and were pre-soaked in transfer buffer immediately prior to use. The transfer assembly was set up in the following order

to form a sandwich within the blotting chamber: anode, two pre-soaked Whatman filter papers, nitrocellulose membrane, gel, two additional pre-soaked Whatman filter papers, and then the cathode. The transfer process was conducted at room temperature for a duration of 90 to 150 minutes, with a constant voltage of 90 V and a current of 400 mA.

3.6.3 Membrane detection

Following protein transfer, remaining protein-binding sites on the nitrocellulose membranes were blocked with a solution of 5% milk in PBS with Tween-20 (PBST) for 1 hour on a shaker. The membranes were then washed three times with either Tris-Buffered Saline with Tween-20 (TBST) or PBST for 30 minutes each. Subsequently, the membranes were incubated overnight at 4 °C on a shaker with the primary antibody, diluted in either PBST or TBST, in accordance with the manufacturer's guidelines. The next day, the membranes were again washed three times with either TBS or PBST for 30 minutes each. The membranes were then incubated with the secondary antibody, diluted in either PBST or TBST-milk, for 1 hour at room temperature on a shaker. Finally, the membranes were washed three more times with PBST or TBST for 30 minutes each. The bound antibodies were visualized either using a LI-COR Odyssey® Infrared Imager or via chemiluminescence with an enhanced chemiluminescence (ECL) system. In the latter case, the membrane was incubated with the ECL substrate solution for 1–2 minutes, then exposed to an X-ray film for a few seconds. The film was subsequently developed in an automatic X-ray film processor.

3.7 IL8 ELISA

HT1080 cells were seeded at a density of 2 x 10^4 cells per well in 96-well cell culture plates. The following day, HT1080 cells were challenged in the presence of HEK293 cells expressing respective anchoring targets/receptors together with increasing concentration of 18D1-N297A-AD fusion proteins. Meanwhile, 96-well ELISA plates were coated overnight with a human anti-IL8 antibody (from the OptEIA ELISA Kit), in accordance with the manufacturer's protocol. After an additional 24 hours, cell culture supernatants were collected and analyzed for their IL8 content utilizing a human IL8

ELISA kit (BD Biosciences, Heidelberg, Germany), following the manufacturer's instructions. ELISA plates were first washed three times with PBS-Tween and blocked with Assay Diluent, followed by a one-hour incubation at room temperature (RT). After the incubation, plates were washed again three times with PBS-Tween. The supernatants from the stimulated cell culture plates were subsequently transferred to the ELISA plates and incubated for two hours at RT. In addition, a standard curve of IL8 (2-0.5 ng/ml) was generated on these plates to allow precise quantification of the IL8 concentrations within the samples. Following an additional five washes, a mixture of biotinylated anti-IL8 antibody and streptavidin-HRP was added to the plates for an hour-long incubation at RT. After incubation and an additional seven washing steps, the amount of bound IL8 was quantified by adding the HRP substrate, ABTS. The optical density was measured at a wavelength of 405 nm using an ELISA plate reader, which allowed for the calculation of IL8 concentrations in the samples.

3.8 The synthesis of modified polylysine (MPL)

3.8.1 MPL synthesis

The modification of poly-L-lysine (ε-PL) to produce modified poly-L-lysine (MPL) was achieved by reacting it with 2,3-dimethyl maleic anhydride (DMMA). This reaction modified the amino group on the lysine side chain into an amide bond and a negatively charged carboxyl group. Initially, 0.165 mmol of ε-PL was dissolved in 25 mL of deionized water. Subsequently, 5 mmol of DMMA, 5 mmol of N-hydroxysuccinimide (NHS), and 6 mmol of 1-ethyl-3-(3-dimethylaminopropyl) carbodiimide hydrochloride (EDCI) were added to the ε-PL solution. The pH of the solution was adjusted to 8.5 by adding triethylamine, and the mixture was stirred at 25 °C for 48 hours. The reaction mixture was then subjected to ultrafiltration using a dialysis tube with a molecular weight cutoff of 1000 Da. Following dialysis, the solution was freeze-dried and sample was collected.

3.8.2 MPL characterization by FTIR

Characterization of MPL by Fourier-transform infrared spectroscopy (FTIR); 10 mg of sample powder was pressed into a thin film, which was fixed on the holder for testing.

The samples were scanned in the IR range from 400 to 4000 cm^{-1}. Several peaks are marked in the figure with explanations for the stretches.

3.9 Synthesis of gold nanoparticles (AuNPs)

The protocol for the synthesis of gold nanoparticles (AuNPs) was adapted from a method previously established by our group (Aido et al., 2021b). Briefly, 14.3 mg of tetrachloroauric acid trihydrate was dissolved in 90 mL of deionized water to prepare a 0.4 mM chloroauric acid solution. This 0.4 mM chloroauric acid solution was transferred into a clean 300 mL glass flask and heated on a hot plate while being stirred at 300 rpm with a magnetic stirrer. The top of the flask was covered with aluminum foil to facilitate heating and reduce evaporation. The solution was heated until it reached a steady boil. At this point, 1 mL of a 38.8 mM trisodium citrate solution was added to the boiling chloroauric acid solution. The reaction was allowed to proceed for an additional 20 minutes under continuous heating. Following this reaction, spherical monodisperse AuNPs of approximately 50 nm in diameter were obtained. The size distribution and average diameter of the synthesized AuNPs were characterized using a Zetasizer, with the procedure described in the subsequent section.

3.10 Gold nanoparticles functionalization

The surface of the gold nanoparticles was functionalized by introducing carboxyl groups. This was achieved by adding thiol-polyethylene glycol (PEG)-acetic acid to the gold nanoparticle solution until a final concentration of 100 µg/mL was reached. The solution was stirred for 1 hour to facilitate the binding of the carboxyl groups to the surface of the gold nanoparticles. Following this, the carboxyl-functionalized gold nanoparticles (AuNP-COOH) were centrifuged at 22,000 rpm for 15 minutes, and the supernatant was subsequently discarded. The AuNP-COOH pellets were resuspended and washed three times with a solution containing 330 µg/mL methoxy PEG-thiol (mPEG-thiol) in water, in order to remove any unreacted thiol-PEG-acetic acid. After the final wash, the solution containing the AuNP-COOH was collected in an Eppendorf tube for further use or analysis.

3.11 Gold nanoparticles activation and antibodies crosslinking

The carboxyl-functionalized gold nanoparticles (AuNP-COOH) solution was centrifuged at 22,000 rpm for 15 minutes. The supernatant was discarded and the AuNP-COOH pellet was resuspended in activation/coupling buffer (50 mM MES, pH 6.0). The solution was then washed three times in the same buffer and the pellet was finally resuspended in 1 mL of activation buffer. Next, 120 µL of a 100 mM EDC solution and 240 µL of a 200 mM NHS solution were added to the AuNP-COOH solution. The mixture was stirred and incubated for 30 minutes at room temperature to allow for activation. Following incubation, the activated AuNP-COOH was washed with activation buffer to remove any unreacted EDC and NHS. 500 µL of the activated AuNP-COOH solution were then incubated with 500 µL of the antibody of interest, ranging in concentration from 300 ng/mL to 1 µg/mL, and left to react overnight at room temperature. The resulting antibody-conjugated AuNPs were then washed with a blocking buffer (50 mM Tris in 330 µg/mL mPEG-SH) to remove any remaining unconjugated antibodies and to block any free activated carboxyl sites on the surface of the gold nanoparticles. Finally, the antibody-conjugated AuNPs were resuspended in the blocking buffer for storage or further experimentation.

3.12 Construction of modified polylysine coated gold nanoparticles (MPL-AuNP-Ab)

A quantity of 1.5 mg, 1 mg, or 0.5 mg of MPL was introduced into 0.9 mL of phosphate-buffered saline (PBS) at varying pH levels (6.5, 7, and 7.5), respectively. These solutions underwent sonication for 20 seconds at 50% intensity and an 80% duty cycle to ensure thorough dispersion of MPL. Subsequently, 100 µL of antibody-coated gold nanoparticle (AuNP-Ab) solution was incorporated into each mixture. These mixtures were then sonicated for an additional 10 seconds, following the same sonication parameters, and subsequently allowed to incubate overnight. Samples were collected on the following day for downstream analysis or applications.

3.13 Particle Characterization

3.13.1 UV-Vis

Following synthesis, the gold nanoparticles (AuNPs) were collected, and their optical properties assessed using UV-Vis spectrophotometry on a SpectraMax instrument. Absorption spectra were recorded in the wavelength range of 450 to 650 nm, with a step size of 5 nm.

3.13.2 DLS and zeta potential

The hydrodynamic diameters and zeta potentials of the synthesized AuNPs - unPEGylated, PEGylated, antibody-conjugated, and MPL-coated forms - were analyzed using a Zetasizer from Malvern Instruments. For dynamic light scattering (DLS) measurements, as well as for determining the zeta potentials of EDC/NHS-modified AuNPs and monoclonal antibody (mAb)-AuNPs, samples were suitably diluted with deionized water by factors ranging from 10 to 1000, depending on their initial concentration or dispersion density. Each diluted sample was thoroughly suspended before analysis. For zeta potential measurements of MPL, MPL powder (0.5, 1, 1.5 mg) was individually dispersed in 1 mL of PBS that had been pre-adjusted to various pH values. The samples were then sonicated for 30 seconds to ensure complete dispersion of the MPL powder. Subsequently, 1 mL of each MPL dispersion was mixed with 10 µL of the antibody-AuNP solution. This mixture was subjected to 10 seconds of sonication before being transferred into a folded capillary cell (Malvern, Worcestershire, UK) in preparation for zeta potential measurements using a Zetasizer Nano ZS instrument.

3.14 MPL-antibody-AuNPs release study

The release profiles of MPL-PDL192-AuNPs and MPL-5B6-AuNPs in PBS of pH 6.5, 7.0 and 7.5. MPL (0.5 mg) was premixed with PDL192-AuNPs and 5B6-AuNPs, respectively, and then the mixture was introduced into solutions with varying pH levels. At specific time intervals, a 1uL sample was extracted from the solution, and the UV absorbance was measured at the wavelength of 280 nm using NanoDrop (ND-1000, Thermal Fisher Scientific, UK).

3.15 Functionality analysis of MPL-antibody-AuNPs

HT1080 cells were seeded at a density of 2 x 10^4 cells per well in 96-well cell culture plates. The following day, the cell culture media were refreshed and adjusted to pH levels of 6.5, 7 and 7.5. Subsequently, cells were stimulated with increasing concentration of MPL-PDL192-AuNPs, MPL-5B6-AuNPs, and Flag-TWEAK (pH 7.5) in the presence and absence of anti-Flag. The next day, IL-8 concentrations in the cell supernatants were analyzed using ELISA as a readout for the activation Fn14-induced NFκB signaling, utilizing a human IL8 ELISA kit (BD Biosciences, Heidelberg, Germany), following the manufacturer's instructions. For the details of ELISA procedure, see in section 3.7.

3.16 Statistical analysis

All figures presented in this study were generated using Microsoft Office Excel 2007, GraphPad Prism 5.0, CorelDRAW Graphics Suite X4, and EndNote X9 software.

4. Results

Antibodies against a variety of TNFRSF receptors (TNFRs) are effective in inducing potent receptor activation upon binding to Fc gamma receptors (FcγRs). Furthermore, antibody fusion proteins with an anchoring domain were reported to induce potent receptor activation in a FcγR-independent manner when bound with their anchoring domain (AD) to a plasma membrane exposed target (Nelke et al., 2020). In recent years, there is an emergence of novel synthesis methods of nanoparticle-based formulations, and among these methods, bioconjugation has gained lots of attention. Bioconjugation involves functionalizing and crosslinking of nanoparticles to molecules with active pharmaceutical effect by biological or chemical means. The goal of this doctoral thesis was to develop a formulation of target-release FcγR-independent antibody-coated gold nanoparticles. For the first step, to validate crosslinking is indispensible for Fn14 activation, this doctoral thesis examined a group of bispecific antibody-AD fusion proteins of the Fn14-specific antibody PDL192 and 5B6 on their effectiveness for binding to their anchoring target and Fn14 activation. After validating the importance of secondary crosslinking by plasma membrane-associated presentation for Fn14 activation, gold nanoparticle (AuNPs) were synthesized and utilized as a platform for antibody immobilization to empower the antibodies to crosslink and activate Fn14. At last, modified polylysine (MPL) was used as a tumor-microenvironment control-release layer on the surface of antibody-coated gold nanoparticles.

4.1.1 Production of various bispecific 18D1-N297A-AD fusion proteins

DNA fragments encoding either an scFv fragment or a single-chain ligand trimer of the TNFSF were cloned to the C-terminus of the heavy chain of the 18D1-N297A antibody using standard techniques. N297A refers to a mutation in the human IgG1 heavy chain changing the alanine (A) at position 297 to asparagine (N) (Figure 4). This substitution significantly prevents IgG binding to FcγRs. The 18D1 antibody is a mouse-human cross-reactive llama-derived recombinant Fn14-specific antibody (Trebing et al., 2014). Thirteen 18D1-N297A-AD fusion proteins were produced upon co-expression of the corresponding heavy chain varaints with the shared 18D1 light chain in HEK293 cells. These 18D1-N297A-AD fusion proteins carried anchoring domains recognizing

hCD20 (scFv:CD20), hCD70 (scFv:CD70), the human Baff receptors BaffR and BCMA (scBaff, scFv:BCMA), hCD19 (scFv:CD19), hCD38 (scFv:CD38), hTNFR2 (scFv:TNFR2), PDL1 (scFv:muPDL1), muCD70 (scFv:muCD70), muCD20 (scFv:muCD20), the human IL2 receptor (hIL2) as well as murine TNFR2 (scmuTNF80) (Figure 4).

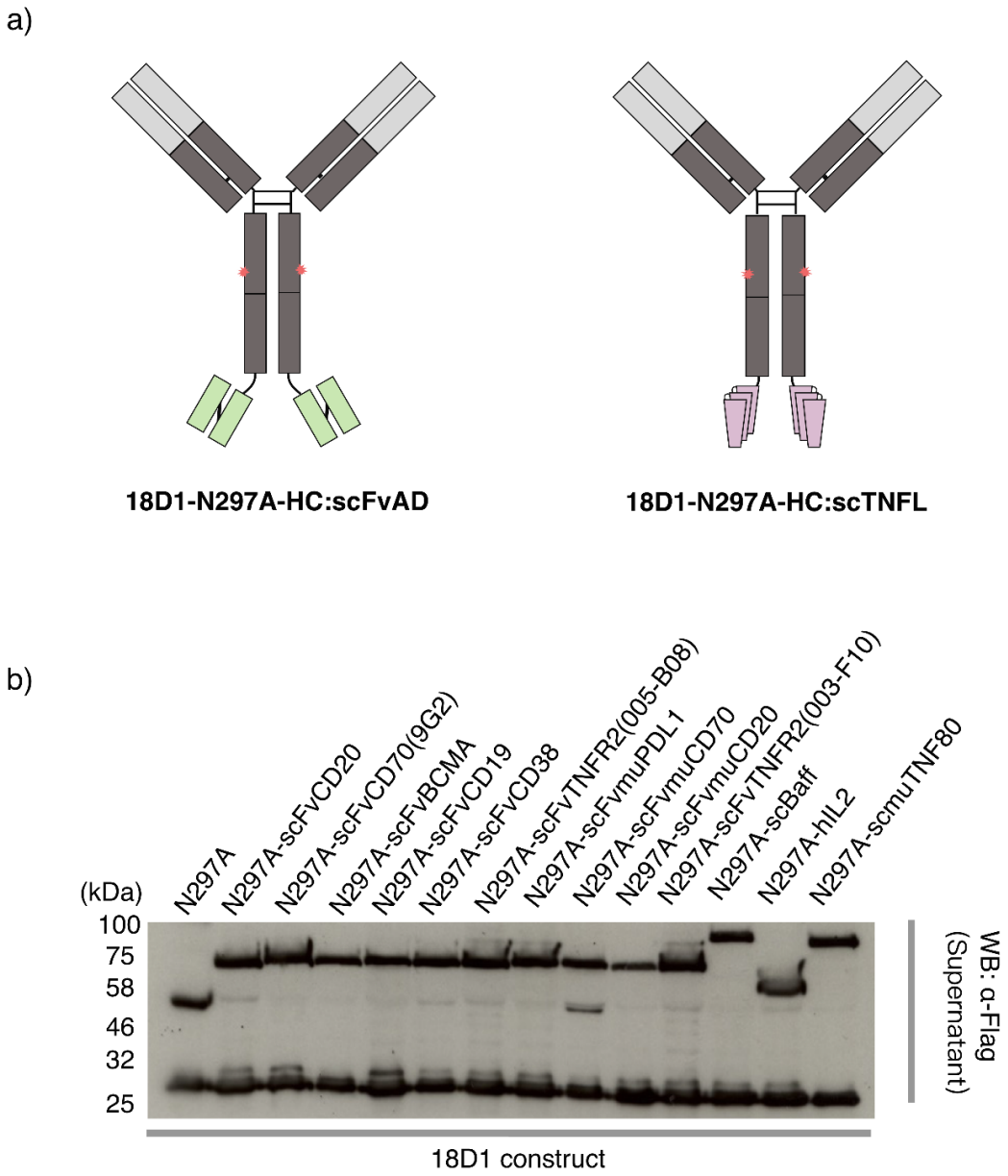

Figure 4: 18D1-N297A-AD fusion proteins investigated in this work. Schematic structure (a) and WB (b) of the 18D1-N297A-AD antibody fusion proteins studied in this work.

4.1.2 Analysis of binding of the 18D1-N297A-AD fusion proteins to their anchoring targets

To evaluate the affinity of the different C-terminal anchoring domains of the various 18D1-N297A-AD fusion proteins to their corresponding targets, binding studies were performed with Gaussia princeps luciferase (GpL)-tagged variants of the 18D1-N297A-AD fusion proteins. It has been previously demostrated that a GpL tag C-terminally coupled to the light chain of an antibody does not affect the binding ability of antibodies (Kums et al., 2017; (Figure 5)). These fusion proteins were produced upon expression in HEK293 cells and quantified by western blotting (Figure 5).

For binding studies with these GpL-tagged 18D1-N297A-AD antibody fusion proteins, HEK293 cells were transiently transfected with the receptors/targets recognized by the various anchoring domains. FACS experiments demonstrated that control cells transfected with empty vector did not express any of the receptors/targets studied, whereas HEK293 cells transfected with BaffR-, CD20(mu)-, CD38-, CD19-, BCMA-, CD20-, CD25-, CD70-, TNFR2-, CD70(mu)-, PDL1-, CD27L- and CD27L(mu)-encoding expression vectors all expressed the respective anchoring receptors/targets (Figure 6). As illustrated, 18D1-N297A-AD fusion proteins specific for hCD38 (scFv:CD38), hCD70 (scFv:CD70), murine TNF2 (scmuTNF80), hTNFR2 (scFv:TNFR2), hCD20 (scFv:CD20) and hCD19 (scFv:CD19) exhibited significant affinity for their anchoring receptors/targets between 500 and 2000 ng/ml (Figure 7). In contract, 18D1-N297A-AD fusion proteins specific for the human Baff receptors BaffR/BCMA (scBaff, scFv:BCMA) and muCD70 (scFv:muCD70) showed only a relatively low affinity to their corresponding receptors, and 18D1-N297A-AD fusion proteins specific for PDL1 (scFv:muPDL1) and muCD20 (scFv:muCD20) displayed no binding to their corresponding receptors.

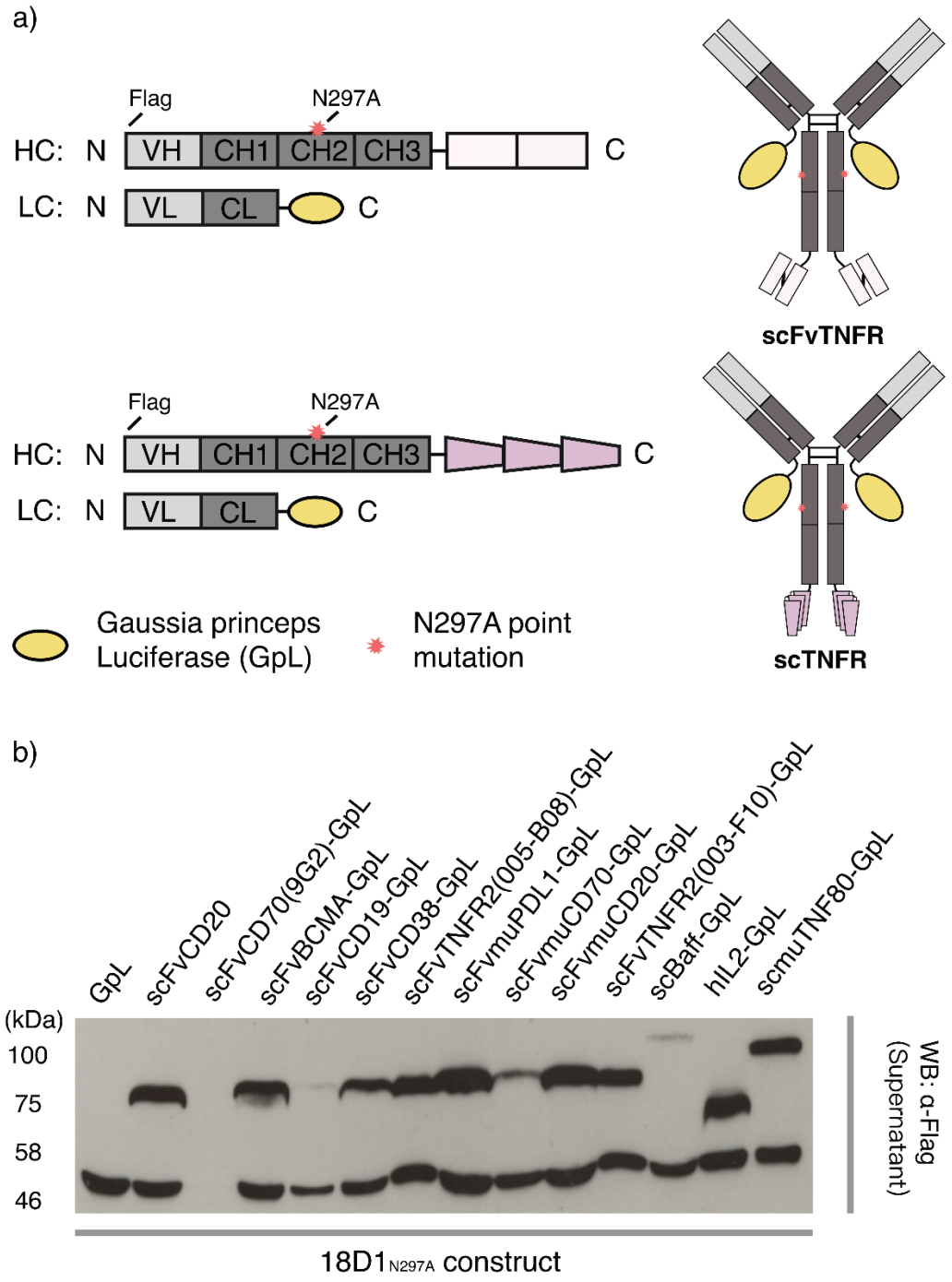

Figure 5: Domain architecture of 18D1-N297A-AD fusion proteins. a) Schematic structure of the GpL-anchored antibody fusion proteins (this figure is modified based on Nelke et al., 2020); b) Western blotting of 18D1-N297A-AD fusion proteins with GpL fused to the C-terminus of the antibody light chains.

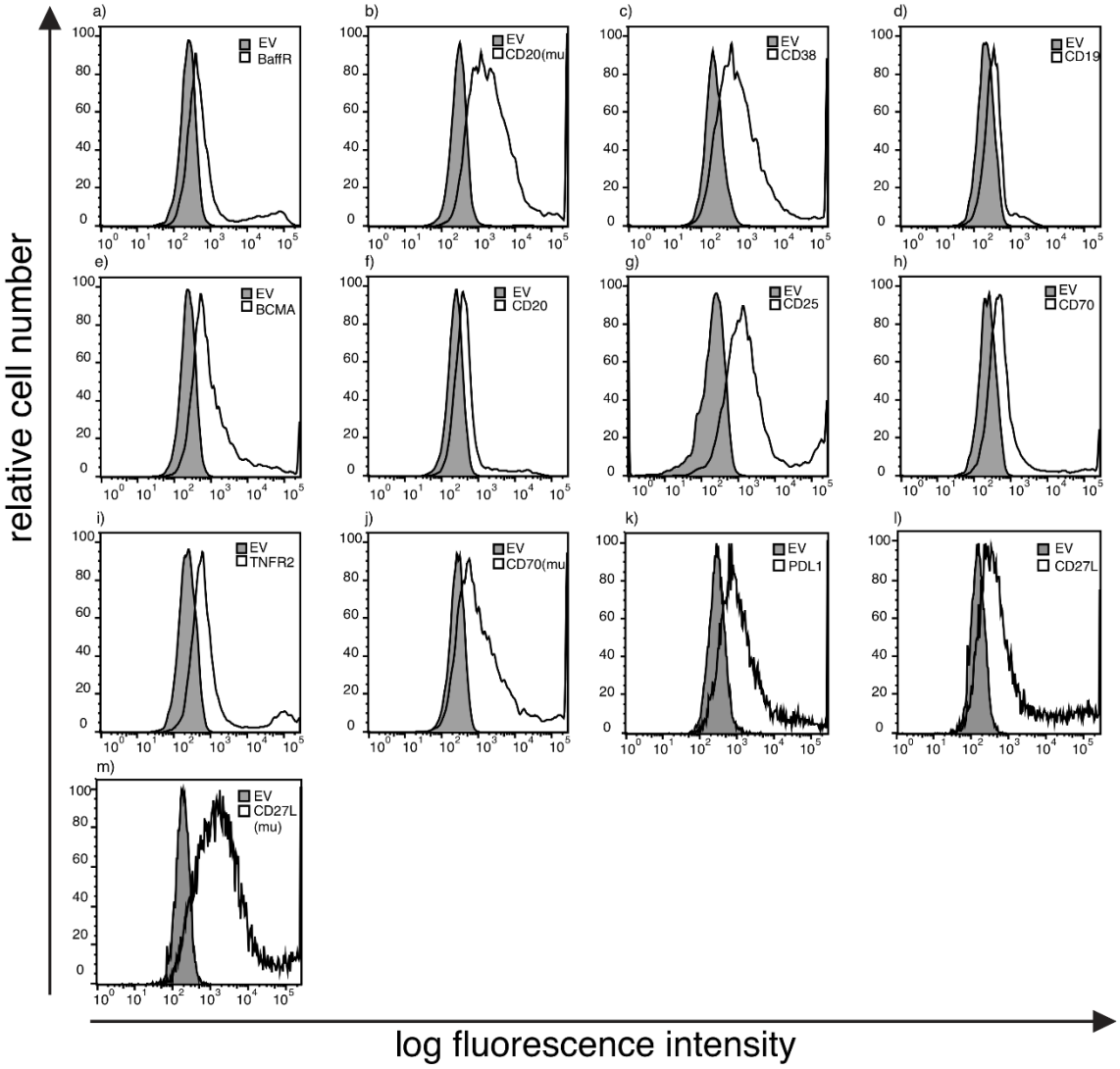

Figure 6: Evaluation of various receptor expression by Flow cytometry. HEK293 cells transiently transfected with expression plasmids encoding a) BAFFR, b) CD20(mu), c) CD38, d) CD19, e) BCMA, f) CD20, g) CD25, h) CD70, i) TNFR2, j) CD70(mu), k) PDL1, l) CD27L, m) CD27L(mu) (blank area) or transfected with empty vector (EV, filled area) were incubated with 1 µg/ml PE-labelled, FITC-labelled or APC-labelled antibody specific for the anchoring target of interest for 30 minutes at 4 °C (blank area). After washing, cell-bound antibodies were quantified by flow cytometry.

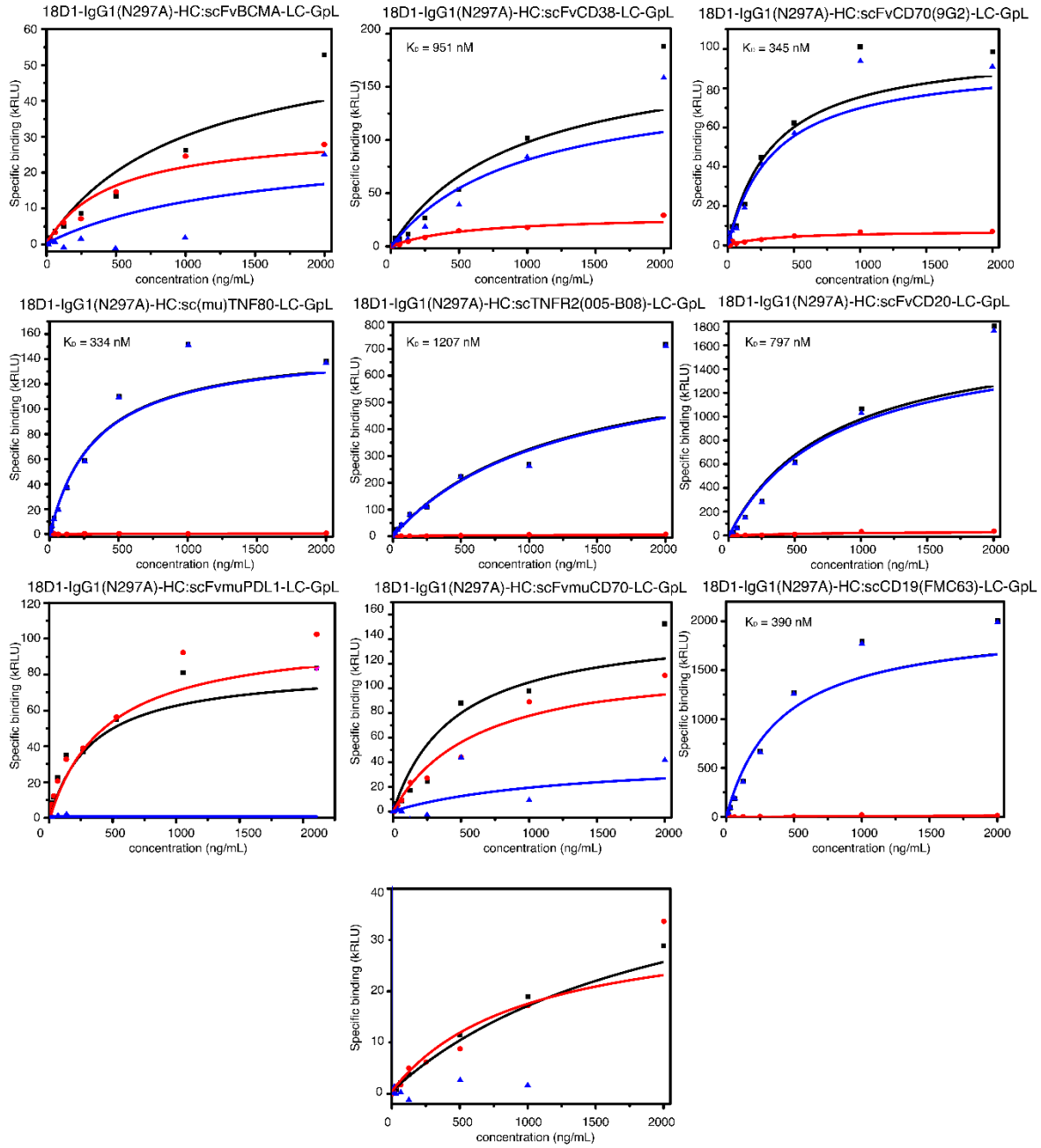

Figure 7: In vitro binding studies of GpL-tagged 18D1-N297A-AD fusion proteins to the AD-specific receptors/targets. HEK293 cells were transiently transfected with plasmids encoding the AD corresponding target proteins and served to determine total binding (black squares). HEK293 cells transfected with empty vector (EV) were used to determine nonspecific binding (red dots). Specific binding (blue triangles) was calculated by subtracting nonspecific binding values from the corresponding total binding values. Kd values of specific binding were also provided.

4.1.3 Functional analysis of the antibody-scBaff fusion proteins.

For analyzing the functionality of 18D1-N297A-AD fusion proteins to the AD-specific receptors/targets, IL8 ELISA experiments were conducted as experimental readout parameters. HT1080 cells were co-cultured with HEK293 cells transfected with the receptors/targets recognized by the various anchoring domains, and stimulated with different concentrations of the 18D1-N297A-AD fusion proteins. HT1080 cells were also co-cultured with HEK293 cells tranfected with EV as a negative control. ELISA results demonstrated 18D1-IgG1(N297A)-HC:scTNF80(mu), 18D1-IgG1(N297A)-HC:scFvCD70, 18D1-IgG1(N297A)-HC:scFvBCMA, 18D1-IgG1(N297A)-HC:scFvCD20, 18D1-IgG1(N297A)-HC:scFvmuPDL1, 18D1-IgG1(N297A)-HC:scFvTNFR2(005-B08), 18D1-IgG1(N297A)-HC:schIL2 and 18D1-IgG1(N297A)-HC:scBaff induced secretion of IL8 in a concentration-dependent manner in the presence of HEK293 cells expressing respective anchoring targets/receptors (Figure 8), and 18D1-N297A-AD stimulated potent IL8 production was observed at the concentration between 222 and 2000 ng/mL. In contrast, only insignificant levels of Fn14 activation were observed for 18D1-IgG1(N297A)-HC:scFvmuCD70, 18D1-IgG1(N297A)-HC:scFvmuCD20, 18D1-IgG1(N297A)-HC:scFvCD38 and 18D1-IgG1(N297A)-HC:scFvTNFR2(003-F10), as the IL8 concentrations were less than 0.5 ng/mL. Although the 18D1-IgG1(N297A)-HC:scFvCD19 also led to concentration-dependent IL8 secretion in the presence of HT1080 and HEK293 cell expressing CD19, 18D1-IgG1(N297A)-HC:scFvCD19 also induced potent Fn14 activation in co-cultures with HT1080 and EV HEK293 cells.

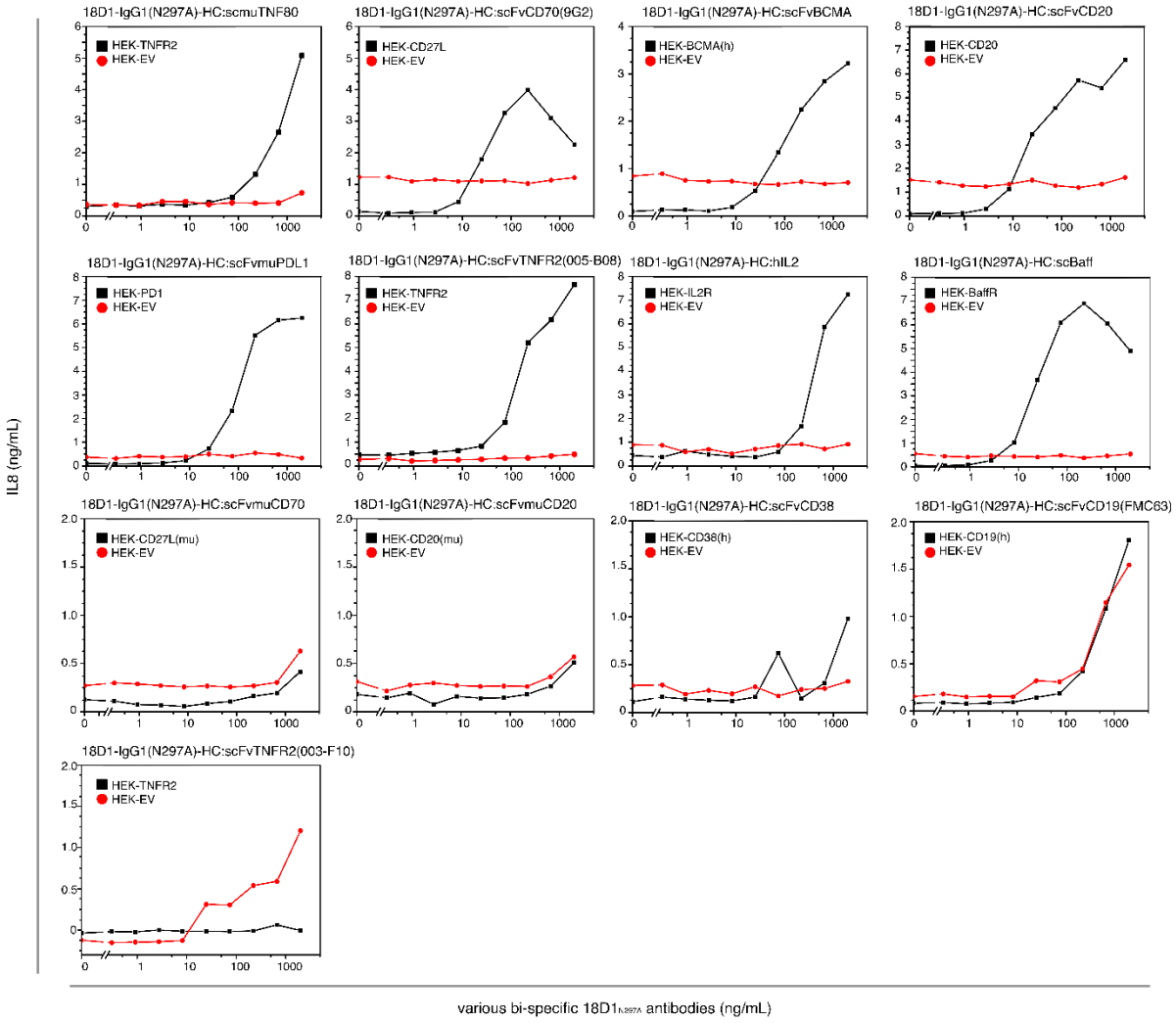

Figure 8: Activation of Fn14 by 18D1-N297A-AD fusion proteins. HT1080 were cultivated in 96-well plates and were challenged in the presence of HEK293 cells expressing respective anchoring targets/receptors together with increasing concentration of 18D1-N297A-AD fusion proteins. After 8 h, the supernatants were collected and analyzed by ELISA for the production of IL8.

4.2 Construction of modified-polylysine-coated antibody-gold nanoparticles and their functionality evaluation

Gold nanoparticles (AuNPs) were synthesized and used as a platform for antibody immonilization. Subsequently, relevant in vitro efficacy analysis were conducted. Finally, modified polylysine (MPL) was utilized as a tumor microenvironment-controlled release layer on the surface of antibody-coated gold nanoparticles.

4.2.1.1 Construction and surface-funcationalization of gold nanoparticles (AuNPs)

The protocol for AuNPs synthesis was adapted from Aido et al (Aido et al., 2021a). In general, a 400 mg/L gold (III) chloride trihydragte solution was mixed with a 38.8 mM trisodium citrate solution, which functioned as a stabilizing agent providing a negtive charge. The mixture was heated and maintained at boiling for 10 mins to ensure the stable formation and homogeneous size distribution of AuNPs. Dynamic light scattering (DLS) and Ultraviolet-visible spectroscopy (UV-vis) were employed to characterize the freshly prepared AuNPs. The size of AuNPs was consistent with previous reports (Figure 9a) (Aido et al., 2021a), and the highest UV-vis absorption was detected at the wavelength of 530 nm (Figure 10a).

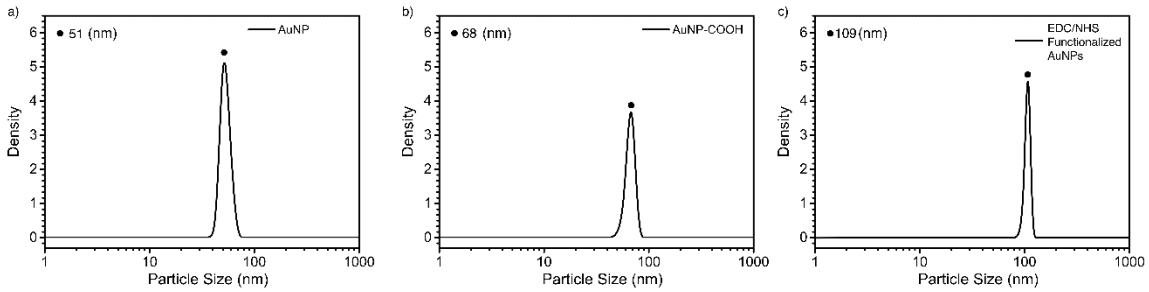

Figure 9: Dynamic light scattering measurements of AuNPs. Size of a) AuNPs, b) AuNP-COOH and c) EDC/NHS functionalized AuNPs measured by dynamic light scattering (DLS) using a Zetasizer Nano ZS instrument. In general, 1 µL of sample suspension was transferred into 1 mL MilliQ water, and the mixture was thoroughly

suspended and analyzed. All DLS experiments were carried out at a temperature of 25 °C.

To ensure the stability of AuNPs during the purification process, AuNPs were carboxylated. The carboxylated AuNPs (AuNP-COOH) were prepared by adding a positive-charged carboxyl-carrying polymer, HOOC-PEG-SH. Given the strong negative charge of the AuNPs, HOOC-PEG-SH was electromagnetically drawn towards them, leading to adsorption onto the nanoparticle surfaces. The particle size of charboxylated AuNPs was characterized by DLS. Upon carboxylation, an increase in AuNP size was measured with a diameter reaching approximately 68 nm (Figure 9b). Futher confirming the size increase, UV- visible spectroscopic analysis revealed a spectral redshift of 10 nm post-carboxylation, evidencing an amplified wavelength, and consequently indicating an increase in nanoparticle size (Figure 10b).

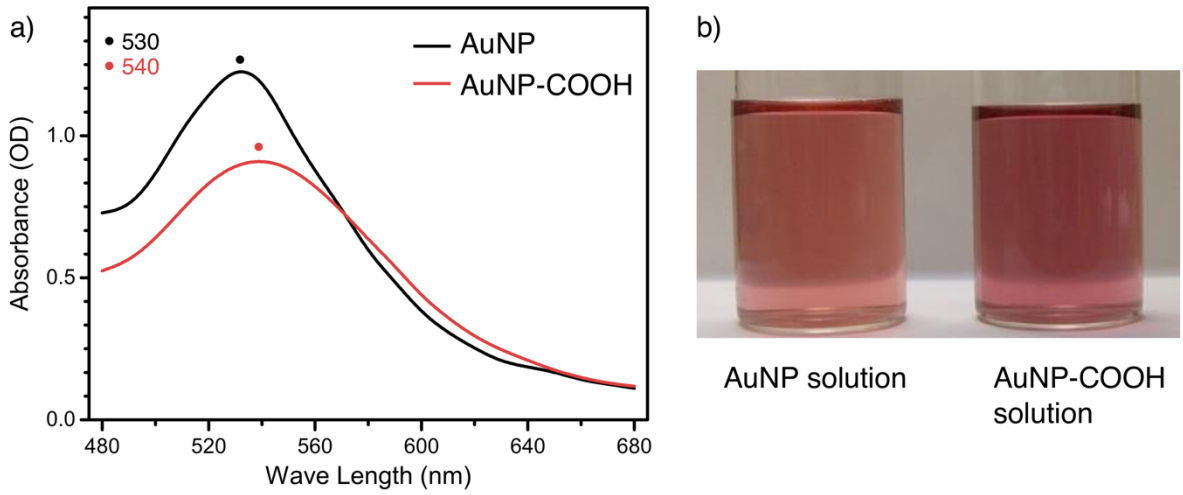

Figure 10: a) Ultraviolet-visible spectroscopy (UV-vis) of AuNPs and COOH-modified AuNPs; b) appearance of AuNP solution and AuNP-COOH solution under natural light.

4.2.1.2 Surface activation of AuNP-COOH by EDC/NHS

AuNP-COOH were activated using the carbodiimide crosslinker N-ethyl-N'-(3-(dimethylamino)propyl)carbodiimide (EDC) and purified antibodies. EDC selectively reacted with the carboxyl moieties present on AuNP-COOH, generating an activated intermediate primed for subsequent displacement by the amino groups of a protein, here the antibody. Given that EDC's reactivity is diminished under neutral pH conditions and in the presence of a phosphate buffer, N-hydroxysuccinimide (NHS) was concomitantly introduced to catalyze the conjugation reaction. Following this functionalization process, the particle size of EDC/NHS functionalized AuNPs was confirmed using dynamic light scattering (DLS). The particle size of EDC/NHS activated AuNPs was 109 nm, thus exhibiting an increase of 41nm compared to the initial size of AuNP-COOH (Figure 9c).

4.2.2 Antibody conjugation to AuNPs

Following the surface activation of the AuNPs with EDC/NHS, anti-Fn14 antibodies were conjugated, specifically PDL192 and 5B6. Subsequently the resulting antibody-conjugated AuNPs, PDL192-AuNPs and 5B6-AuNPs, were characterized with respect to particle size and zeta potential values (Table 6).

Table 10: Zeta potentials and particle sizes of EDC/NHS-modified AuNPs before and after antibody coupling.

Sample	Zeta potential	Particle size
EDC/NHS activated AuNPs	-25 mV	109 ± 3 nm
PDL192-AuNPs	11 mV	127 ± 10 nm
5B6-AuNPs	8 mV	133 ± 19 nm

4.2.3 Modification and characterization of modified polylysine (MPL)

Poly-L-lysine, a biodegradable and biocompatible polypeptide, is characterized by abundant free amino groups. These reactive moieties confer the potential for structural modification, thereby influencing the responsiveness of poly-L-lysine towards external stimuli such as enzymatic action, pH fluctuations, and temperature shifts (Chen et al., 2021). For the construction of a protective shell around antibody-conjugated gold nanoparticles (mAb-AuNP), the poly-L-lysine shell was chemically modified designed to undergo degradation exclusively within the tumor microenvironment (TME). The method employed for poly-L-lysine modification was adapted from (Qian et al., 2020) with certain changes. The molecule of MPL was synthesized through a chemical modification process in which ε-poly-L-lysine (ε-PL) was reacted with 2,3-dimethyl maleic anhydride (DMMA). This procedure facilitated the conversion of the amino group present on the lysine side chain into an amide bond, concurrently producing a carboxyl group that carries a negative charge. This carboxyl functionality is a significant result of the modification and plays a crucial role in the behavior and properties of the resultant MPL molecule.

To confirm the successful modification poly-L-lysine and its modified variant (MPL) were analyzed by Fourier transform infrared (FTIR) spectroscopy. Key absorption peaks within the mid-infrared and CH-stretching regions were identified for subsequent analysis (Figure 11). The vibrational peak frequencies and assignments for the poly-L-lysine were found to be consistent with those reported in prior literature (Jordan et al., 1994; De Campos Vidal & Mello, 2011). The mid-infrared spectrum of the MPL exhibited distinct peaks at 1711 and 1035 cm^{-1} that are absent in the unmodified poly-L-lysine spectrum. The peak at 1711 cm^{-1} is attributed to the COOH stretching vibrations of the carboxylic moieties, while the peak at 1035 cm^{-1} is assigned to the C-O stretching vibrations of the same groups. The presence of these peaks confirmed the introduction of carboxyl groups, thereby confirming the successful structural modification of the poly-L-lysine with DMMA.

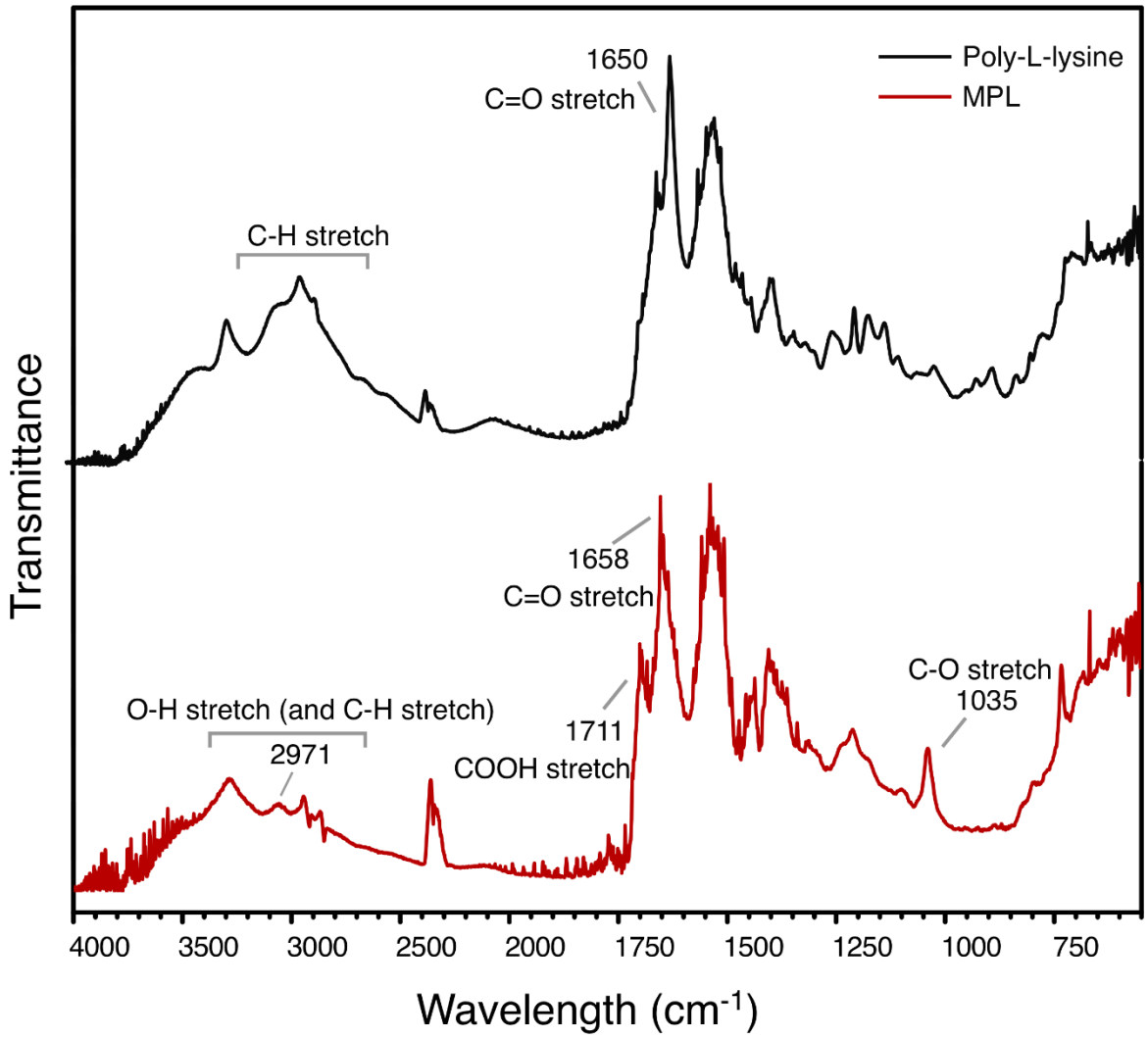

Figure 11: Characterization of MPL by Fourier-transform infrared spectroscopy. 10 mg of sample powder was pressed into a thin film, which was fixed on the holder for testing. The samples were scanned in the IR range from 400 to 4000 cm^{-1}. Several peaks are marked in the figure with explanations for the stretches.

Given the proposed mechanism wherein MPL engages in electrostatically interaction with antibody-AuNPs to establish the MPL shell, the zeta potential of MPL is crucial in determining the formation and stability of the MPL-antibody-AuNPs complex. Consequently, the zeta potentials of both MPL and the poly-L-lysine were assessed

(Figure 12). Poly-L-lysine, being a potent cationic polymer, demonstrates a pH-dependent trend in its aqueous zeta potentials, experiencing a decrease as pH values rise (Naassaoui & Aschi, 2019). The zeta potential from this study was close to the value reported in the referenced research (Naassaoui & Aschi, 2019). The zeta potential of MPL was ascertained to be 16.9 mV, reflecting a reduction of 21.4 mV from the original poly-L-lysine zeta potential. This decrease in zeta potential can be attributed to the introduction of carboxyl groups during the modification process, thereby enhancing the pH-responsiveness of MPL.

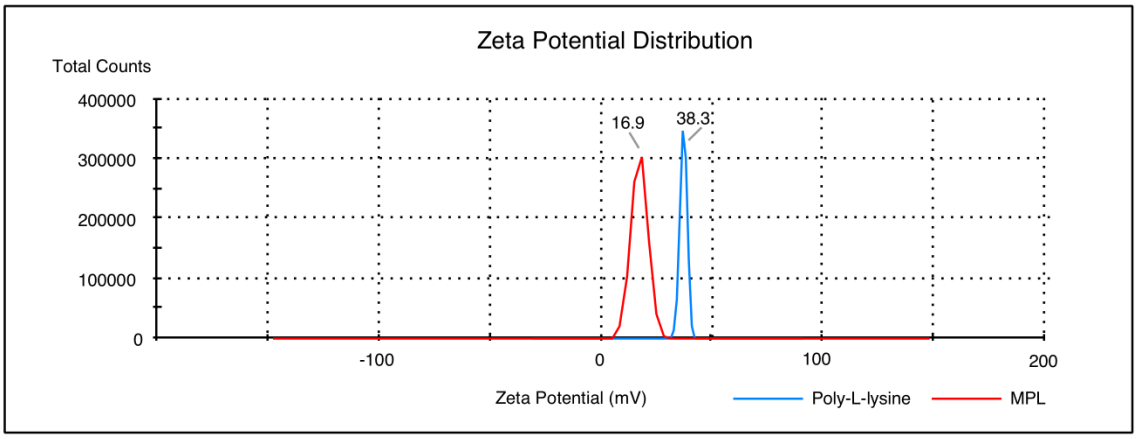

Figure 12: Zeta potential distribution of MPL. 2 mg of MPL powder was dispersed in 2 mL of phosphate-buffered saline (PBS) solution at pH 7.2. The sample was sonicated for 30 seconds until the MPL powder was fully dispersed. 1 mL of MPL dispersion was transferred into a folded capillary cell (Malvern, Worcestershire, UK) and the zeta potential was analyzed by utilizing a Zetasizer Nano ZS instrument.

4.2.4 Construction, characterization and functional analysis of MPL-PDL192-AuNPs and MPL-5B6-AuNPs complex

4.2.4.1 Construction and characterization of MPL-antibody-AuNP complexes

The MPL-antibody-AuNP complexes were synthesized by dispersing MPL powder into a solution containing PDL192-AuNP or 5B6-AuNP. The chemical modification of MPL yielded a positively charged polymer, while the antibody-AuNPs inherently carried a negative charge. The admixture of positively charged MPL with the negatively charged antibody-AuNPs enabled electrostatic interaction between the two components. This process facilitated the polyelectrolytes binding and subsequent neutralization of charges inherent to MPL and antibody-AuNP resulting in the formation of MPL-PDL192-AuNPs and MPL-5B6-AuNPs complex.

Subsequent to their formation, the MPL-antibody-AuNPs were suspended in phosphate-buffered saline (PBS) with varying pH levels (pH 6.0, 6.5, 7.0 and 7.5) to study the influence of the solution's environment on the stability of MPL-antibody-AuNP complexes. Particle sizes were characterized by Zetasizer (Figure 13). At neutral pH (7.5), the particle size reached 141 nm, and the broad size distribution indicated the occurrence of particle flocculation. Flocculation refers to a random process in which particles with opposite charges bind nondirectionally and non-selectively (Murthy et al., 2004). In this context, the concentrations of MPL and antibody-AuNPs significantly influenced the extent of aggregation observed for the MPL-antibody-AuNPs.

It was anticipated that a decrease in solution acidity would correspond with a reduction in particle size. Indeed, when the pH value fell below 6.5, the particle size reduced to 91 nm or lower. Given 91 nm closely matches the size of antibody-AuNPs, this observation suggests the disintegration of the MPL shell and the release of antibody-AuNPs from MPL-antibody-AuNP complexes. As reported in prior research (Qian et

al., 2020), increasing solution acidity diminishes the positive charge of MPL, thereby disrupting the charge equilibrium between MPL and antibody-AuNP.

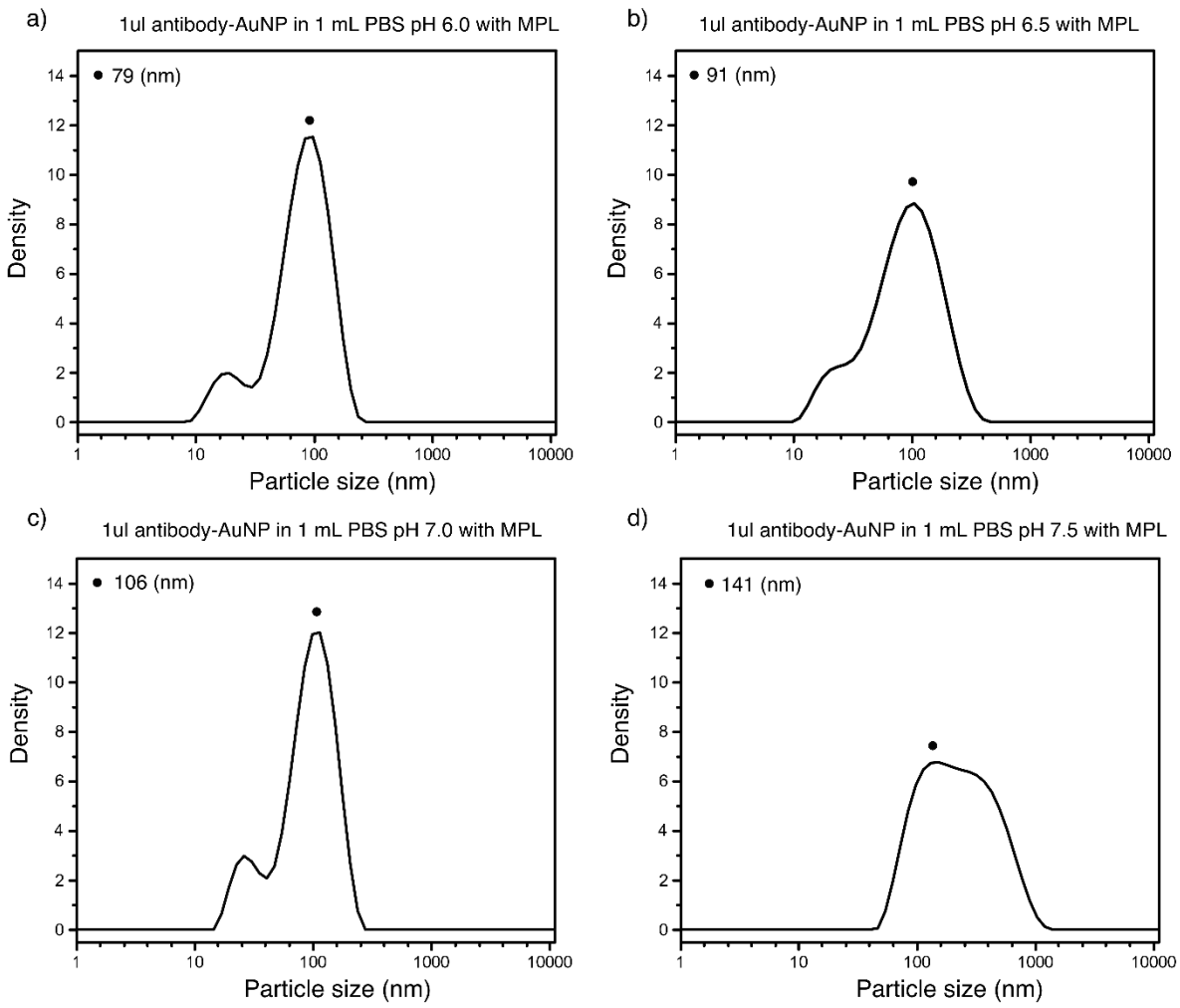

Figure 13: Size of antibody-AuNPs in PBS mixed with MPL at various pH levels a) 6, b) 6.5, c) 7 and d) 7.5 quantified by dynamic light scattering (DLS) using a Zetasizer Nano ZS instrument. In general, an aliquot of 10 µL of sample suspension was transferred into 1ml MilliQ water and the mixture was fully suspended and analyzed. All DLS experiments were carried out at a temperature of 25 °C.

Upon exposure of MPL to the low pH conditions of the TME, a reversal in its electric charge is induced. Consequently, the now negative-charged MPL and antibody-

AuNPs repel each other. To ensure the effective release of antibody-AuNPs within the TME, varying amount of MPL were incorporated into the MPL-antibody-AuNPs complex, and the resulting zeta potentials were quantified by Zetasizer.

As illustrated in Figure 14, the zeta potential exhibited a direct correlation with the amount of MPL employed, although only a negligible difference in zeta potential was observed between samples prepared with 1.5 mg and 1 mg MPL. This observation could potentially be ascribed to a saturation effect in the binding between MPL and antibody-AuNPs. Additionally, a progressive increase in the MPL shell breaking point was noted with escalating amount of MPL for all test groups. When 1.5 mg of MPL was utilized in the formulation, the shell breaking point was observed to occur between pH 7.0 and 7.5. Thus, for subsequent experimental procedures, MPL-antibody-AuNPs were prepared using 0.5 mg of MPL.

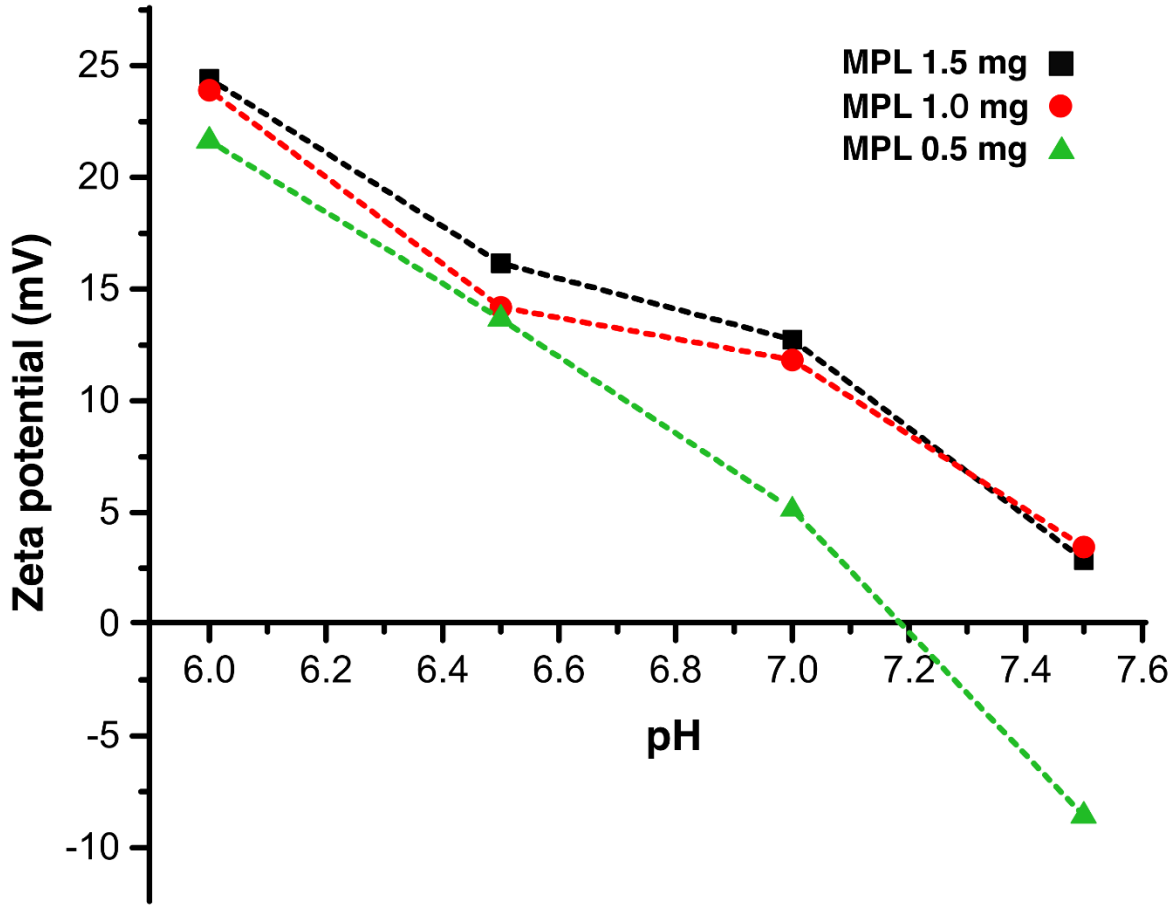

Figure 14: The zeta potential of antibody-AuNP in PBS with varying amount of MPL and at different pH conditions. MPL powder (0.5, 1, 1.5 mg) was separately dispersed in 1 mL of PBS pre-adjusted to different pH values. The samples were then sonicated for a duration of 30 seconds to ensure complete dispersion of the MPL powder. Subsequently, 1 mL of the MPL dispersion was mixed with 10 µL of the antibody-AuNPs solution. This mixture underwent 10 seconds sonication before being transferred into a folded capillary cell (Malvern, Worcestershire, UK) in preparation for zeta potential measurement using a Zetasizer Nano ZS instrument.

4.2.4.2 Release study and functionality analysis of MPL-antibody-AuNPs

An in vitro release study was conducted to evaluate both the stability of MPL-antibody-AuNPs in a neutral environment and their potential for releasing antibody-AuNPs within the TME. Given the inherent pH gradient between physiological body fluids and the TME, the release profiles of MPL-antibody-AuNPs were investigated under three distinct pH conditions: 6.5, 7 and 7.5.

As depicted in Figure 15, MPL-antibody-AuNPs reached a release plateau within the initial hour of observation. Notably, across all release profiles, both MPL-PDL192-AuNPs and MPL-5B6-AuNPs reached their peak concentrations within the pH 6.5 media, amounting to 0.6 mg/mL for MPL-PDL192-AuNPs and 0.3 mg/mL for MPL-5B6-AuNPs. As anticipated, a rise in media pH correlated with a decrease in both antibody-AuNPs concentrations and their release rates, suggesting that media acidity facilitated the dissolution of the MPL shell, thereby promoting the release of antibody-AuNPs. Furthermore, the release rates and maximum concentrations of MPL-PDL192-AuNPs in the three media exceeded those of MPL-5B6-AuNPs. This observation aligns with the theoretical expectation that the pKa difference between PDL192 and 5B6 would exert an impact on their respective release rates.

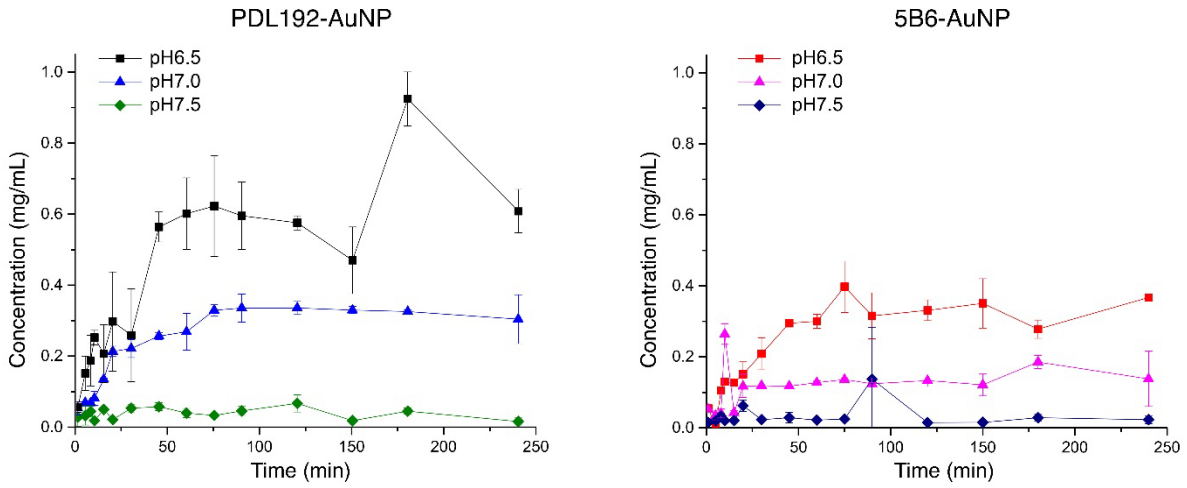

Figure 15: The release profiles of MPL-PDL192-AuNPs and MPL-5B6-AuNPs in PBS of pH 6.5, 7.0 and 7.5. MPL (0.5 mg) was premixed with PDL192-AuNPs and 5B6-AuNPs, respectively, and then the mixture was introduced into solutions with varying pH levels. At specific time intervals, a 1uL sample was extracted from the solution, and the UV absorbance was measured at the wavelength of 280 nm using NanoDrop (ND-1000, Thermal Fisher Scientific, UK).

To verify the efficacy of MPL-PDL192-AuNPs and MPL-5B6-AuNPs within a neutral environment and the TME, a series of in vitro functional assays were implemented. In brief, HT1080 cells were cultured in 96-well plates. The following day, the cell culture media were refreshed and adjusted to pH levels of 6.5, 7 and 7.5. Subsequently, cells were stimulated with MPL-PDL192-AuNPs, MPL-5B6-AuNPs, and Flag-TWEAK (pH 7.5) in the presence and absence of anti-Flag. The next day, IL-8 concentrations in the cell supernatants were analyzed using ELISA as a readout for the activation Fn14-induced NFκB signaling. As illustrated (Figure 16), both MPL-PDL192-AuNPs and MPL-5B6-AuNPs demonstrated potent agonistic effect at pH 6.5, similar to the effect of TWEAK in the presence of anti-Flag. As the acidity of the cell culture media decreased, a corresponding weakening of the agonistic effect was observed.

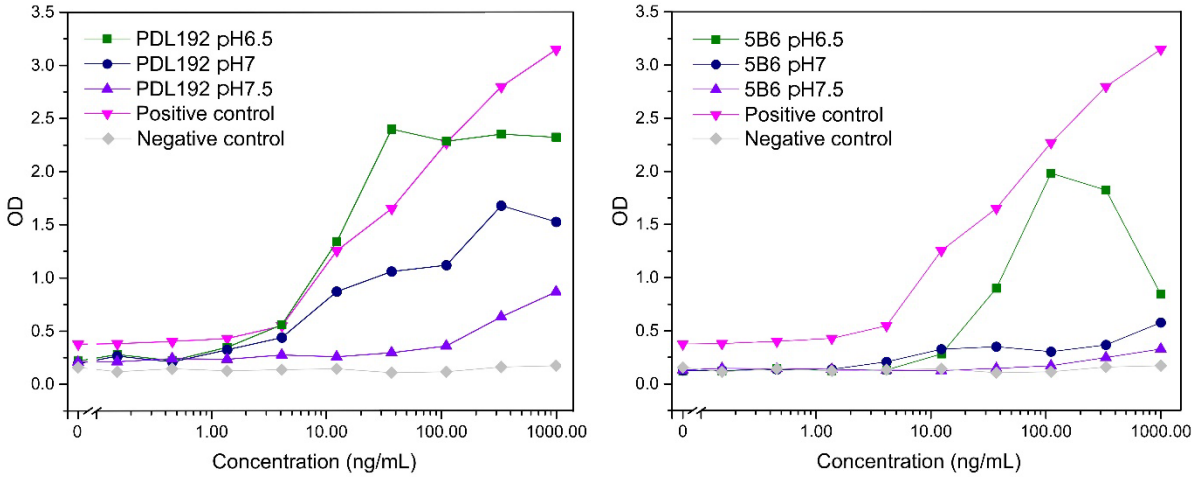

Figure 16: Functionality analysis of MPL-antibody-AuNPs. HT1080 cells were cultured in 96-well plates, and the following day, the cell culture media were refreshed and adjusted to pH levels of 6.5, 7 and 7.5. Subsequently, cells were stimulated with MPL-PDL192-AuNPs, MPL-5B6-AuNPs, and Flag-TWEAK, both in the presence and absence of anti-Flag (served as negative and positive control, respectively). The next day, IL-8 concentration in the cell supernatants were analyzed using ELISA as a readout for the activation of NFκB signaling.

5 Discussion:

5.1 The activation of Fn14 by Fn14-targeting bispecific antibody fusion proteins

Over the past decade, significant progress has been made towards developing innovative antibody-based immunotherapies that target TNF family receptors/ligands. Nevertheless, the clinical applicability of these therapies is constrained by formidable challenges. These impediments include the induction of destructive autoimmunity, the inadequacy of effective delivery of tumor antigens to immune cells, non-specific and/or off-target effects, the tumor microenvironment's self-attenuation, and the inadequate penetration of immunotherapeutic agents into the tumor's aberrant extracellular matrix (ECM) (Phan et al., 2003; Munn & Bronte, 2016; Buabeid et al., 2020a). To address these challenges, ongoing research efforts are focused on the development of novel strategies, such as design of immunotherapeutic agents with enhanced activity, the optimization of dosing schedules, and the integration of these therapies with other therapeutic modalities, such as chemotherapy or radiotherapy (Le et al., 2022; Z. Zhang et al., 2022).

The Fn14/TWEAK pathway, due to its multi-faceted role in oncogenesis, presents a compelling target for immunotherapy. Nevertheless, Fn14 is acknowledged to be one of the TNFRSF receptors (TNFRs) that can only be fully activated by membrane-bound ligand molecules (Grell et al., 1995; Grell, Wajant, Zimmermann, & Scheurich, 1998; Kucka&Wajant, 2021). In this context, the capacity of Fn14-targeted drugs to establish Fn14 complexes influences the Fn14 response to these interventions. Aiming to augment the effectiveness of non-membrane-associated Fn14-targeted agents, we generated a panel of bispecific antibodies against Fn14 in this study. As depicted in the schematic structure of the examined antibody fusion proteins (Figure 4), single-chain fragment variable (scFv) domains are linked to the C-terminus of the 18D1 anti-Fn14 antibody heavy chains. The scFvs served as anchoring domains because these domains are capable of recognizing tumor antigens exposed on the

cell surface or antigens present in the tumor stroma (Wajant, 2015; Wajant, 2019). The use of an anchor domain (AD) not only converts soluble TNFLs or anti-TNFR antibody fusion proteins into potent TNFR agonists, but also provides space for a secondary activity. In a prior study from our group, antibodies specific for the TNFRSF members CD40 and CD95 were genetically conjoined with a single-chain B-cell activating factor (scBaff) trimer, serving as a C-terminal myeloma-specific anchoring domain (Nelke et al., 2020). The resultant bispecific antibody fusion proteins manifested a robust agonistic effect on CD40- and CD95-responsive cells when co-cultured with BaffR, BCMA, or TACI-expressing anchoring cells, whereas only minor receptor stimulation was discerned in co-cultures with cells devoid of Baff-interacting receptor expression. Within the present study, binding analyses of the 13 18D1-AD fusion proteins were conducted on HEK293 cells transiently expressing the anchoring targets by help of 18D1-AD variants with a GpL reporter domain (Figures 5, 6, and 7). The results demonstrated that 18D1-AD fusion proteins with ADs specific for hCD38 (scFv:CD38), hCD70 (scFv:CD70), murine TNF2 (scmuTNF80), hTNFR2 (scFv:TNFR2), hCD20 (scFv:CD20), and hCD19 (scFv:CD19) indeed, bind with high affinity towards their corresponding targets (Figure 7). In contrast, 18D1-AD fusion proteins anchoring to human Baff receptors BaffR/BCMA (scBaff, scFv:BCMA) and muCD70 (scFv:muCD70) exhibited a relatively low affinity for their corresponding targets. Additionally, the 18D1 fusion proteins binding to PDL1 (scFv:muPDL1) and muCD20 (scFv:muCD20) demonstrated no detectable binding affinity for the corresponding receptors expressed on HEK293 cells.

In the subsequent functionality analysis, most of the 18D1-AD fusion proteins exhibited robust Fn14 receptor activation capability in the presence of cells expressing the corresponding anchoring target (Figure 8). These findings ascertain that crosslinking and oligomerization significantly augment the potency of bispecific 18D1-AD fusion proteins. Similarly, antibody fusion proteins with an anchoring domain have been reported to induce potent receptor activation in a FcγR-independent manner upon binding to their respective anchoring domain on an exposed plasma membrane-bound

target (Nelke et al., 2020). It is clear that the boosted responsiveness of category II TNFRs to antibody-AD fusion proteins does not arise from augmented receptor occupancy, but rather from an enhanced capacity of plasma membrane-anchored antibodies to promote TNFR oligomerization (Wajant, 2014). Moreover, controlled oligomerization of soluble TNFL trimers can also be achieved through genetic engineering, such as an N-terminal Flag tag plus anti-flag antibody or fusion with a multimerization domain, thereby resulting in molecules with defined stoichiometry (Bossen et al., 2008b; Medler et al., 2019; Wyzgol et al., 2009). It is imperative to note that oligomerization of soluble TNFLs does not intrinsically increase their affinity for TNFRs (Fick et al., 2012a; Lang et al., 2012). Studies indicate that soluble TNFLs can be converted into potent category II TNFR agonists by physically linking two or more ligand trimers (Kucka & Wajant, 2021). Furthermore, natural oligomerization of soluble TNFLs has been reported, as demonstrated in soluble CD95L found in bronchoalveolar lavage fluid of acute lung injury patients, wherein oxidation-triggered aggregation enhances CD95-mediated cell death (Herrero et al., 2011). Similarly, soluble Baff appears as both a trimeric protein and a 60-mer, with the latter exhibiting a hundred-fold higher TACI signaling capacity (Bossen et al., 2008a).

5.2 Construction and functional analysis of MPL-antibody-AuNPs

5.2.1 Construction of antibody-gold nanoparticles (antibody-AuNPs)

Despite considerable progress in immunotherapies over the past decade, numerous obstacles concerning therapeutic efficacy and safety continue to impede their potential. For instance, the incidence of hepatotoxicity and immunogenicity, provoking nonspecific liver toxicity and inflammatory responses respectively, complicates the treatment of inaccessible tumors (Le et al., 2022). Moreover, the intricate tumor microenvironment (TME) poses a considerable barrier that restricts the application of existing immunotherapies (Han et al., 2020). In addition to these, the inherent instability and short half-life of such immunotherapies necessitate high doses of

therapeutic agents, potentially leading to toxicity and severe side effects in a subset of patients. As a consequence, numerous studies have explored the combination of immunotherapy and nanoparticulate systems to enhance the therapeutic index. This approach aims to facilitate the delivery of immunotherapeutic agents directly to the target tumor site, increasing local accumulation and efficacy, while minimizing systemic toxicity associated with dose-dependent effects (Buabeid et al., 2020b).

In recent years, AuNPs have been extensively exploited in the scientific community as platforms for bioconjugation and biosensing, primarily due to their unique surface characteristics, optical properties, stability, and uniformity (Sardar et al., 2009). The ability to modify the surface of AuNPs enables the attachment of a wide array of molecules, ranging from peptides, oligonucleotides, enzymes, and DNA, to antibodies via physical adsorption or chemical bonding (L. Zhang et al., 2020). In this study, a formulation that combines MPL with AuNPs was developed to facilitate the delivery of Fn14-targeting antibodies. In this context, the AuNP served as an anchoring platform that promoted their oligomerization. Techniques including ultraviolet-visible spectroscopy (UV-vis) and dynamic light scattering (DLS) were utilized to characterize the in-situ properties of AuNPs and AuNP-COOH. DLS data (Figure 9) revealed the average size of AuNPs to be approximately 51 nm, with a distinct sharp peak that suggested the presence of spherical and stable AuNPs (Haiss et al., 2007; Sardar et al., 2009). The introduction of a positively charged, carboxyl-group bearing polymer, HOOC-PEG-SH, led to a 16 nm increase in the size of AuNPs. This provided evidence of successful conjugation of the carboxyl group (-COOH) to the surface of the AuNPs. Further verification of the carboxyl group attachment was provided by UV-vis spectrum results (Figure 10.a), which showed a shift in the maximum absorption wavelength from 530 nm to 540 nm. Additionally, a color change was observed, reflecting the increment in particle size (Figure 10.b).

Subsequently, 18D1 or 18D1 antibody fusion proteins were conjugated to AuNP-COOH using EDC/NHS as a catalyst. While antibodies can be conjugated to the surface of AuNPs via electrostatic interactions or cysteine group binding, the instability

of antibody-AuNP conjugates under variable physiological conditions could compromise antigen-binding capacity and potentially lead to antibody detachment. As depicted in figure 17, the conjugation process involves EDC reacting with carboxylic acid groups on AuNP-COOH to generate an active O-acylisourea intermediate. The latter is displaced by a nucleophilic attack from primary amino groups present in the mixture, resulting in the formation of an amide bond with the original carboxyl group, and subsequent release of an EDC by-product as a soluble urea derivative (de Mol & Fischer, 2010). However, the O-acylisourea intermediate is unstable in aqueous environments, and failure to react with an amine from antibodies results in hydrolysis, regeneration of carboxyls, and release of N-unsubstituted urea. While EDC crosslinking is optimal under acidic conditions (pH 4.5), antibodies exhibit stability in phosphate buffer at a neutral pH (approximately 7.2). While this condition is compatible with the reaction chemistry, the efficiency is significantly reduced. Therefore, NHS was incorporated into the reaction to enhance efficiency and establish dry-stable (amine-reactive) intermediates. EDC facilitates the coupling of NHS to carboxyls, creating an NHS ester, a more stable derivative than the O-acylisourea intermediate, thereby promoting effective conjugation to primary amines under physiological pH conditions.

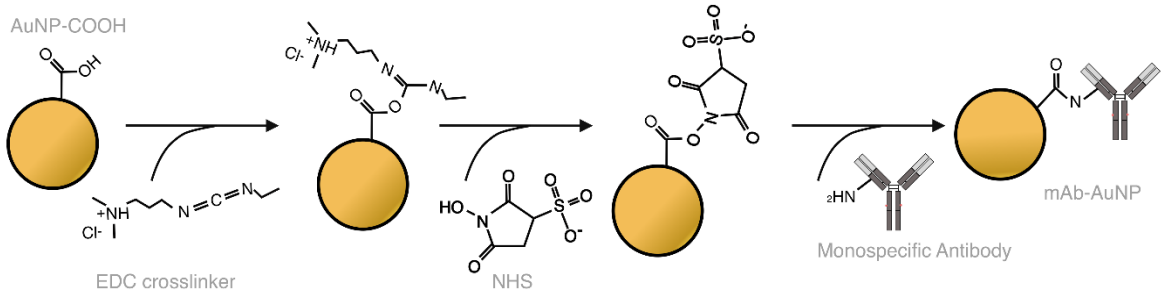

Figure 17: Antibody crosslinking to AuNP-COOH assisted by EDC/NHS.

Following the conjugation reaction, DLS measurements of each antibody-AuNP displayed an increase in diameter due to surface passivation and the successful antibody conjugation (Figure 9 and Table 6). The observed increase of approximately 26 nm aligns with previous reports indicating that the longest axis of an antibody measures around 30 nm, under the assumption that no other factors are contributing (James & Driskell, 2013). To assure complete coverage of AuNP-COOH with antibodies, an antibody solution with a concentration of app. 500 µg/ml was necessary. Suboptimal antibody concentrations could potentially facilitate the formation of dimers and trimers of AuNP-COOH, leading to stable intermediates via dipole interactions from asymmetric charge distributions. This scenario might precipitate aggregation and resultant undesirable particle sizes (Montenegro et al., 2013; A. Wang et al., 2016). Additionally, following conjugation, a marked rise in the ζ-potential of the particles was noted, indicating an alteration in the surface charge due to the antibody binding. The changes in ζ-potential correlate with the DLS diameters by number (Table 6), with the most prominent ζ-potential value alterations coinciding with the most significant increases in size.

5.2.2 Modification and characterization of MPL

Poly-L-lysine, a biodegradable and biocompatible polymer, exhibits robust interaction with DNA and negatively charged proteins, rendering it a subject of extensive exploration for biomedical utilities, such as gene therapy vehicles and anti-cancer drug delivery (Eetezadi et al., 2015; M. Zheng et al., 2021). As a cationic polypeptide, poly-L-lysine possesses numerous free amino groups, offering potential for structural modification. The interaction between cationic poly-L-lysine and the anionic membranes of erythrocytes and vascular endothelial cells often causes hemolysis and cytotoxicity (Hall et al., 2015). High-molecular-weight poly-L-lysine is perceived as more cytotoxic than its low-molecular-weight counterpart due to its more substantial adverse effects on mitochondrial oxidative phosphorylation and glycolytic activity,

culminating in severe intracellular ATP depletion and triggering necrotic cell death (Hall et al., 2015). Therefore, this study utilizes low-molecular-weight poly-L-lysine (3 kDa). By altering the structure of poly-L-lysine, a decline in the ζ-potential is anticipated, subsequently diminishing cytotoxicity. Fourier Transform Infrared (FTIR) spectroscopy was employed to confirm successful structural modification (Figure 11). The MPL spectrum exhibited peaks at 1711 and 1035 cm^{-1}, assignable to the COOH stretch of carboxyl acid groups and the C-O stretch of carboxylic acid groups, respectively. Further evidence for the successful chemical modification was provided by the ζ-potential (Figure 12). The metric declined from 38.3 mV to 16.9 mV, indicating a reduction in the “cationicity” of the polymer. Strong cationic charges associated with poly-L-lysine have been reported to result in the formation of a spherical floc structure of poly-L-lysine AuNPs, with particle size escalating over time due to charge-induced flocculation and particle aggregation. This phenomenon occurs when polyelectrolyte molecules adsorb onto several oppositely charged colloidal particles, and these particles can bind to multiple polyelectrolyte chains (Murthy et al., 2004). Hence, the decrease in cationic charge following the transition from poly-L-lysine to MPL assists in preventing a substantial size increase when MPL is mixed with antibody-AuNPs.

5.2.3 Composition of MPL-antibody-AuNPs

For decades, electrostatic charging has been utilized in the synthesis of composite micro- and nanoparticles, control of nanoparticle size, and production of various categories of non-spherical polymer particles via interparticle interactions during particle growth (Koehler et al., 2014). In this study, the MPL-antibody-AuNPs were synthesized via electrostatic attraction by dispersing MPL powder into the antibody-AuNP solution. MPL was chemically modified into a negatively charged polymer when exposed to neutral environment, while antibody-AuNPs carried a positive charge. The introduction of negatively charged MPL into the positively charged antibody-AuNP solution led to electrostatic interaction between MPL and antibody-AuNPs. During this

process, the polyelectrolytes formed a complex and the charges on MPL and antibody-AuNP were neutralized, leading to the formation of MPL-antibody-AuNPs. To achieve TME-targeted release of MPL-antibody-AuNPs, the shell of MPL-antibody-AuNPs should undergo disintegration upon entry into the TME, subsequently releasing the antibody-AuNPs. The mechanism here involves a pH shift from a normal physiological environment (pH 7.2) to the TME (pH 6.8), triggering the charge reversal of MPL from negative to positive (Figure 18). Therefore, the charge reversal of MPL in response to environmental pH changes is of significant interest. To ensure that the MPL charge reversal point is achieved when the solution's pH is altered to 6.5, different MPL quantities were mixed with antibody-AuNPs: 0.5, 1, and 1.5 mg.

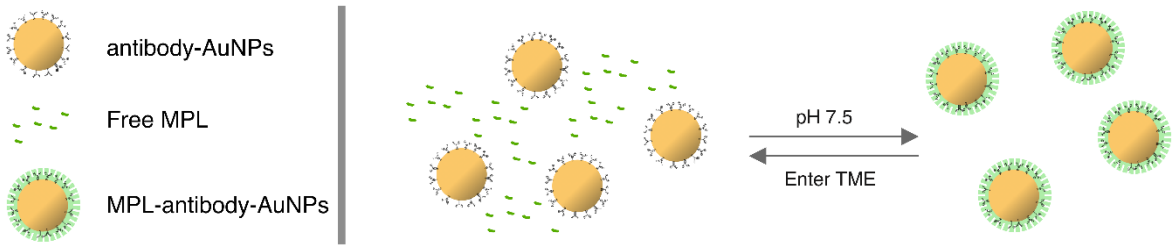

Figure 18: schematic illustration of composition and decomposition of MPL-antibody-AuNPs

As depicted in Figure 14, the ζ-potential demonstrated a consistent trend with pH alteration at a fixed MPL quantity, indicating that the ζ-potential of MPL-antibody-AuNPs decreased with increasing pH. This observation aligns with results obtained from parallel studies (Naassaoui & Aschi, 2019). Additionally, the ζ-potential increases with an increment in the MPL quantity, which is anticipated given that MPL in its isolated state carries a positive charge. For the 1.0 mg and 1.5 mg MPL groups, the ζ-potential persisted as positive throughout the entire pH spectrum. Interestingly, when 0.5 mg of MPL was mixed with antibody-AuNPs, the ζ-potential slightly transitioned from positive to negative, indicating the negative surface charge of MPL. Under this

condition, the electrostatic attraction between negatively charged MPL and positively charged antibody-AuNPs became significant, leading to the formation of MPL-antibody-AuNPs. Based on this observation, MPL-18D1-AuNPs were prepared using this specific MPL: antibody-AuNP ratio.

To further confirm the successful construction of MPL-antibody-AuNPs complexes at pH 7.5, and the effective release of antibody-AuNPs at pH 6.5, freshly prepared MPL-antibody-AuNPs were dispersed in PBS of varied pH values, and the particle size was analyzed by DLS (Figure 13). As predicted, the particle size decreased in accordance with the increased acidity of the solution; when the pH fell below 6.5, the particle size diminished to 91 nm or lower. As reported in existing literature (Qian et al., 2020), the increase in solution acidity reduces the negative charge of MPL and triggers an electric charge reversal, thereby disrupting the charge equilibrium between MPL and antibody-AuNP. Under this circumstance, the positively charged MPL and antibody-AuNPs engaged in a repulsive interaction, leading to the release of the antibody-AuNP. Given that 91 nm is closely approximated to the size of antibody-AuNP, this finding implies the disassembly of the MPL shell and the subsequent release of antibody-AuNP from the MPL-antibody-AuNPs.

5.3 Release study and functionality analysis of MPL-antibody-AuNPs

Advancements in nanotechnology and material science have facilitated the development of diverse polymeric nanoparticles, which display superior properties such as biodegradability, biocompatibility, aqueous solubility, chemical stability, and a high capacity for encapsulating immunostimulants (S. Li et al., 2018). Furthermore, polymeric nanoparticle-based drug delivery systems possess properties such as an extensive range of flexible particle size (from 1 nm to 10 mm), controllable release profiles, and the capability for targeted delivery of therapeutic agents to cancer tissues, together with wide-ranging applicability to various forms of cancer (Madej et al., 2022).

A study by Qian et al., 2020, reported the use of MPL as a shell for encapsulating drug-peptide conjugates (Qian et al., 2020). The MPL shell exhibited pH-dependent disintegration properties, maintaining its stability in neutral or basic buffer conditions (pH equal or greater than 7.0), but undergoing decomposition in acidic buffer conditions (pH less than 7.0). This phenomenon has been attributed to the charge-switching property of MPL, which maintains a negative charge in normal physiological tissues, but undergoes a transition to a positive charge upon exposure to the acidic TME, thereby facilitating the release of the positively charged drug-peptide conjugate. Following the injection of the MPL-shelled drug-peptide conjugate to murine models, no significant activity was detected in liver, heart, kidney, or spleen sections. In contrast, significant accumulation of the MPL-drug-peptide conjugate was observed at tumor sites, indicating effective delivery of therapeutic agent and high biocompatibility (Qian et al., 2020). Moreover, in vivo antitumor and anti-metastasis efficacy was observed in mice treated with the MPL--drug-peptide conjugate. These observations suggest that MPL could serve as a promising biocompatible polymeric delivery platform for large biomolecules.

In this study, MPL was utilized in a similar fashion to deliver the Fn14-targeting monospecific antibody into the TME. Based on the in vitro release profiles of MPL-PDL192-AuNPs and MPL-5B6-AuNPs, an increase in solution acidity facilitated the release of PDL192-AuNPs and 5B6-AuNPs, reaching peak concentrations of 0.6 mg/mL and 0.35 mg/mL, respectively. The observed variance in release between PDL192 and 5B6 may be attributed to differences in charge, with PDL192 possessing a higher surface charge than 5B6 (Table 6). Research indicates that nanoparticle disintegration can only ensue if the electrostatic disparity between the cargo encapsulated within the nanoparticle (herein, antibody-AuNPs) and the encasing shell (MPL) is substantial enough to instigate effective repulsion (Koehler et al., 2014). As 5B6 exhibits a lower ζ-potential, its negative charge is not as strong as that of PDL192. As a result, the repulsion between 5B6 and MPL at pH 6.5 fails to be potent enough

to dissociate all MPL-5B6-AuNPs, leading to a peak 5B6-AuNPs concentration that is only half of the peak concentration of PDL192.

6. Conclusion:

Over the past decade, significant progress has been taken towards creating innovative antibody-based immunotherapies that target TNF family receptors/ligands, while some of these potential treatments have moved into various clinical research stages. Nevertheless, their clinical applicability is constrained by formidable challenges. The major challenge remains formulating an immunotherapeutic agent that demonstrates potent antitumor efficacy while exhibiting excellent tumor-targeting properties and low cytotoxicity on normal cells. Consequently, numerous studies have explored the combination of immunotherapy and nanoparticulate systems to enhance the therapeutic index. This approach aims to facilitate the delivery of immunotherapeutic agents directly to the target tumor site, increasing local accumulation and efficacy, while minimizing systemic toxicity associated with dose-dependent effects. Gold nanoparticles have been extensively exploited in the scientific community as platforms for bioconjugation and biosensing in recent years, primarily due to their unique surface characteristics, optical properties, stability, and uniformity. The ability to modify the surface of AuNPs enables the attachment of a wide array of molecules, ranging from peptides, oligonucleotides, enzymes, and DNA, to antibodies via physical adsorption or chemical bonding.

In this study, we developed an innovative nanoparticle formulation to facilitate the delivery of antitumor antibodies to tumor sites. The study commenced with the utilization of 13 bispecific antibody fusion proteins, which targeted the Fn14 receptor, thereby validating the pivotal role of crosslinking in Fn14 receptor activation. Subsequently, gold nanoparticles were activated using COOH-PEG-SH in combination with EDC/NHS, and subsequently conjugated with two Fn14-targeting antibodies, PDL192 and 5B6. Following this, a pH-sensitive shell was generated on the outer layer of the antibody-coupled gold nanoparticles through the application of chemically modified polylysine. The resultant complexes, termed MPL-antibody-AuNP, demonstrated a release profile reminiscent of the tumor microenvironment (TME). Notably, these complexes released antibody-AuNPs only in slightly acidic conditions while remaining intact in neutral or basic environments. Functionality analysis further affirmed the pH-sensitive property of MPL-antibody-AuNPs, demonstrating that the antibodies only initiated potent Fn14 activation in slightly acidic environments. This formulation holds potential for applicability to antibodies or ligands targeting the

TNFRSF family, given that gold nanoparticles successfully served as platforms for antibody crosslinking, thereby transforming these antibodies into potent agonists. Moreover, the TME disintegration profile of MPL mitigates the potential cytotoxic effects of antibodies, thereby circumventing associated adverse side effects.

This study not only showcases the potential of nanoparticle formulations in targeted therapy, but also provides a solid foundation for further investigations on their clinical application in the context of targeting category II TNFRSF receptors with antibodies or ligands.

7. Schlussfolgerung:

Im vergangenen Jahrzehnt wurden bedeutende Fortschritte bei der Entwicklung innovativer, auf Antikörpern basierender Immuntherapien gemacht, die auf TNF-Familienrezeptoren/-liganden abzielen. Einige dieser potenziellen Behandlungen haben verschiedene klinische Forschungsphasen erreicht. Dennoch wird ihre klinische Anwendbarkeit durch erhebliche Herausforderungen eingeschränkt. Die größte Herausforderung besteht darin, einen immuntherapeutischen Wirkstoff zu formulieren, der eine starke antitumorale Wirksamkeit zeigt, hervorragende tumorzielende Eigenschaften aufweist und eine geringe Zytotoxizität auf normalen Zellen hat. Folglich haben zahlreiche Studien die Kombination von Immuntherapie und nanopartikulären Systemen untersucht, um den therapeutischen Index zu erhöhen. Dieser Ansatz zielt darauf ab, die Lieferung von immuntherapeutischen Wirkstoffen direkt zur Ziel-Tumor-Stelle zu erleichtern, die lokale Ansammlung und Wirksamkeit zu erhöhen und gleichzeitig die systemische Toxizität zu minimieren, die mit dosisabhängigen Effekten verbunden ist. Goldnanopartikel wurden in der wissenschaftlichen Gemeinschaft in den letzten Jahren umfassend als Plattformen für Bio-Konjugation und Biosensorik genutzt, hauptsächlich aufgrund ihrer einzigartigen Oberflächeneigenschaften, optischen Eigenschaften, Stabilität und Gleichförmigkeit. Die Fähigkeit, die Oberfläche von AuNPs zu modifizieren, ermöglicht die Anbindung einer Vielzahl von Molekülen, von Peptiden, Oligonukleotiden, Enzymen und DNA bis hin zu Antikörpern durch physikalische Adsorption oder chemische Bindung.

In dieser Studie entwickelten wir eine innovative Nanopartikel-Formulierung, um die Lieferung von Antitumor-Antikörpern zu Tumorstellen zu erleichtern. Die Studie begann mit der Verwendung von 13 bispezifischen Antikörper-Fusionsproteinen, die den Fn14-Rezeptor zielten, wodurch die zentrale Rolle des Crosslinkings bei der Fn14-Rezeptoraktivierung validiert wurde. Anschließend wurden Goldnanopartikel mit COOH-PEG-SH in Kombination mit EDC/NHS aktiviert und anschließend mit zwei Fn14-zielenden Antikörpern, PDL192 und 5B6, konjugiert. Danach wurde eine pH-sensitive Hülle auf der äußeren Schicht der mit Antikörpern gekoppelten Goldnanopartikel erzeugt, durch die Anwendung von chemisch modifiziertem Polylysin. Die resultierenden Komplexe, als MPL-Antikörper-AuNP bezeichnet, zeigten ein Freisetzungsprofil, das an das Tumormikroumfeld (TME) erinnert.

Bemerkenswerterweise setzten diese Komplexe Antikörper-AuNPs nur in leicht sauren Bedingungen frei, während sie in neutralen oder basischen Umgebungen intakt blieben. Eine Funktionalitätsanalyse bestätigte weiterhin die pH-sensitive Eigenschaft von MPL-Antikörper-Au

8. Reference

Aido, A., Zaitseva, O., Wajant, H., Buzgo, M., & Simaite, A. (2021a). Anti-fn14 antibody-conjugated nanoparticles display membrane tweak-like agonism. *Pharmaceutics*, *13*(7). https://doi.org/10.3390/pharmaceutics13071072

Aido, A., Zaitseva, O., Wajant, H., Buzgo, M., & Simaite, A. (2021b). Anti-fn14 antibody-conjugated nanoparticles display membrane tweak-like agonism. *Pharmaceutics*, *13*(7). https://doi.org/10.3390/PHARMACEUTICS13071072/S1

Amina, S. J., & Guo, B. (2020). A review on the synthesis and functionalization of gold nanoparticles as a drug delivery vehicle. *International Journal of Nanomedicine*, *15*, 9823–9857. https://doi.org/10.2147/IJN.S279094

Aronin, A., Amsili, S., Prigozhina, T. B., Tzdaka, K., Rachmilewitz, J., Shani, N., Tykocinski, M. L., & Dranitzki Elhalel, M. (2013). Fn14•TRAIL effectively inhibits hepatocellular carcinoma growth. *PloS One*, *8*(10). https://doi.org/10.1371/JOURNAL.PONE.0077050

Avilés-Jurado, F. X., Terra, X., Gómez, D., Flores, J. C., Raventós, A., Maymó-Masip, E., León, X., Serrano-Gonzalvo, V., Vendrell, J., Figuerola, E., & Chacón, M. R. (2015). Low blood levels of sTWEAK are related to locoregional failure in head and neck cancer. *European Archives of Oto-Rhino-Laryngology : Official Journal of the European Federation of Oto-Rhino-Laryngological Societies (EUFOS) : Affiliated with the German Society for Oto-Rhino-Laryngology - Head and Neck Surgery*, *272*(7), 1733–1741. https://doi.org/10.1007/S00405-014-3095-2

Bacher, S., & Schmitz, M. L. (2005). The NF-kB Pathway as a Potential Target for Autoimmune Disease Therapy. *Current Pharmaceutical Design*, *10*(23), 2827–2837. https://doi.org/10.2174/1381612043383584

Baxter, F. O., Came, P. J., Abell, K., Kedjouar, B., Huth, M., Rajewsky, K., Pasparakis, M., & Watson, C. J. (2006). IKKβ/2 induces TWEAK and apoptosis in mammary epithelial cells. *Development*, *133*(17), 3485–3494. https://doi.org/10.1242/DEV.02502

Bossen, C., Cachero, T. G., Tardivel, A., Ingold, K., Willen, L., Dobles, M., Scott, M. L., Maquelin, A., Belnoue, E., Siegrist, C. A., Chevrier, S., Acha-Orbea, H., Leung, H., Mackay, F., Tschopp, J., & Schneider, P. (2008). TACI, unlike BAFF-R, is solely activated by oligomeric BAFF and APRIL to support survival of activated B cells and plasmablasts. *Blood*, *111*(3), 1004–1012. https://doi.org/10.1182/BLOOD-2007-09-110874

Bover, L. C., Cardó-Vila, M., Kuniyasu, A., Sun, J., Rangel, R., Takeya, M., Aggarwal, B. B., Arap, W., & Pasqualini, R. (2007). A previously unrecognized protein-protein interaction

between TWEAK and CD163: potential biological implications. *Journal of Immunology (Baltimore, Md. : 1950)*, *178*(12), 8183–8194. https://doi.org/10.4049/JIMMUNOL.178.12.8183

Brown, S. A. N., Ghosh, A., & Winkles, J. A. (2010). Full-length, membrane-anchored TWEAK can function as a juxtacrine signaling molecule and activate the NF-κB pathway. *Journal of Biological Chemistry*, *285*(23), 17432–17441. https://doi.org/10.1074/jbc.M110.131979

Buabeid, M. A., Arafa, E. S. A., & Murtaza, G. (2020a). Emerging Prospects for Nanoparticle-Enabled Cancer Immunotherapy. *Journal of Immunology Research*, *2020*. https://doi.org/10.1155/2020/9624532

Buabeid, M. A., Arafa, E. S. A., & Murtaza, G. (2020b). Emerging Prospects for Nanoparticle-Enabled Cancer Immunotherapy. *Journal of Immunology Research*, *2020*. https://doi.org/10.1155/2020/9624532

Burkly, L. C., Michaelson, J. S., & Zheng, T. S. (2011). TWEAK/Fn14 pathway: an immunological switch for shaping tissue responses. *Immunological Reviews*, *244*(1), 99–114. https://doi.org/10.1111/J.1600-065X.2011.01054.X

Chao, D. T., Su, M., Tanlimco, S., Sho, M., Choi, D., Fox, M., Ye, S., Hsi, E. D., Durkin, L., Yin, J., Zhang, Y., Kim, H., Starling, G. C., & Culp, P. A. (2013). Expression of TweakR in breast cancer and preclinical activity of enavatuzumab, a humanized anti-TweakR mAb. *Journal of Cancer Research and Clinical Oncology*, *139*(2), 315–325. https://doi.org/10.1007/S00432-012-1332-X/FIGURES/4

Chen, Q., Chen, J., Yang, Z., Xu, J., Xu, L., Liang, C., Han, X., & Liu, Z. (2019). Nanoparticle-Enhanced Radiotherapy to Trigger Robust Cancer Immunotherapy. *Advanced Materials*, *31*(10), 1–12. https://doi.org/10.1002/adma.201802228

Chen, Q., Xu, L., Liang, C., Wang, C., Peng, R., & Liu, Z. (2016). Photothermal therapy with immune-adjuvant nanoparticles together with checkpoint blockade for effective cancer immunotherapy. *Nature Communications*, *7*. https://doi.org/10.1038/NCOMMS13193

Cheng, E., Armstrong, C. L., Galisteo, R., & Winkles, J. A. (2013). TWEAK/Fn14 Axis-Targeted Therapeutics: Moving Basic Science Discoveries to the Clinic. *Frontiers in Immunology*, *4*(DEC). https://doi.org/10.3389/FIMMU.2013.00473

Cherry, E. M., Lee, D. W., Jung, J. U., & Sitcheran, R. (2015). Tumor necrosis factor-like weak inducer of apoptosis (TWEAK) promotes glioma cell invasion through induction of NF-

κB-inducing kinase (NIK) and noncanonical NF-κB signaling. *Molecular Cancer*, *14*(1). https://doi.org/10.1186/S12943-014-0273-1

Chiang, C. S., Lin, Y. J., Lee, R., Lai, Y. H., Cheng, H. W., Hsieh, C. H., Shyu, W. C., & Chen, S. Y. (2018). Combination of fucoidan-based magnetic nanoparticles and immunomodulators enhances tumour-localized immunotherapy. *Nature Nanotechnology*, *13*(8), 746–754. https://doi.org/10.1038/S41565-018-0146-7

Chicheportiche, Y., Bourdon, P. R., Xu, H., Hsu, Y. M., Scott, H., Hession, C., Garcia, I., & Browning, J. L. (1997). TWEAK, a new secreted ligand in the tumor necrosis factor family that weakly induces apoptosis. *The Journal of Biological Chemistry*, *272*(51), 32401–32410. https://doi.org/10.1074/JBC.272.51.32401

Chicheportiche, Y., Fossati-Jimack, L., Moll, S., Ibnou-Zekri, N., & Izui, S. (2000). Down-regulated expression of TWEAK mRNA in acute and chronic inflammatory pathologies. *Biochemical and Biophysical Research Communications*, *279*(1), 162–165. https://doi.org/10.1006/BBRC.2000.3913

Chopra, M., Brandl, A., Siegmund, D., Mottok, A., Schäfer, V., Biehl, M., Kraus, S., Bäuerlein, C. A., Ritz, M., Mattenheimer, K., Schwinn, S., Seher, A., Grabinger, T., Einsele, H., Rosenwald, A., Brunner, T., Beilhack, A., & Wajant, H. (2015). Blocking TWEAK-Fn14 interaction inhibits hematopoietic stem cell transplantation-induced intestinal cell death and reduces GVHD. *Blood*, *126*(4), 437–444. https://doi.org/10.1182/BLOOD-2015-01-620583

De Campos Vidal, B., & Mello, M. L. S. (2011). Collagen type I amide I band infrared spectroscopy. *Micron*, *42*(3), 283–289. https://doi.org/10.1016/J.MICRON.2010.09.010

de Mol, N. J., & Fischer, M. J. E. (2010). Surface Plasmon Resonance: Methods and Protocols. *Life Sciences*, 255. https://doi.org/10.1007/978-1-60761-670-2

De Plater, L., Vincent, A. S., Berger, F., Nicolas, A., Vacher, S., Gravier, E., Thuleau, A., Karboul, N., Richardson, M., Elbaz, C., Marangoni, E., Bie, I., Paoletti, X., Roman-Roman, S., Culp, P. A., Asselain, B., Diéras, V., & Decaudin, D. (2014). Predictive gene signature of response to the anti-TweakR mAb PDL192 in patient-derived breast cancer xenografts. *PloS One*, *9*(11). https://doi.org/10.1371/JOURNAL.PONE.0104227

Desplat-Jego, S., Feuillet, L., Creidy, R., Malikova, I., Rance, R., Khrestchatisky, M., Hahm, K., Burkly, L. C., Pelletier, J., & Boucraut, J. (2009). TWEAK is expressed at the cell surface of monocytes during multiple sclerosis. *Journal of Leukocyte Biology*, *85*(1), 132–135. https://doi.org/10.1189/JLB.0608347

Dickens, L. S., Powley, I. R., Hughes, M. A., & MacFarlane, M. (2012). The “complexities” of life and death: death receptor signalling platforms. *Experimental Cell Research*, *318*(11), 1269–1277. https://doi.org/10.1016/J.YEXCR.2012.04.005

Din, F. U., Aman, W., Ullah, I., Qureshi, O. S., Mustapha, O., Shafique, S., & Zeb, A. (2017). Effective use of nanocarriers as drug delivery systems for the treatment of selected tumors. *International Journal of Nanomedicine*, *12*, 7291–7309. https://doi.org/10.2147/IJN.S146315

Donohue, P. J., Richards, C. M., Brown, S. A. N., Hanscom, H. N., Buschman, J., Thangada, S., Hla, T., Williams, M. S., & Winkles, J. A. (2003). TWEAK is an endothelial cell growth and chemotactic factor that also potentiates FGF-2 and VEGF-A mitogenic activity. *Arteriosclerosis, Thrombosis, and Vascular Biology*, *23*(4), 594–600. https://doi.org/10.1161/01.ATV.0000062883.93715.37

Duckett, C. S., & Thompson, C. B. (1997). CD30-dependent degradation of TRAF2: implications for negative regulation of TRAF signaling and the control of cell survival. *Genes & Development*, *11*(21), 2810. https://doi.org/10.1101/GAD.11.21.2810

Dwyer, B. J., Jarman, E. J., Gogoi-Tiwari, J., Ferreira-Gonzalez, S., Boulter, L., Guest, R. V., Kendall, T. J., Kurian, D., Kilpatrick, A. M., Robson, A. J., O’Duibhir, E., Man, T. Y., Campana, L., Starkey Lewis, P. J., Wigmore, S. J., Olynyk, J. K., Ramm, G. A., Tirnitz-Parker, J. E. E., & Forbes, S. J. (2021). TWEAK/Fn14 signalling promotes cholangiocarcinoma niche formation and progression. *Journal of Hepatology*, *74*(4), 860–872. https://doi.org/10.1016/J.JHEP.2020.11.018

Dykman, L. A., Staroverov, S. A., Fomin, A. S., Khanadeev, V. A., Khlebtsov, B. N., & Bogatyrev, V. A. (2018). Gold nanoparticles as an adjuvant: Influence of size, shape, and technique of combination with CpG on antibody production. *International Immunopharmacology*, *54*, 163–168. https://doi.org/10.1016/J.INTIMP.2017.11.008

Eetezadi, S., Ekdawi, S. N., & Allen, C. (2015). The challenges facing block copolymer micelles for cancer therapy: In vivo barriers and clinical translation. *Advanced Drug Delivery Reviews*, *91*, 7–22. https://doi.org/10.1016/J.ADDR.2014.10.001

Fadel, T. R., Sharp, F. A., Vudattu, N., Ragheb, R., Garyu, J., Kim, D., Hong, E., Li, N., Haller, G. L., Pfefferle, L. D., Justesen, S., Harold, K. C., & Fahmy, T. M. (2014). A carbon nanotube-polymer composite for T-cell therapy. *Nature Nanotechnology*, *9*(8), 639–647. https://doi.org/10.1038/NNANO.2014.154

Fallarini, S., Paoletti, T., Battaglini, C. O., Ronchi, P., Lay, L., Bonomi, R., Jha, S., Mancin, F., Scrimin, P., & Lombardi, G. (2013). Factors affecting T cell responses induced by fully synthetic glyco-gold-nanoparticles. *Nanoscale*, *5*(1), 390–400. https://doi.org/10.1039/C2NR32338A

Fan, Y., Kuai, R., Xu, Y., Ochyl, L. J., Irvine, D. J., & Moon, J. J. (2017). Immunogenic Cell Death Amplified by Co-localized Adjuvant Delivery for Cancer Immunotherapy. *Nano Letters*, *17*(12), 7387–7393. https://doi.org/10.1021/ACS.NANOLETT.7B03218

Felli, N., Pedini, F., Zeuner, A., Petrucci, E., Testa, U., Conticello, C., Biffoni, M., Di Cataldo, A., Winkles, J. A., Peschle, C., & De Maria, R. (2005). Multiple members of the TNF superfamily contribute to IFN-gamma-mediated inhibition of erythropoiesis. *Journal of Immunology (Baltimore, Md.: 1950)*, *175*(3), 1464–1472. https://doi.org/10.4049/JIMMUNOL.175.3.1464

Feng, X., Xu, W., Li, Z., Song, W., Ding, J., Chen Feng, X. X., Xu, W., Li, Z., Song, W., Ding, J., Chen, X., & Feng, X. (2019). Immunomodulatory Nanosystems. *Advanced Science*, *6*(17), 1900101. https://doi.org/10.1002/ADVS.201900101

Fick, A., Lang, I., Schäfer, V., Seher, A., Trebing, J., Weisenberger, D., & Wajant, H. (2012). Studies of binding of tumor necrosis factor (TNF)-like weak inducer of apoptosis (TWEAK) to fibroblast growth factor inducible 14 (Fn14). *The Journal of Biological Chemistry*, *287*(1), 484–495. https://doi.org/10.1074/JBC.M111.287656

Fulda, S., & Vucic, D. (2012). Targeting IAP proteins for therapeutic intervention in cancer. *Nature Reviews. Drug Discovery*, *11*(2), 109–124. https://doi.org/10.1038/NRD3627

Gaudineau, B., Fougère, M., Guaddachi, F., Lemoine, F., de la Grange, P., & Jauliac, S. (2012). Lipocalin 2, the TNF-like receptor TWEAKR and its ligand TWEAK act downstream of NFAT1 to regulate breast cancer cell invasion. *Journal of Cell Science*, *125*(Pt 19), 4475–4486. https://doi.org/10.1242/JCS.099879

Gonzalvez, F., Lawrence, D., Yang, B., Yee, S., Pitti, R., Marsters, S., Pham, V. C., Stephan, J. P., Lill, J., & Ashkenazi, A. (2012). TRAF2 Sets a threshold for extrinsic apoptosis by tagging caspase-8 with a ubiquitin shutoff timer. *Molecular Cell*, *48*(6), 888–899. https://doi.org/10.1016/J.MOLCEL.2012.09.031

Grell, M., Douni, E., Wajant, H., Löhden, M., Clauss, M., Maxeiner, B., Georgopoulos, S., Lesslauer, W., Kollias, G., Pfizenmaier, K., & Scheurich, P. (1995). The transmembrane form of tumor necrosis factor is the prime activating ligand of the 80 kDa tumor necrosis factor receptor. *Cell*, *83*(5), 793–802. https://doi.org/10.1016/0092-8674(95)90192-2

Grell, M., Wajant, H., Zimmermann, G., & Scheurich, P. (1998). The type 1 receptor (CD120a) is the high-affinity receptor for soluble tumor necrosis factor. *Proceedings of the National Academy of Sciences of the United States of America*, *95*(2), 570–575. https://doi.org/10.1073/PNAS.95.2.570

Grell, M., Zimmermann, G., Gottfried, E., Chen, C. M., Grünwald, U., Huang, D. C. S., Wu Lee, Y. H., Dürkop, H., Engelmann, H., Scheurich, P., Wajant, H., & Strasser, A. (1999). Induction of cell death by tumour necrosis factor (TNF) receptor 2, CD40 and CD30: a role for TNF-R1 activation by endogenous membrane-anchored TNF. *The EMBO Journal*, *18*(11), 3034–3043. https://doi.org/10.1093/EMBOJ/18.11.3034

Gu, L., Dai, L., Cao, C., Zhu, J., Ding, C., Xu, H. B., Qiu, L., & Di, W. (2013). Functional expression of TWEAK and the receptor Fn14 in human malignant ovarian tumors: possible implication for ovarian tumor intervention. *PloS One*, *8*(3). https://doi.org/10.1371/JOURNAL.PONE.0057436

Haile, W. B., Echeverry, R., Wu, F., Guzman, J., An, J., Wu, J., & Yepes, M. (2010). TUMOR NECROSIS FACTOR-LIKE WEAK INDUCER OF APOPTOSIS (TWEAK) AND FIBROBLAST GROWTH FACTOR-INDUCIBLE 14 (Fn14) MEDIATE CEREBRAL ISCHEMIA-INDUCED POLY(ADP-RIBOSE) POLYMERASE-1 ACTIVATION AND NEURONAL DEATH. *Neuroscience*, *171*(4), 1256. https://doi.org/10.1016/J.NEUROSCIENCE.2010.10.029

Haiss, W., Thanh, N. T. K., Aveyard, J., & Fernig, D. G. (2007). Determination of size and concentration of gold nanoparticles from UV-Vis spectra. *Analytical Chemistry*, *79*(11), 4215–4221. https://doi.org/10.1021/AC0702084

Hall, A., Wu, L. P., Parhamifar, L., & Moghimi, S. M. (2015). Differential Modulation of Cellular Bioenergetics by Poly(l-lysine)s of Different Molecular Weights. *Biomacromolecules*, *16*(7), 2119–2126. https://doi.org/10.1021/ACS.BIOMAC.5B00533

Hamdy, S., Molavi, O., Ma, Z., Haddadi, A., Alshamsan, A., Gobti, Z., Elhasi, S., Samuel, J., & Lavasanifar, A. (2008). Co-delivery of cancer-associated antigen and Toll-like receptor 4 ligand in PLGA nanoparticles induces potent CD8+ T cell-mediated anti-tumor immunity. *Vaccine*, *26*(39), 5046–5057. https://doi.org/10.1016/J.VACCINE.2008.07.035

Han, S., Huang, K., Gu, Z., & Wu, J. (2020). Tumor immune microenvironment modulation-based drug delivery strategies for cancer immunotherapy. *Nanoscale*, *12*(2), 413–436. https://doi.org/10.1039/C9NR08086D

Hayden, M. S., & Ghosh, S. (2012). NF-κB, the first quarter-century: remarkable progress and outstanding questions. *Genes & Development*, *26*(3), 203. https://doi.org/10.1101/GAD.183434.111

Hehlgans, T., & Pfeffer, K. (2005). The intriguing biology of the tumour necrosis factor/tumour necrosis factor receptor superfamily: Players, rules and the games. In *Immunology* (Vol. 115, Issue 1, pp. 1–20). Wiley-Blackwell. https://doi.org/10.1111/j.1365-2567.2005.02143.x

Herrero, R., Kajikawa, O., Matute-Bello, G., Wang, Y., Hagimoto, N., Mongovin, S., Wong, V., Park, D. R., Brot, N., Heinecke, J. W., Rosen, H., Goodman, R. B., Fu, X., & Martin, T. R. (2011). The biological activity of FasL in human and mouse lungs is determined by the structure of its stalk region. *The Journal of Clinical Investigation*, *121*(3), 1174–1190. https://doi.org/10.1172/JCI43004

Ho, D. H., Vu, H., Brown, S. A. N., Donohue, P. J., Hanscom, H. N., & Winkles, J. A. (2004). Soluble tumor necrosis factor-like weak inducer of apoptosis overexpression in HEK293 cells promotes tumor growth and angiogenesis in athymic nude mice. *Cancer Research*, *64*(24), 8968–8972. https://doi.org/10.1158/0008-5472.CAN-04-1879

Hoffmann, U., Fischereder, M., Marx, M., Schweda, F., Lang, B., Straub, R. H., & Krämer, B. K. (2003). Induction of cytokines and adhesion molecules in stable hemodialysis patients: is there an effect of membrane material? *American Journal of Nephrology*, *23*(6), 442–447. https://doi.org/10.1159/000074536

Holler, N., Tardivel, A., Kovacsovics-Bankowski, M., Hertig, S., Gaide, O., Martinon, F., Tinel, A., Deperthes, D., Calderara, S., Schulthess, T., Engel, J., Schneider, P., & Tschopp, J. (2003). Two adjacent trimeric Fas ligands are required for Fas signaling and formation of a death-inducing signaling complex. *Molecular and Cellular Biology*, *23*(4), 1428–1440. https://doi.org/10.1128/MCB.23.4.1428-1440.2003

Hosokawa, Y., Hosokawa, I., Ozaki, K., Nakae, H., & Matsuo, T. (2006). Proinflammatory effects of tumour necrosis factor-like weak inducer of apoptosis (TWEAK) on human gingival fibroblasts. *Clinical and Experimental Immunology*, *146*(3), 540–549. https://doi.org/10.1111/J.1365-2249.2006.03233.X

Hu, G., Zeng, W., & Xia, Y. (2017). TWEAK/Fn14 signaling in tumors. *Tumor Biology*, *39*(6). https://doi.org/10.1177/1010428317714624/ASSET/IMAGES/LARGE/10.1177_1010428317714624-FIG2.JPEG

Huang, M., Narita, S., Tsuchiya, N., Ma, Z., Numakura, K., Obara, T., Tsuruta, H., Saito, M., Inoue, T., Horikawa, Y., Satoh, S., & Habuchi, T. (2011). Overexpression of Fn14 promotes androgen-independent prostate cancer progression through MMP-9 and correlates with poor treatment outcome. *Carcinogenesis*, *32*(11), 1589–1596. https://doi.org/10.1093/CARCIN/BGR182

Ingold, K., Zumsteg, A., Tardivel, A., Huard, B., Steiner, Q. G., Cachero, T. G., Qiang, F., Gorelik, L., Kalled, S. L., Acha-Orbea, H., Rennert, P. D., Tschopp, J., & Schneider, P. (2005). Identification of proteoglycans as the APRIL-specific binding partners. *The Journal of Experimental Medicine*, *201*(9), 1375–1383. https://doi.org/10.1084/JEM.20042309

James, A. E., & Driskell, J. D. (2013). Monitoring gold nanoparticle conjugation and analysis of biomolecular binding with nanoparticle tracking analysis (NTA) and dynamic light scattering (DLS). *The Analyst*, *138*(4), 1212–1218. https://doi.org/10.1039/C2AN36467K

Jiao, Q., Li, L., Mu, Q., & Zhang, Q. (2014). Immunomodulation of nanoparticles in nanomedicine applications. *BioMed Research International*, *2014*. https://doi.org/10.1155/2014/426028

Joo, H. M., Coquery, C., Xue, Y., Gayet, I., Dillon, S. R., Punaro, M., Zurawski, G., Banchereau, J., Pascual, V., & Oh, S. K. (2012). Serum from patients with SLE instructs monocytes to promote IgG and IgA plasmablast differentiation. *The Journal of Experimental Medicine*, *209*(7), 1335–1348. https://doi.org/10.1084/JEM.20111644

Jordan, C. E., Frey, B. L., Kornguth, S., & Com, R. M. (1994). Characterization of Poly-L-lysine Adsorption onto Alkanethiol-Modified Gold Surfaces with Polarization-Modulation Fourier Transform Infrared Spectroscopy and Surface Plasmon Resonance Measurements. *Langmuir*, *10*(10), 3642–3648. https://doi.org/10.1021/la00022a043

Kaur, H., Chaurasia, S. S., Agrawal, V., & Wilson, S. E. (2009). Expression of PDGF Receptor-α in Corneal Myofibroblasts In Situ. *Experimental Eye Research*, *89*(3), 432. https://doi.org/10.1016/J.EXER.2009.03.017

Kawakita, T., Shiraki, K., Yamanaka, Y., Yamaguchi, Y., Saitou, Y., Enokimura, N., Yamamoto, N., Okano, H., Sugimoto, K., Murata, K., & Nakano, T. (2004). Functional expression of TWEAK in human hepatocellular carcinoma: Possible implication in cell proliferation and tumor angiogenesis. *Biochemical and Biophysical Research Communications*, *318*(3), 726–733. https://doi.org/10.1016/j.bbrc.2004.04.084

Kim, H., Niu, L., Larson, P., Kucaba, T. A., Murphy, K. A., James, B. R., Ferguson, D. M., Griffith, T. S., & Panyam, J. (2018a). Polymeric nanoparticles encapsulating novel TLR7/8 agonists as immunostimulatory adjuvants for enhanced cancer immunotherapy. *Biomaterials*, *164*, 38–53. https://doi.org/10.1016/J.BIOMATERIALS.2018.02.034

Kim, H., Niu, L., Larson, P., Kucaba, T. A., Murphy, K. A., James, B. R., Ferguson, D. M., Griffith, T. S., & Panyam, J. (2018b). Polymeric nanoparticles encapsulating novel TLR7/8 agonists as immunostimulatory adjuvants for enhanced cancer immunotherapy. *Biomaterials*, *164*, 38–53. https://doi.org/10.1016/J.BIOMATERIALS.2018.02.034

Koehler, J. M., Visaveliya, N., & Knauer, A. (2014). Controlling formation and assembling of nanoparticles by control of electrical charging, polarization, and electrochemical potential. *Nanotechnology Reviews*, *3*(6), 553–568. https://doi.org/10.1515/NTREV-2014-0006/MACHINEREADABLECITATION/RIS

Kucka, K., & Wajant, H. (2021). Receptor Oligomerization and Its Relevance for Signaling by Receptors of the Tumor Necrosis Factor Receptor Superfamily. *Frontiers in Cell and Developmental Biology*, *8*, 1890. https://doi.org/10.3389/FCELL.2020.615141/BIBTEX

Kumar, M., Makonchuk, D. Y., Li, H., Mittal, A., & Kumar, A. (2009). TNF-like weak inducer of apoptosis (TWEAK) activates proinflammatory signaling pathways and gene expression through the activation of TGF-beta-activated kinase 1. *Journal of Immunology (Baltimore, Md. : 1950)*, *182*(4), 2439–2448. https://doi.org/10.4049/JIMMUNOL.0803357

Kums, J., Nelke, J., Rüth, B., Schäfer, V., Siegmund, D., & Wajant, H. (2017). Quantitative analysis of cell surface antigen-antibody interaction using Gaussia princeps luciferase antibody fusion proteins. *MAbs*, *9*(3), 506–520. https://doi.org/10.1080/19420862.2016.1274844

Kwon, O. H., Park, S. J., Kang, T. W., Kim, M., Kim, J. H., Noh, S. M., Song, K. S., Yoo, H. S., Wang, Y., Pocalyko, D., Paik, S. G., Kim, Y. H., Kim, S. Y., & Kim, Y. S. (2012). Elevated fibroblast growth factor-inducible 14 expression promotes gastric cancer growth via nuclear factor-κB and is associated with poor patient outcome. *Cancer Letters*, *314*(1), 73–81. https://doi.org/10.1016/J.CANLET.2011.09.016

Lalaoui, N., Merino, D., Giner, G., Vaillant, F., Chau, D., Liu, L., Kratina, T., Pal, B., Whittle, J. R., Etemadi, N., Berthelet, J., Gräsel, J., Hall, C., Ritchie, M. E., Ernst, M., Smyth, G. K., Vaux, D. L., Visvader, J. E., Lindeman, G. J., & Silke, J. (2020). Targeting triple-negative breast cancers with the Smac-mimetic birinapant. *Cell Death & Differentiation 2020 27:10*, *27*(10), 2768–2780. https://doi.org/10.1038/s41418-020-0541-0

Lang, I., Fick, A., Schäfer, V., Giner, T., Siegmund, D., & Wajant, H. (2012). Signaling active CD95 receptor molecules trigger co-translocation of inactive CD95 molecules into lipid rafts. *The Journal of Biological Chemistry*, *287*(28), 24026–24042. https://doi.org/10.1074/JBC.M111.328211

Lassen, U. N., Meulendijks, D., Siu, L. L., Karanikas, V., Mau-Sorensen, M., Schellens, J. H. M., Jonker, D. J., Hansen, A. R., Simcox, M. E., Schostack, K. J., Bottino, D., Zhong, H., Roessler, M., Vega-Harring, S. M., Jarutat, T., Geho, D., Wang, K., Demario, M., & Goss, G. D. (2015). A phase I monotherapy study of RG7212, a first-in- class monoclonal antibody targeting TWEAK signaling in patients with advanced cancers. *Clinical Cancer Research*, *21*(2), 258–266. https://doi.org/10.1158/1078-0432.CCR-14-1334/86440/AM/A-PHASE-I-MONOTHERAPY-STUDY-OF-RG7212-A-FIRST-IN

Le, T. M. D., Yoon, A. R., Thambi, T., & Yun, C. O. (2022). Polymeric Systems for Cancer Immunotherapy: A Review. *Frontiers in Immunology*, *13*, 440. https://doi.org/10.3389/FIMMU.2022.826876/BIBTEX

Lee Ventola, C. (2017). Cancer Immunotherapy, Part 1: Current Strategies and Agents. *Pharmacy and Therapeutics*, *42*(6), 375. /pmc/articles/PMC5440098/

Li, N., Hu, W. J., Shi, J., Xue, J., Guo, W. X., Zhang, Y., Guan, D. X., Liu, S. P., Cheng, Y. Q., Wu, M. C., Xie, D., Liu, S. R., & Cheng, S. Q. (2013). Roles of fibroblast growth factor-inducible 14 in hepatocellular carcinoma. *Asian Pacific Journal of Cancer Prevention : APJCP*, *14*(6), 3509–3514. https://doi.org/10.7314/APJCP.2013.14.6.3509

Li, S., Feng, X., Wang, J., He, L., Wang, C., Ding, J., & Chen, X. (2018). Polymer nanoparticles as adjuvants in cancer immunotherapy. *Nano Research 2018 11:11*, *11*(11), 5769–5786. https://doi.org/10.1007/S12274-018-2124-7

Li, S. Y., Liu, Y., Xu, C. F., Shen, S., Sun, R., Du, X. J., Xia, J. X., Zhu, Y. H., & Wang, J. (2016). Restoring anti-tumor functions of T cells via nanoparticle-mediated immune checkpoint modulation. *Journal of Controlled Release : Official Journal of the Controlled Release Society*, *231*, 17–28. https://doi.org/10.1016/J.JCONREL.2016.01.044

Li, X., Zhu, W., Chen, Z., Luo, L., Huang, J., Zhang, F., Li, M., Guo, Y., & Guo, L. (2014). Fibroblast growth factor-inducible 14 regulates cell growth and multidrug resistance of small-cell lung cancer through the nuclear factor-KB pathway. *Anti-Cancer Drugs*, *25*(10), 1152–1164. https://doi.org/10.1097/CAD.0000000000000153

Lin, B. R., Huang, M. T., Chen, S. T., Jeng, Y. M., Li, Y. J., Liang, J. T., Lee, P. H., Chang, K. J., & Chang, C. C. (2012). Prognostic significance of TWEAK expression in colorectal

cancer and effect of its inhibition on invasion. *Annals of Surgical Oncology*, *19 Suppl 3*(SUPPL. 3). https://doi.org/10.1245/S10434-011-1825-X

Liu, H., Moynihan, K. D., Zheng, Y., Szeto, G. L., Li, A. V., Huang, B., Van Egeren, D. S., Park, C., & Irvine, D. J. (2014). Structure-based programming of lymph-node targeting in molecular vaccines. *Nature*, *507*(7493), 519–522. https://doi.org/10.1038/NATURE12978

Locksley, R. M., Killeen, N., & Lenardo, M. J. (2001a). The TNF and TNF receptor superfamilies: integrating mammalian biology. *Cell*, *104*(4), 487–501. https://doi.org/10.1016/S0092-8674(01)00237-9

Locksley, R. M., Killeen, N., & Lenardo, M. J. (2001b). The TNF and TNF receptor superfamilies: Integrating mammalian biology. In *Cell* (Vol. 104, Issue 4, pp. 487–501). Cell Press. https://doi.org/10.1016/S0092-8674(01)00237-9

Madej, M., Kurowska, N., & Strzalka-Mrozik, B. (2022). Polymeric Nanoparticles—Tools in a Drug Delivery System in Selected Cancer Therapies. *Applied Sciences 2022, Vol. 12, Page 9479*, *12*(19), 9479. https://doi.org/10.3390/APP12199479

Maecker, H., Varfolomeev, E., Kischkel, F., Lawrence, D., LeBlanc, H., Lee, W., Hurst, S., Danilenko, D., Li, J., Filvaroff, E., Yang, B., Daniel, D., & Ashkenazi, A. (2005). TWEAK attenuates the transition from innate to adaptive immunity. *Cell*, *123*(5), 931–944. https://doi.org/10.1016/J.CELL.2005.09.022

Medler, J., Nelke, J., Weisenberger, D., Steinfatt, T., Rothaug, M., Berr, S., Hünig, T., Beilhack, A., & Wajant, H. (2019). TNFRSF receptor-specific antibody fusion proteins with targeting controlled FcγR-independent agonistic activity. *Cell Death & Disease 2019 10:3*, *10*(3), 1–13. https://doi.org/10.1038/s41419-019-1456-x

Mi, Y., Smith, C. C., Yang, F., Qi, Y., Roche, K. C., Serody, J. S., Vincent, B. G., & Wang, A. Z. (2018). A Dual Immunotherapy Nanoparticle Improves T-Cell Activation and Cancer Immunotherapy. *Advanced Materials (Deerfield Beach, Fla.)*, *30*(25). https://doi.org/10.1002/ADMA.201706098

Michaelson, J. S., Amatucci, A., Kelly, R., Su, L., Garber, E., Day, E. S., Berquist, L., Cho, S., Li, Y., Parr, M., Willen, L., Schneider, P., Wortham, K., Burkly, L. C., Hsu, Y. M., & Joseph, I. B. J. K. (2011). Development of an Fn14 agonistic antibody as an anti-tumor agent. *MAbs*, *3*(4), 362–375. https://doi.org/10.4161/MABS.3.4.16090

Michaelson, J. S., Cho, S., Browning, B., Zheng, T. S., Lincecum, J. M., Wang, M. Z., Hsu, Y. M., & Burkly, L. C. (2005). Tweak induces mammary epithelial branching morphogenesis. *Oncogene*, *24*(16), 2613–2624. https://doi.org/10.1038/SJ.ONC.1208208

Michaelson, J. S., Kelly, R., Yang, L., Zhang, X., Wortham, K., & Joseph, I. B. J. K. (2012). The anti-Fn14 antibody BIIB036 inhibits tumor growth in xenografts and patient derived primary tumor models and enhances efficacy of chemotherapeutic agents in multiple xenograft models. *Cancer Biology & Therapy*, *13*(9), 812–821. https://doi.org/10.4161/CBT.20564

Mitchell, S., Vargas, J., & Hoffmann, A. (2016). Signaling via the NFκB system. *Wiley Interdisciplinary Reviews. Systems Biology and Medicine*, *8*(3), 227–241. https://doi.org/10.1002/WSBM.1331

Montenegro, J. M., Grazu, V., Sukhanova, A., Agarwal, S., de la Fuente, J. M., Nabiev, I., Greiner, A., & Parak, W. J. (2013). Controlled antibody/(bio-) conjugation of inorganic nanoparticles for targeted delivery. *Advanced Drug Delivery Reviews*, *65*(5), 677–688. https://doi.org/10.1016/J.ADDR.2012.12.003

Munn, D. H., & Bronte, V. (2016). Immune suppressive mechanisms in the tumor microenvironment. *Current Opinion in Immunology*, *39*, 1–6. https://doi.org/10.1016/J.COI.2015.10.009

Murthy, V. S., Cha, J. N., Stucky, G. D., & Wong, M. S. (2004). Charge-Driven Flocculation of Poly(L-lysine)-Gold Nanoparticle Assemblies Leading to Hollow Microspheres. *Journal of the American Chemical Society*, *126*(16), 5292–5299. https://doi.org/10.1021/ja038953v

Naassaoui, I., & Aschi, A. (2019). Evaluation of Properties and Structural Transitions of Poly-L-lysine: Effects of pH and Temperature. *Journal of Macromolecular Science, Part B: Physics*, *58*(10), 673–688. https://doi.org/10.1080/00222348.2019.1638593

Nakayama, M., Ishidoh, K., Kayagaki, N., Kojima, Y., Yamaguchi, N., Nakano, H., Kominami, E., Okumura, K., & Yagita, H. (2002). Multiple pathways of TWEAK-induced cell death. *Journal of Immunology (Baltimore, Md.: 1950)*, *168*(2), 734–743. https://doi.org/10.4049/JIMMUNOL.168.2.734

Nakayama, M., Ishidoh, K., Kojima, Y., Harada, N., Kominami, E., Okumura, K., & Yagita, H. (2003). Fibroblast growth factor-inducible 14 mediates multiple pathways of TWEAK-induced cell death. *Journal of Immunology (Baltimore, Md.: 1950)*, *170*(1), 341–348. https://doi.org/10.4049/JIMMUNOL.170.1.341

Nakayama, M., Kayagaki, N., Yamaguchi, N., Okumura, K., & Yagita, H. (2000). Involvement of Tweak in Interferon γ–Stimulated Monocyte Cytotoxicity. *The Journal of Experimental Medicine*, *192*(9), 1373. https://doi.org/10.1084/JEM.192.9.1373

Nelke, J., Medler, J., Weisenberger, D., Beilhack, A., & Wajant, H. (2020). CD40- and CD95-specific antibody single chain-Baff fusion proteins display BaffR-, TACI- and BCMA-restricted agonism. *MAbs*, *12*(1). https://doi.org/10.1080/19420862.2020.1807721

Nishikori, M. (n.d.). *Classical and Alternative NF-k B Activation Pathways and Their Roles in Lymphoid Malignancies*.

Niu, Y., Li, Y., Zang, J., Huang, H., Deng, J., Cui, Z., Yu, D., & Deng, J. (2012). Death receptor 5 and neuroproliferation. *Cellular and Molecular Neurobiology*, *32*(2), 255–265. https://doi.org/10.1007/S10571-011-9757-3

Noh, Y. W., Kim, S. Y., Kim, J. E., Kim, S., Ryu, J., Kim, I., Lee, E., Um, S. H., & Lim, Y. T. (2017). Multifaceted Immunomodulatory Nanoliposomes: Reshaping Tumors into Vaccines for Enhanced Cancer Immunotherapy. *Advanced Functional Materials*, *27*(8), 1605398. https://doi.org/10.1002/ADFM.201605398

Ou, W., Thapa, R. K., Jiang, L., Soe, Z. C., Gautam, M., Chang, J. H., Jeong, J. H., Ku, S. K., Choi, H. G., Yong, C. S., & Kim, J. O. (2018). Regulatory T cell-targeted hybrid nanoparticles combined with immuno-checkpoint blockage for cancer immunotherapy. *Journal of Controlled Release : Official Journal of the Controlled Release Society*, *281*, 84–96. https://doi.org/10.1016/J.JCONREL.2018.05.018

Park, K. (2014). Absence of in vivo-in vitro correlation in per-oral drug delivery. *Journal of Controlled Release : Official Journal of the Controlled Release Society*, *180*, 150. https://doi.org/10.1016/j.jconrel.2014.03.020

Pettersen, I., Baryawno, N., Abel, F., Bakkelund, W. H., Zykova, S. N., Winberg, J. O., Moens, U., Rasmuson, A., Kogner, P., Johnsen, J. I., & Sveinbjörnsson, B. (2013). Expression of TWEAK/Fn14 in neuroblastoma: implications in tumorigenesis. *International Journal of Oncology*, *42*(4), 1239–1248. https://doi.org/10.3892/IJO.2013.1800

Phan, G. Q., Yang, J. C., Sherry, R. M., Hwu, P., Topalian, S. L., Schwartzentruber, D. J., Restifo, N. P., Haworth, L. R., Seipp, C. A., Freezer, L. J., Morton, K. E., Mavroukakis, S. A., Duray, P. H., Steinberg, S. M., Allison, J. P., Davis, T. A., & Rosenberg, S. A. (2003). Cancer regression and autoimmunity induced by cytotoxic T lymphocyte-associated antigen 4 blockade in patients with metastatic melanoma. *Proceedings of the National*

Academy of Sciences of the United States of America, *100*(14), 8372–8377. https://doi.org/10.1073/PNAS.1533209100

Plebanek, M. P., Bhaumik, D., Bryce, P. J., & Shad Thaxton, C. (2018). Scavenger Receptor Type B1 and Lipoprotein Nanoparticle Inhibit Myeloid-Derived Suppressor Cells. *Molecular Cancer Therapeutics*, *17*(3), 686–697. https://doi.org/10.1158/1535-7163.MCT-17-0981

Prada, J. P., Wangorsch, G., Kucka, K., Lang, I., Dandekar, T., & Wajant, H. (2021). A systems-biology model of the tumor necrosis factor (TNF) interactions with TNF receptor 1 and 2. *Bioinformatics (Oxford, England)*, *37*(5), 669–676. https://doi.org/10.1093/BIOINFORMATICS/BTAA844

Qian, C., Wang, J., Qian, Y., Hu, R., Zou, J., Zhu, C., Zhu, C., Zhu, Y., Qi, S., Jia, X., Wu, L., Li, W., & Chen, Z. (2020). Tumor-Cell-Surface Adherable Peptide-Drug Conjugate Prodrug Nanoparticles Inhibit Tumor Metastasis and Augment Treatment Efficacy. *Nano Letters*, *20*(6), 4153–4161. https://doi.org/10.1021/acs.nanolett.0c00152

Qiu, F., Becker, K. W., Knight, F. C., Baljon, J. J., Sevimli, S., Shae, D., Gilchuk, P., Joyce, S., & Wilson, J. T. (2018). Poly(propylacrylic acid)-peptide nanoplexes as a platform for enhancing the immunogenicity of neoantigen cancer vaccines. *Biomaterials*, *182*, 82–91. https://doi.org/10.1016/J.BIOMATERIALS.2018.07.052

Ratajczak, W., Atkinson, S. D., & Kelly, C. (2022). *The TWEAK / Fn14 / CD163 axis — implications for metabolic disease*. *September 2021*, 449–462.

Richards, D. M., Marschall, V., Billian-Frey, K., Heinonen, K., Merz, C., Redondo Müller, M., Sefrin, J. P., Schröder, M., Sykora, J., Fricke, H., Hill, O., Gieffers, C., & Thiemann, M. (2019). HERA-GITRL activates T cells and promotes anti-tumor efficacy independent of FcγR-binding functionality. *Journal for Immunotherapy of Cancer*, *7*(1). https://doi.org/10.1186/S40425-019-0671-4

Riley, R. S., June, C. H., Langer, R., & Mitchell, M. J. (2019). Delivery technologies for cancer immunotherapy. *Nature Reviews. Drug Discovery*, *18*(3), 175–196. https://doi.org/10.1038/S41573-018-0006-Z

Rodell, C. B., Arlauckas, S. P., Cuccarese, M. F., Garris, C. S., Li, R., Ahmed, M. S., Kohler, R. H., Pittet, M. J., & Weissleder, R. (2018). TLR7/8-agonist-loaded nanoparticles promote the polarization of tumour-associated macrophages to enhance cancer immunotherapy. *Nature Biomedical Engineering*, *2*(8), 578–588. https://doi.org/10.1038/S41551-018-0236-8

Roos, C., Wicovsky, A., Müller, N., Salzmann, S., Rosenthal, T., Kalthoff, H., Trauzold, A., Seher, A., Henkler, F., Kneitz, C., & Wajant, H. (2010). Soluble and transmembrane TNF-like weak inducer of apoptosis differentially activate the classical and noncanonical NF-kappa B pathway. *Journal of Immunology (Baltimore, Md.: 1950)*, *185*(3), 1593–1605. https://doi.org/10.4049/JIMMUNOL.0903555

Rosalia, R. A., Cruz, L. J., van Duikeren, S., Tromp, A. T., Silva, A. L., Jiskoot, W., de Gruijl, T., Löwik, C., Oostendorp, J., van der Burg, S. H., & Ossendorp, F. (2015). CD40-targeted dendritic cell delivery of PLGA-nanoparticle vaccines induce potent anti-tumor responses. *Biomaterials*, *40*, 88–97. https://doi.org/10.1016/J.BIOMATERIALS.2014.10.053

Sabour Alaoui, S., Dessirier, V., de Araujo, E., Alexaki, V. I., Pelekanou, V., Lkhider, M., Stathopoulos, E. N., Castanas, E., Bagot, M., Bensussan, A., & Tsapis, A. (2012). TWEAK Affects Keratinocyte G2/M Growth Arrest and Induces Apoptosis through the Translocation of the AIF Protein to the Nucleus. *PLOS ONE*, *7*(3), e33609. https://doi.org/10.1371/JOURNAL.PONE.0033609

Saha, S., Xiong, X., Chakraborty, P. K., Shameer, K., Arvizo, R. R., Kudgus, R. A., Dwivedi, S. K. D., Hossen, M. N., Gillies, E. M., Robertson, J. D., Dudley, J. T., Urrutia, R. A., Postier, R. G., Bhattacharya, R., & Mukherjee, P. (2016). Gold Nanoparticle Reprograms Pancreatic Tumor Microenvironment and Inhibits Tumor Growth. *ACS Nano*, *10*(12), 10636–10651. https://doi.org/10.1021/ACSNANO.6B02231

Saitoh, T., Nakayama, M., Nakano, H., Yagita, H., Yamamoto, N., & Yamaoka, S. (2003). TWEAK induces NF-kappaB2 p100 processing and long lasting NF-kappaB activation. *The Journal of Biological Chemistry*, *278*(38), 36005–36012. https://doi.org/10.1074/JBC.M304266200

Salzmann, S., Seher, A., Trebing, J., Weisenberger, D., Rosenthal, A., Siegmund, D., & Wajant, H. (2013). Fibroblast Growth Factor Inducible (Fn14)-specific Antibodies Concomitantly Display Signaling Pathway-specific Agonistic and Antagonistic Activity. *The Journal of Biological Chemistry*, *288*(19), 13455. https://doi.org/10.1074/JBC.M112.435917

Sanz, A. B., Sanchez-Niño, M. D., Carrasco, S., Manzarbeitia, F., Ruiz-Andres, O., Selgas, R., Ruiz-Ortega, M., Gonzalez-Enguita, C., Egido, J., & Ortiz, A. (2012). Inflammatory cytokines and survival factors from serum modulate tweak-induced apoptosis in PC-3 prostate cancer cells. *PloS One*, *7*(10). https://doi.org/10.1371/JOURNAL.PONE.0047440

Sardar, R., Funston, A. M., Mulvaney, P., & Murray, R. W. (2009). Gold nanoparticles: Past, present, and future. *Langmuir*, *25*(24), 13840–13851. https://doi.org/10.1021/LA9019475

Sasso, M. S., Lollo, G., Pitorre, M., Solito, S., Pinton, L., Valpione, S., Bastiat, G., Mandruzzato, S., Bronte, V., Marigo, I., & Benoit, J. P. (2016). Low dose gemcitabine-loaded lipid nanocapsules target monocytic myeloid-derived suppressor cells and potentiate cancer immunotherapy. *Biomaterials*, *96*, 47–62. https://doi.org/10.1016/J.BIOMATERIALS.2016.04.010

Sau, S., Alsaab, H. O., Bhise, K., Alzhrani, R., Nabil, G., & Iyer, A. K. (2018). Multifunctional nanoparticles for cancer immunotherapy: A groundbreaking approach for reprogramming malfunctioned tumor environment. *Journal of Controlled Release : Official Journal of the Controlled Release Society*, *274*, 24–34. https://doi.org/10.1016/J.JCONREL.2018.01.028

Schmid, D., Park, C. G., Hartl, C. A., Subedi, N., Cartwright, A. N., Puerto, R. B., Zheng, Y., Maiarana, J., Freeman, G. J., Wucherpfennig, K. W., Irvine, D. J., & Goldberg, M. S. (2017). T cell-targeting nanoparticles focus delivery of immunotherapy to improve antitumor immunity. *Nature Communications*, *8*(1). https://doi.org/10.1038/S41467-017-01830-8

Schneider, C. S., Perez, J. G., Cheng, E., Zhang, C., Mastorakos, P., Hanes, J., Winkles, J. A., Woodworth, G. F., & Kim, A. J. (2015). Minimizing the non-specific binding of nanoparticles to the brain enables active targeting of Fn14-positive glioblastoma cells. *Biomaterials*, *42*, 42–51. https://doi.org/10.1016/J.BIOMATERIALS.2014.11.054

Schneider, P., Holler, N., Bodmer, J. L., Hahne, M., Frei, K., Fontana, A., & Tschopp, J. (1998). Conversion of membrane-bound Fas(CD95) ligand to its soluble form is associated with downregulation of its proapoptotic activity and loss of liver toxicity. *The Journal of Experimental Medicine*, *187*(8), 1205–1213. https://doi.org/10.1084/JEM.187.8.1205

Shi, C., Liu, T., Guo, Z., Zhuang, R., Zhang, X., & Chen, X. (2018). Reprogramming Tumor-Associated Macrophages by Nanoparticle-Based Reactive Oxygen Species Photogeneration. *Nano Letters*, *18*(11), 7330–7342. https://doi.org/10.1021/ACS.NANOLETT.8B03568

Shimada, K., Fujii, T., Tsujikawa, K., Anai, S., Fujimoto, K., & Konishi, N. (2012). ALKBH3 contributes to survival and angiogenesis of human urothelial carcinoma cells through NADPH oxidase and Tweak/Fn14/VEGF signals. *Clinical Cancer Research*, *18*(19), 5247–5255. https://doi.org/10.1158/1078-0432.CCR-12-0955/286444/AM/ALKBH3-CONTRIBUTES-TO-SURVIVAL-AND-ANGIOGENESIS-OF

Siegmund, D., Ehrenschwender, M., & Wajant, H. (2018). TNFR2 unlocks a RIPK1 kinase activity-dependent mode of proinflammatory TNFR1 signaling. *Cell Death & Disease*, *9*(9). https://doi.org/10.1038/S41419-018-0973-3

Siegmund, D., Lang, I., & Wajant, H. (2017). Cell death-independent activities of the death receptors CD95, TRAILR1, and TRAILR2. *The FEBS Journal*, *284*(8), 1131–1159. https://doi.org/10.1111/FEBS.13968

Siemienski, K., Weiss, T., Grell, M., Pfizenmaier, K., Scheurich, P., & Wajant, H. (1997). TNFR80-dependent enhancement of TNFR60-induced cell death is mediated by TRAF2 and is specific for TNFR60. *Immunobiology*, *197*(2–4), 198.

Sims, J. J., Scavone, F., Cooper, E. M., Kane, L. A., Youle, R. J., Boeke, J. D., & Cohen, R. E. (2012). Polyubiquitin-sensor proteins reveal localization and linkage-type dependence of cellular ubiquitin signaling. *Nature Methods*, *9*(3), 303–309. https://doi.org/10.1038/NMETH.1888

Suda, T., Hashimoto, H., Tanaka, M., Ochi, T., & Nagata, S. (1997). Membrane Fas ligand kills human peripheral blood T lymphocytes, and soluble Fas ligand blocks the killing. *The Journal of Experimental Medicine*, *186*(12), 2045–2050. https://doi.org/10.1084/JEM.186.12.2045

Sun, Y., Han, Y., Wang, X., Wang, W., Wang, X., Wen, M., Xia, J., Xing, H., Li, X., & Zhang, Z. (2016). Correlation of EGFR Del 19 with Fn14/JAK/STAT signaling molecules in non-small cell lung cancer. *Oncology Reports*, *36*(2), 1030–1040. https://doi.org/10.3892/OR.2016.4905

Tajrishi, M. M., Zheng, T. S., Burkly, L. C., & Kumar, A. (2014). The TWEAK-Fn14 Pathway: A Potent Regulator of Skeletal Muscle Biology in Health and Disease. *Cytokine & Growth Factor Reviews*, *25*(2), 215. https://doi.org/10.1016/J.CYTOGFR.2013.12.004

Tran, N. L., McDonough, W. S., Savitch, B. A., Fortin, S. P., Winkles, J. A., Symons, M., Nakada, M., Cunliffe, H. E., Hostetter, G., Hoelzinger, D. B., Rennert, J. L., Michaelson, J. S., Burkly, L. C., Lipinski, C. A., Loftus, J. C., Mariani, L., & Berens, M. E. (2006). Increased Fibroblast Growth Factor-Inducible 14 Expression Levels Promote Glioma Cell Invasion via Rac1 and Nuclear Factor-κB and Correlate with Poor Patient Outcome. *Cancer Research*, *66*(19), 9535–9542. https://doi.org/10.1158/0008-5472.CAN-06-0418

Trebing, J., El-Mesery, M., Schäfer, V., Weisenberger, D., Siegmund, D., Silence, K., & Wajant, H. (2014). CD70-restricted specific activation of TRAILR1 or TRAILR2 using scFv-

targeted TRAIL mutants. *Cell Death & Disease*, *5*(1). https://doi.org/10.1038/CDDIS.2013.555

Trebing, J., Lang, I., Chopra, M., Salzmann, S., Moshir, M., Silence, K., S Riedel, S., Siegmund, D., Beilhack, A., Otto, C., & Wajant, H. (2014). A novel llama antibody targeting Fn14 exhibits anti-metastatic activity in vivo. *MAbs*, *6*(1), 297–308. https://doi.org/10.4161/MABS.26709

Tsui, R., Kearns, J. D., Lynch, C., Vu, D., Ngo, K. A., Basak, S., Ghosh, G., & Hoffmann, A. (2015). IκBβ enhances the generation of the low-affinity NFκB/RelA homodimer. *Nature Communications*, *6*, 7068–7068. https://doi.org/10.1038/NCOMMS8068

Varfolomeev, E., Goncharov, T., Maecker, H., Zobel, K., Kömüves, L. G., Deshayes, K., & Vucic, D. (2012). Cellular inhibitors of apoptosis are global regulators of NF-κB and MAPK activation by members of the TNF family of receptors. *Science Signaling*, *5*(216). https://doi.org/10.1126/SCISIGNAL.2001878

Vince, J. E., Chau, D., Callus, B., Wong, W. W. L., Hawkins, C. J., Schneider, P., McKinlay, M., Benetatos, C. A., Condon, S. M., Chunduru, S. K., Yeoh, G., Brink, R., Vaux, D. L., & Silke, J. (2008). TWEAK-FN14 signaling induces lysosomal degradation of a cIAP1-TRAF2 complex to sensitize tumor cells to TNFalpha. *The Journal of Cell Biology*, *182*(1), 171–184. https://doi.org/10.1083/JCB.200801010

Wajant, H. (2013). The TWEAK-Fn14 system as a potential drug target. *British Journal of Pharmacology*, *170*(4), 748–764. https://doi.org/10.1111/bph.12337

Wajant, H. (2015). Principles of antibody-mediated TNF receptor activation. *Cell Death and Differentiation*, *22*(11), 1727–1741. https://doi.org/10.1038/CDD.2015.109

Wajant, H. (2019). Molecular Mode of Action of TRAIL Receptor Agonists—Common Principles and Their Translational Exploitation. *Cancers*, *11*(7). https://doi.org/10.3390/CANCERS11070954

Wang, A., Perera, Y. R., Davidson, M. B., & Fitzkee, N. C. (2016). Electrostatic Interactions and Protein Competition Reveal a Dynamic Surface in Gold Nanoparticle-Protein Adsorption. *Journal of Physical Chemistry C*, *120*(42), 24231–24239. https://doi.org/10.1021/ACS.JPCC.6B08469/SUPPL_FILE/JP6B08469_SI_001.PDF

Wang, Y., Song, W., Hu, M., An, S., Xu, L., Li, J., Kinghorn, K. A., Liu, R., & Huang, L. (2018). Nanoparticle-mediated HMGA1 Silencing Promotes Lymphocyte Infiltration and Boosts Checkpoint Blockade Immunotherapy for Cancer. *Advanced Functional Materials*, *28*(36). https://doi.org/10.1002/ADFM.201802847

Watts, G. S., Tran, N. L., Berens, M. E., Bhattacharyya, A. K., Nelson, M. A., Montgomery, E. A., & Sampliner, R. E. (2007). Identification of Fn14/TWEAK receptor as a potential therapeutic target in esophageal adenocarcinoma. *International Journal of Cancer*, *121*(10), 2132–2139. https://doi.org/10.1002/IJC.22898

Whitsett, T. G., Cheng, E., Inge, L., Asrani, K., Jameson, N. M., Hostetter, G., Weiss, G. J., Kingsley, C. B., Loftus, J. C., Bremner, R., Tran, N. L., & Winkles, J. A. (2012). Elevated expression of Fn14 in non-small cell lung cancer correlates with activated EGFR and promotes tumor cell migration and invasion. *The American Journal of Pathology*, *181*(1), 111–120. https://doi.org/10.1016/J.AJPATH.2012.03.026

Wicovsky, A., Salzmann, S., Roos, C., Ehrenschwender, M., Rosenthal, T., Siegmund, D., Henkler, F., Gohlke, F., Kneitz, C., & Wajant, H. (2009). TNF-like weak inducer of apoptosis inhibits proinflammatory TNF receptor-1 signaling. *Cell Death & Differentiation 2009 16:11*, *16*(11), 1445–1459. https://doi.org/10.1038/cdd.2009.80

Wiley, S. R., Cassiano, L., Lofton, T., Davis-Smith, T., Winkles, J. A., Lindner, V., Liu, H., Daniel, T. O., Smith, C. A., & Fanslow, W. C. (2001). A novel TNF receptor family member binds TWEAK and is implicated in angiogenesis. *Immunity*, *15*(5), 837–846. https://doi.org/10.1016/S1074-7613(01)00232-1

Winkles, J. A. (2008). The TWEAK-Fn14 cytokine-receptor axis: discovery, biology and therapeutic targeting. *Nature Reviews. Drug Discovery*, *7*(5), 411–425. https://doi.org/10.1038/NRD2488

Winkles, J. A., Tran, N. L., Brown, S. A. N., Stains, N., Cunliffe, H. E., & Berens, M. E. (2007). Role of TWEAK and Fn14 in tumor biology. *Frontiers in Bioscience : A Journal and Virtual Library*, *12*(7), 2761–2771. https://doi.org/10.2741/2270

Wyzgol, A., Müller, N., Fick, A., Munkel, S., Grigoleit, G. U., Pfizenmaier, K., & Wajant, H. (2009). Trimer stabilization, oligomerization, and antibody-mediated cell surface immobilization improve the activity of soluble trimers of CD27L, CD40L, 41BBL, and glucocorticoid-induced TNF receptor ligand. *Journal of Immunology (Baltimore, Md. : 1950)*, *183*(3), 1851–1861. https://doi.org/10.4049/JIMMUNOL.0802597

Xie, P. (2013). TRAF molecules in cell signaling and in human diseases. *Journal of Molecular Signaling*, *8*(1). https://doi.org/10.1186/1750-2187-8-7

Xu, Z., Wang, Y., Zhang, L., & Huang, L. (2014). Nanoparticle-delivered transforming growth factor-β siRNA enhances vaccination against advanced melanoma by modifying tumor microenvironment. *ACS Nano*, *8*(4), 3636–3645. https://doi.org/10.1021/NN500216Y

Xue, J., Zhao, Z., Zhang, L., Xue, L., Shen, S., Wen, Y., Wei, Z., Wang, L., Kong, L., Sun, H., Ping, Q., Mo, R., & Zhang, C. (2017). Neutrophil-mediated anticancer drug delivery for suppression of postoperative malignant glioma recurrence. *Nature Nanotechnology*, *12*(7), 692–700. https://doi.org/10.1038/NNANO.2017.54

Yang, G., Xu, L., Xu, J., Zhang, R., Song, G., Chao, Y., Feng, L., Han, F., Dong, Z., Li, B., & Liu, Z. (2018). Smart Nanoreactors for pH-Responsive Tumor Homing, Mitochondria-Targeting, and Enhanced Photodynamic-Immunotherapy of Cancer. *Nano Letters*, *18*(4), 2475–2484. https://doi.org/10.1021/ACS.NANOLETT.8B00040

Yin, J. J., Liu, Y. N., Tillman, H., Barrett, B., Hewitt, S., Ylaya, K., Fang, L., Lake, R., Corey, E., Morrissey, C., Vessella, R., & Kelly, K. (2014). AR-regulated TWEAK-FN14 pathway promotes prostate cancer bone metastasis. *Cancer Research*, *74*(16), 4306–4317. https://doi.org/10.1158/0008-5472.CAN-13-3233

Yoriki, R., Akashi, S., Sho, M., Nomi, T., Yamato, I., Hotta, H., Takayama, T., Matsumoto, S., Wakatsuki, K., Migita, K. M., Yagita, H., & Nakajima, Y. (2011). Therapeutic potential of the TWEAK/Fn14 pathway in intractable gastrointestinal cancer. *Experimental and Therapeutic Medicine*, *2*(1), 103–108. https://doi.org/10.3892/ETM.2010.181

Yuan, H., Jiang, W., Von Roemeling, C. A., Qie, Y., Liu, X., Chen, Y., Wang, Y., Wharen, R. E., Yun, K., Bu, G., Knutson, K. L., & Kim, B. Y. S. (2017). Multivalent bi-specific nanobioconjugate engager for targeted cancer immunotherapy. *Nature Nanotechnology*, *12*(8), 763–769. https://doi.org/10.1038/NNANO.2017.69

Zhang, L., Mazouzi, Y., Salmain, M., Liedberg, B., & Boujday, S. (2020). Antibody-Gold Nanoparticle Bioconjugates for Biosensors: Synthesis, Characterization and Selected Applications. *Biosensors and Bioelectronics*, *165*, 112370. https://doi.org/10.1016/J.BIOS.2020.112370

Zhang, Q., Wei, W., Wang, P., Zuo, L., Li, F., Xu, J., Xi, X., Gao, X., Ma, G., & Xie, H. Y. (2017). Biomimetic Magnetosomes as Versatile Artificial Antigen-Presenting Cells to Potentiate T-Cell-Based Anticancer Therapy. *ACS Nano*, *11*(11), 10724–10732. https://doi.org/10.1021/ACSNANO.7B04955

Zhang, Z., Liu, X., Chen, D., & Yu, J. (2022). Radiotherapy combined with immunotherapy: the dawn of cancer treatment. *Signal Transduction and Targeted Therapy 2022 7:1*, *7*(1), 1–34. https://doi.org/10.1038/s41392-022-01102-y

Zhao, L., Seth, A., Wibowo, N., Zhao, C. X., Mitter, N., Yu, C., & Middelberg, A. P. J. (2014). Nanoparticle vaccines. *Vaccine*, *32*(3), 327–337. https://doi.org/10.1016/J.VACCINE.2013.11.069

Zheng, L., Lv, Z., Gong, Z., Sheng, Q., Gao, Z., Zhang, Y., Yu, S., Zhou, J., Xi, Z., & Wang, X. (2017). Fn14 hepatic progenitor cells are associated with liver fibrosis in biliary atresia. *Pediatric Surgery International*, *33*(5), 593–599. https://doi.org/10.1007/S00383-017-4068-5/TABLES/2

Zheng, M., Pan, M., Zhang, W., Lin, H., Wu, S., Lu, C., Tang, S., Liu, D., & Cai, J. (2021). Poly(α-l-lysine)-based nanomaterials for versatile biomedical applications: Current advances and perspectives. *Bioactive Materials*, *6*(7), 1878–1909. https://doi.org/10.1016/J.BIOACTMAT.2020.12.001

Zhou, H., Mohamedali, K. A., Gonzalez-Angulo, A. M., Cao, Y., Migliorini, M., Cheung, L. H., LoBello, J., Lei, X., Qi, Y., Hittelman, W. N., Winkles, J. A., Tran, N. L., & Rosenblum, M. G. (2014). Development of human serine protease-based therapeutics targeting Fn14 and identification of Fn14 as a new target overexpressed in TNBC. *Molecular Cancer Therapeutics*, *13*(11), 2688–2705. https://doi.org/10.1158/1535-7163.MCT-14-0346/175435/AM/DEVELOPMENT-OF-HUMAN-SERINE-PROTEASE-BASED

Zhou, Q., Zhang, Y., Du, J., Li, Y., Zhou, Y., Fu, Q., Zhang, J., Wang, X., & Zhan, L. (2016). Different-Sized Gold Nanoparticle Activator/Antigen Increases Dendritic Cells Accumulation in Liver-Draining Lymph Nodes and CD8+ T Cell Responses. *ACS Nano*, *10*(2), 2678–2692. https://doi.org/10.1021/ACSNANO.5B07716

9. Appendix

9.1 Abbreviations

Table 11. Abbreviations

AD	Anchoring domain
ADCC	Antibody-dependent cellular cytotoxicity
APCs	Antigen-presenting cells
APS	Ammonium persulfate
AuNPs	Gold nanoparticles
AuNP-COOH	carboxyl-functionalized gold nanoparticles
Baff	B-cell activating factor receptor
BCMA	B-cell maturation antigen
BMDC	Bone marrow-derived dendritic cells
BSA	Bovine serum albumin
cIAP	Cellular inhibitor of apoptosis
CRD	Cysteine-rich domains
DD	Death domain
DDA	Dimethyl-dioctadecylammonium
DLS	Dynamic light scattering
DMMA	2,3-dimethyl maleic anhydride
DMSO	Dimethyl sulfoxide
ECL	Enhanced chemiluminescence
ECM	Extracellular matrix
EDC	1-ethyl-3-(3-dimethylaminopropyl) carbodiimide hydrochloride
EDTA	Ethylenediaminetetraacetic acid
ELISA	Enzyme-linked immunosorbent assay
EV	Empty vector
FBS	Fetal bovine serum
FcγRs	Fc gamma receptors
FDA	Food and Drug Administration
FGF	Fibroblast growth factor
Fn14	Fibroblast growth factor inducible 14
FTIR	Fourier transform infrared spectroscopy
GPI	Glycosylphosphatidylinositol
GPL	Gaussia princeps luciferase
HPV	Human papillomavirus
IAP	Inhibitor of apoptosis
IFN-γ	Interferon-γ
IKK	Inhibitor of kappaB kinase
LPS	Lipopolysaccharides

mAb	Monoclonal antibody
MAPK	Mitogen-activated protein kinases
MES	2-(N-morpholino) ethane sulfonic acid
MPL	Modified polylysine
MPLA	Monophosphoryl lipid A
NFκB	Nuclear factor κB
NHS	N-hydroxysuccinimide(1-hydroxy-2,5 pyrrolidine Dione) sodium salt
NP	Nnanoparticles
PBS	Phosphate buffered saline
PBST	Phosphate buffered saline with tween
PDL	Programmed death-ligand
PEG	Polyethylene glycol
PEI	Poly ethylenimine
PGA	Poly (g-glutamic acid)
ε-PL	Poly-L-lysine
PLG	Poly(lactic-co-glycolic)
PLGA	Poly(lactic-co-glycolic acid)
PMB	Polymyxin B
P/S	Penicillin/Streptomycin
RT	Room temperature
scFv	Single chain fragment variable
scBaff	Single-chain B-cell activating factor
SDS	Sodium dodecyl sulfate
SDS-PAGE	Sodium Dodecyl Sulfate Polyacrylamide Gel Electrophoresis
sTNFL	Soluble TNF ligands
TACI	Transmembrane activator and cyclophilin ligand interactor
TBS	Tris-buffered saline
TBST	Tris-buffered saline with tween
TEMED	Tetramethylethylenediamine
TGF	Tumor growth factor
THD	TNF homology domain
TLR	Toll-like receptor
TM	Transmembrane domain
TME	Tumor microenvironment
TNF	Tumor necrosis factor
TNFL	Tumor necrosis factor ligand
TNFR	Tumor necrosis factor receptor
TNFRSF	Tumor necrosis factor receptor superfamily
TRAF	TNFR associated factor
TRAIL	TNF-related apoptosis-inducing ligand

TRP	Tyrosinase-related protein
TWEAK	Tumor necrosis factor like weak inducer of apoptosis
UV-Vis	Ultraviolet-visible spectroscopy

9.2 List of Publications

Tengyu Zhang, Nienke Hesen, Olena Zaitseva, Ahmed Aido, Harald Wajant. Development of Modified polylysine based antibody conjugated nanoparticles with tumor-restricted, FcγR-independent stimulatory activity by targeting Fn14. (Manuscript)

Kucka, K., Lang, I., Zhang, T., Siegmund, D., Medler, J., & Wajant, H. (2021). Membrane lymphotoxin-α2β is a novel tumor necrosis factor (TNF) receptor 2 (TNFR2) agonist. *Cell Death & Disease*, *12*(4). https://doi.org/10.1038/S41419-021-03633-8

Medler, J., Kucka, K., Melo, V., Zhang, T., Von Rotenhan, S., Ulrich, J., Bremer, E., Hudecek, M., Beilhack, A., & Wajant, H. (2022). CD40- and 41BB-specific antibody fusion proteins with PDL1 blockade-restricted agonism. *Theranostics*, *12*(4), 1486–1499. https://doi.org/10.7150/THNO.66119

Meng, F., Zou, L., Zhang, T., Jiang, L., Ding, Y., Yu, P., & Peng, J. (2018). Using LC-MS/MS-based targeted proteomics to monitor the pattern of ABC transporters expression in the development of drug resistance. *Cancer Management and Research*, *10*, 2859–2870. https://doi.org/10.2147/CMAR.S164766

Olena Zaitseva, Annett Hoffmann, Magareta Loest, Mohamed Anany, Tengyu Zhang, Kirstin Kucka, Armin Wiegering, Christoph Otto and Harald Wajant. Antibody-based soluble and membrane-bound TWEAK mimicking agonists with FcγR-independent activity. Frontiers in Immunology (Accepted)

Zhuo, X., Margrethe Brekstad Kjellin, M., Schaal, Z., Zhang, T., Löbmann, K., & Leng, D. (2022). A Comparative Study between A Protein Based Amorphous Formulation and Other Dissolution Rate Enhancing Approaches: A Case Study with Rifaximin. *Pharmaceutics 2023, Vol. 15, Page 126*, *15*(1), 126. https://doi.org/10.3390/PHARMACEUTICS15010126

9.3 List of Figures

Figure 18: schematic illustration of composition and decomposition of MPL-antibody-AuNPs.

9.4 List of Tables